

**STRATEGIES FOR EXPANDING LIPID COVERAGE AND ACCELERATING  
BIOMARKER DISCOVERY USING MULTISEGMENT INJECTION-  
NONAQUEOUS-CAPILLARY ELECTROPHORESIS-MASS SPECTROMETRY**

**STRATEGIES FOR EXPANDING LIPID COVERAGE AND ACCELERATING  
BIOMARKER DISCOVERY USING MULTISEGMENT INJECTION-  
NONAQUEOUS-CAPILLARY ELECTROPHORESIS-MASS SPECTROMETRY**

By RITCHIE LY, B.SC.

A Thesis Submitted to the School of Graduate Studies in Partial Fulfillment of the  
Requirements of the Degree

Doctor of Philosophy

McMaster University © Copyright by Ritchie Ly

October 2022

DOCTOR OF PHILOSOPHY (2022)  
(Chemistry and Chemical Biology)

McMaster University  
Hamilton, Ontario

TITLE	Strategies for Expanding Lipid Coverage and Accelerating Biomarker Discovery Using Multisegment Injection-Nonaqueous Capillary Electrophoresis-Mass Spectrometry	
AUTHOR	Ritchie Ly, B.Sc.	(McMaster University)
SUPERVISOR	Professor Philip Britz-McKibbin	
PAGES	xvi, 160	

## Abstract

The importance of biomarkers cannot be understated as they have played a key role in revolutionizing public health and disease prevention on a population level. While there is a need to discover more specific and clinically relevant biomarkers, many technical challenges exist especially in the context of the rapidly growing field of lipidomics. This thesis aims to develop new analytical strategies for nontargeted lipid profiling when using multisegment injection-nonaqueous capillary electrophoresis-mass spectrometry (MSI-NACE-MS). *Chapter II* greatly expands metabolome coverage in CE-MS when using a compatible non-aqueous electrolyte system for global analysis of ionic lipids differing widely in their polarity, such as lysophosphatidic acids, phosphatidylinositols, phosphatidylethanolamines and free fatty acids. For the first time, a multi-tiered data workflow was introduced in MSI-NACE-MS using an ultra-high resolution Orbitrap mass analyzer under negative ion mode for credentialing more than 270 lipid features from serum extracts based on their characteristic accurate mass and electrophoretic mobility. Of these, 128 anionic lipids were reliably measured (median CV  $\approx$  13%) in most serum extracts (> 75%) that were applied to stratify a cohort of Japanese non-alcoholic steatohepatitis patients ( $n = 85$ ) based on their disease severity not feasible by conventional biomarkers of liver fibrosis. *Chapter III* expands the analytical performance of MSI-NACE-MS by introducing an innovative two-step chemical derivatization protocol as a charge-switching strategy to resolve zwitter-ionic phospholipids that otherwise co-migrate with the electroosmotic flow. Reaction conditions were optimized to achieve a quantitative yield for methylated phosphatidylcholines, which greatly improved resolution and detectability

when using MSI-NACE-MS under positive ion mode. Overall, this approach expanded lipidome coverage, supported phospholipid structural identification based on their characteristic electrophoretic mobility while also demonstrating the potential for reliable quantitative determination in a human serum reference material (NIST SRM-1950). Importantly, this universal methylation strategy may prove useful in other lipidomic platforms (LC-MS/MS, DI-MS/MS) as it is less hazardous than diazomethane. Lastly, *Chapter IV* involved the application of MSI-NACE-MS technology to discover surrogate biomarkers of omega-3 index (O3I) in two independent placebo-controlled clinical trials involving the ingestion of high-dose omega-3 fatty acids, including fish oil, eicosapentaenoic acid (EPA) or docosahexaenoic acid (DHA). For the first time, we identified a panel of omega-3 containing phosphatidylcholines in serum and plasma ether extracts that exhibited treatment responses in participants that were also positively correlated with independent O3I measurements. This work revealed that specific circulating phospholipids may allow for rapid assessment of omega-3 index without the need for complicated erythrocyte membrane hydrolyzed fatty acid analysis as required for risk assessment of cardiovascular health and sudden cardiac death. Overall, this thesis introduced MSI-NACE-MS as a hitherto unrecognized analytical platform for lipidomics that is complementary to chromatographic methods with improved sample throughput and accelerated data workflows for biomarker discovery in clinical medicine.

### **Acknowledgements**

First and foremost, I would like to graciously thank my supervisor, Dr. Philip Britz-McKibbin, for his continuous support, guidance, and encouragement during my undergraduate and graduate career. There are absolutely no words or actions that can truly express how grateful I am for the experience he has given me through joining his research group and taking a chance with a below average chemistry student from the undergraduate program at McMaster. This single opportunity completely changed the course of my life towards one with purpose and the impact he has had on me is immeasurable. I have had many opportunities to expand my knowledge beyond the field of analytical chemistry that have thoroughly supplied me with an expansive array of tools in my arsenal to be a critical thinker and a well-rounded scientist. Not only am I extremely grateful for the consistent guidance, time, and critical feedback during my studies, I appreciate every opportunity he provided me to creatively explore my own research ideas with trust and faith that I would execute them well. Cultivating this environment helped blossom my skills immensely as I never felt alone throughout the journey. Beyond the science, his door was always open to teach me incredible lessons about life that I will forever cherish in my heart. Although I am absolutely devastated that this time is coming to a close, I only hope that I have and continue to make him proud as I move ahead and put into practice everything that he has taught me – to inspire, spread knowledge, push boundaries and give others the opportunities as he did for me. Not only did I come out of this experience with a lifelong mentor, but I look forward to a future with one of the greatest friends I could have ever asked for.

I would also like to thank my incredible committee members, Dr. Karl Jobst and Dr. Murray Potter for their expertise, constructive feedback and valuable suggestions during committee meetings that pushed me to think outside the box during my graduate studies. Their continuous support helped me stay grounded in research and in life.

I would like to thank all the past and current members of the Britz-McKibbin research group that have contributed to this journey. Their mentorship, advice and guidance continue to inspire me throughout life. I forever cherish the memories we shared, the late-night chats and the continuous and unconditional support you all provided me. To the incredible students that I have had the honor to mentor through my graduate studies, you have taught me more about research and life than you will ever know.

I would also like to acknowledge the remarkable people I had the pleasure to meet in Japan through my multiple summer stays at Human Metabolome Technologies. The kindness, hospitality and support completely changed my perspectives on life. The experiences there are what I strive to bring forward to others. To Douglas Osei-Hyiaman, your support and belief in me as a person and a scientist will forever remain close to my heart.

Last but not least, I would like to express my deepest gratitude to my parents, my brother and my best friend Archie for their continuous love, guidance, and support throughout this journey. They have taught me the invaluable lessons of true hard work and determination and continue to inspire me everyday.

Thank you.

## Table of Contents

### Chapter I: Introduction to Biomarker Discovery and Lipidomics

1.1	The Advent of Lipidomics	2
1.2	Lipid Classes and Biological Functions	3
1.3	Challenges in the Biomarker Discovery Workflow for Lipidomics	5
1.4	Considerations at the Pre-analytical Phase of Biomarker Discovery	7
1.5	Considerations of Analytical Platforms for Biomarker Discovery	10
1.6	Chemical Derivatization Strategies in Lipidomics	13
1.7	Considerations at the Post-analytical Phase for Biomarker Discovery	17
1.8	Thesis Motivations & Objectives: Strategies for Accelerated Screening of Lipid Based Biomarkers Using MSI-NACE-MS	20
1.8.1	Establishing a Structured Nontargeted Data Workflow for MSI-NACE-MS	24
1.8.2	Expanding Coverage of MSI-NACE-MS Using a Convenient Derivatization Strategy for Zwitterionic Lipid Species	25
1.8.3	Screening for Circulating n-3 Phospholipids as Surrogate Markers for Routine Screening of Omega-3 Status	26
1.9	References	27

### Chapter II: Nontargeted Serum Lipid Profiling of Nonalcoholic Steatohepatitis by Multisegment Injection–Nonaqueous Capillary Electrophoresis– Mass Spectrometry: A Multiplexed Separation Platform for Resolving Ionic Lipids

2.1	Abstract	33
2.2	Introduction	34
2.3	Experimental	36
2.3.1	Chemicals and Reagents	36
2.3.2	Serum Lipid Extract Preparation	36
2.3.3	CE-MS Instrumentation and Serial Injection Configuration	37
2.3.4	Data Processing and Statistical Analysis	39
2.4	Results and Discussion	41
2.4.1	NASH Cohort and Serum Lipidomic Workflow in MSI-NACE-MS	43
2.4.2	Serum Lipidome Coverage and Lipid Classification in Mobility Maps	45
2.4.3	Differential Risk Assessment of NASH Patients from Serum Lipid Profiles	49
2.5	Conclusion	55
2.6	References	56
2.7	Supporting Information	59



**Chapter III: Expanding Lipidomic Coverage in Multisegment Injection-Nonaqueous Capillary Electrophoresis-Mass Spectrometry via a Convenient and Quantitative Methylation Strategy**

3.1	Abstract	74
3.2	Introduction	75
3.3	Experimental	78
3.3.1	Chemicals and Materials	78
3.3.2	Plasma Lipid Extraction Using MTBE	79
3.3.3	Chemical Derivatization of Zwitterionic Phospholipids Using Fmoc and MTT	80
3.3.4	CE-MS Instrumentation and Serial Injection Configuration	81
3.4	Results and Discussion	83
3.4.1	Separation Performance Enhancement After Phospholipid Methylation	83
3.4.2	Optimization of Fmoc/MTT Phospholipid Derivatization. Expanded Lipidome Coverage and Classification Via Mobility Maps	85
3.4.3	Characterization of Consensus mPLs from Reference Plasma Sample.	92
3.4.4	Quantification of Plasma mPLs Using Harmonized Reference Lipid Concentrations.	93
3.4.5	Conclusion	99
3.6	References	100
3.7	Supporting Information	104

**Chapter IV: Lipidomics for Identifying Serum Phospholipids as Surrogate Biomarkers of Omega-3 Index using Multisegment Injection-Nonaqueous Capillary Electrophoresis-Mass Spectrometry**

4.1	Abstract	116
4.2	Introduction	117
4.3	Experimental	120
4.3.1	Study Designs, Participants and Cohorts	120
4.3.2	Sample Workup, Extraction and Derivatization Procedure for MSI-NACE-MS	122
4.3.3	Untargeted and Targeted Lipidomics of Serum/Plasma Ether Extracts by MSI-NACE-MS	124
4.3.4	Data Processing and Statistical Analysis	126
4.4	Results and Discussion	127
4.4.1	Rapid Screening for Serum Phospholipids Responsive to High-Dose FO Supplementation	127
4.4.2	Discovery of Serum PC Species and Panels Associated with High-dose FO Supplementation	130

4.4.3	Validation of Serum PC Biomarkers of O3I Status Following DHA or EPA Specific Supplementation	135
4.4.4	Circulating $\omega$ -3 Phosphatidylcholines as Surrogate Markers to Measure Omega-3 Index	137
4.5	Conclusion	142
4.6	References	143
4.7	Supplemental Information	146

## **Chapter V: Future Directions in Lipidomics Using NACE for Biomarker Discovery**

5.1	Overview of Major Thesis Contributions	151
5.2	Further Method Development to Expand Lipid Profiling Capabilities by NACE	154
5.3	Applications of Strategies to Uncover Lipid Based Biomarkers for Cystic Fibrosis Using Neonatal Dried Blood Spots	155
5.4	Uncovering Lipid-Based Biomarkers in Larger Epidemiological Studies Using MSI-NACE-MS	157
5.5	Development of Targeted DI-MS/MS Assay for High-Throughput Screening of Vitamin D and Omega-3 Status	157
5.6	General Conclusions	158
5.7	References	159

### **List of Figures**

<b>Figure 1.1</b>	Overview of typical workflow for metabolomics and lipidomics profiling to uncover differential biomarkers.	5
<b>Figure 1.2</b>	The lipid annotation hierarchy for lipid identification based on the various structural information that is derived from analytical methods.	6
<b>Figure 1.3</b>	Overview of general lipidomics approach.	8
<b>Figure 1.4</b>	Schematic depicting phenomenon inducing separation using MSI-NACE-MS.	13
<b>Figure 1.5</b>	Overview of chemical derivatization scheme involving PEs with $d_6$ -DMBNHS	18
<b>Figure 1.6</b>	Unmodified lipid extract (top trace) and derivatized lipid extracted with $d_6$ -DMB (bottom)	19
<b>Figure 1.7</b>	Overview of various software tools and databases available for handling of lipidomics datasets	20
<b>Figure 2.1</b>	Lipidomics data workflow using a 3-tiered strategy when performing nontargeted lipid profiling	43

<b>Figure 2.2</b>	Representative total and extracted ion electropherograms highlighting the unique selectivity of MSI-NACE-MS for resolving a diverse range of ionic lipids having different polarity. MS/MS spectra from collisional-induced dissociation experiments at an optimal collision energy under negative ion mode for structural elucidation of select anionic lipids by MSI-NACE-MS	49
<b>Figure 2.3</b>	A 2D heat map depicting the ionic serum lipidome from a cohort of NASH patients (n=85) classified into two sub-groups (cluster A, n=26; cluster B, n=59) following a k-means clustering	52
<b>Figure 3.1</b>	Overview of FMOC/MTT derivatization scheme that is used as a safer alternative to diazomethane	84
<b>Figure 3.2</b>	Optimization of FMOC/MTT derivatization conditions as a function of reaction time that highlights a visible change in yellow color intensity with longer reaction times	87
<b>Figure 3.3</b>	Electrophoretic mobility plot as a function of the accurate mass for 76 PLs measured in reference plasma extracts	89
<b>Figure 3.4</b>	Representative extracted ion electropherograms for different mPC species when using customized serial injection configuration in MSI-NACE-MS,	94
<b>Figure 4.1</b>	Overview of data filtering approach using MSI-NACE-MS in both modes to target relevant lipids responsive to FO treatment	128
<b>Figure 4.2</b>	Study design overview of serum samples provided by Stuart Philips with subjects taking either sunflower oil or $\omega$ -3 containing fish oil supplements over an 8-week regime.	131
<b>Figure 4.3</b>	Serum phospholipid trajectory graphs for FO study	132
<b>Figure 4.4</b>	Study design overview for individual DHA/EPA supplementation with treatment response boxplots	137
<b>Figure 4.5</b>	Correlation plot of serum phospholipids to O3I	141
<b>Figure 5.1</b>	Analysis of lipid species using a single dried blood spot	156

### Supporting Figures

<b>Figure S2.1</b>	Schematic of the serial injection configuration for ionic lipids by MSI-NACE-MS, including six serum extracts from NASH patients (n=86) and a pooled sample as quality control (QC, n=17)	61
<b>Figure S2.2</b>	Representative MS/MS spectra from collisional-induced dissociation experiments at an optimal collision energy under negative ion mode for confirming the structural identity of a lysophosphatidylethanolamine (LPE 20:4)	62
<b>Figure S2.3</b>	Results of partitional clustering of NASH patients using a <i>k</i> -means clustering algorithm	63

<b>Figure S3.1</b>	Proposed mechanism for methylation of phospholipids using MTT.	105
<b>Figure S3.2</b>	Reaction scheme depicting p-toluidine by-product generation after methylation of phospholipids from MTT	106
<b>Figure S3.3</b>	An extracted ion electropherogram overlay of purine ( $m/z$ 121.0509) used as reference mass calibrant in the sheath liquid solution under different sample workup conditions following FMOC/MTT derivatization of NIST SRM-1950	107
<b>Figure S3.4</b>	MS/MS spectra acquired after CID experiments on derivatized mSM d34:1 in positive and negative ion mode	108
<b>Figure S3.5.</b>	Mobility map depicting all mPC species (n=50) and mSM species (n=27) detected from NIST SRM-1950 human plasma extracts after FMOC/MTT derivatization using MSI-NACE-MS in positive ion mode with full-scan data acquisition.	109
<b>Figure S3.6</b>	Venn diagram summarizing the coverage of consensus lipids reported by Bowden et al. from NIST SRM-1950 plasma ether extracts when using MSI-NACE-MS under positive (with FMOC/MTT derivatization) and negative ion mode (no derivatization)	110
<b>Figure S4.1</b>	Sub-group analysis of high dose FO supplementation compared to placebo	148
<b>Figure S4.2</b>	Scatter plots showing correlation of serum phospholipids to erythrocyte PL and O3I in FO study	149

### List of Tables

<b>Table 1.1</b>	Structural examples of lipid species	4
<b>Table 1.2</b>	Analysis platforms for metabolomics and lipidomics analysis	11
<b>Table 2.1</b>	Clinical characteristics and grading score of Japanese NASH patients from the full cohort and sub-group of patients identified after a <i>k</i> -means clustering algorithm of their serum lipid profiles	42
<b>Table 3.1</b>	Summary of MSI-NACE-MS validation experiments compared to reported concentrations in Bowden et al. and Thompson et al.	96
<b>Table 4.1</b>	Responsive fasting serum mPCs associated with FO supplementation	135
<b>Table 4.2</b>	Serum phospholipid models and associated Pearson correlation to O3I	139

### Supporting Tables

<b>Table S2.1</b>	Summary of clinical characteristics of a Japanese patient cohort diagnosed with NASH.	64
<b>Table S2.2</b>	List of credentialized saturated fatty acids detected in pooled NASH serum sample.	65

<b>Table S2.3</b>	List of credentialized mono-/polyunsaturated fatty acids detected in pooled NASH serum sample.	66
<b>Table S2.4</b>	List of credentialized phosphatidylcholines (PC) detected in pooled NASH serum sample.	67
<b>Table S2.5</b>	List of credentialized phosphatidylethanolamines (PE) detected in pooled NASH serum sample.	68
<b>Table S2.6</b>	List of credentialized lysophosphatidic acids (LPA) detected in pooled NASH serum sample.	69
<b>Table S2.7</b>	List of credentialized phosphatidylinositols (PI) detected in pooled NASH serum sample.	70
<b>Table S2.8</b>	Unknown serum lipid features that satisfied the three-tiered screening criteria in MSI-NACE-MS. Putative lipid classification assigned for anionic lipids within distinct clusters evident in the mobility map.	71
<b>Table S2.9</b>	Top-ranked serum lipids differentially expressed in NASH patient sub-groups following cluster analysis that satisfied Bonferroni correction and covariate adjustment.	72
<b>Table S3.1</b>	Plasma phospholipids measured from NIST-SRM 1950 serum by MSI-NACE-MS in positive ion mode detection that met acceptance criteria in the lipidomics harmonization study	111
<b>Table S3.2</b>	Plasma phospholipids from NIST SRM-1950 measured by MSI-NACE-MS that did not meet acceptance criteria in the lipidomics harmonization study	114
<b>Table S4.1</b>	Clinical characteristics of participants in separate DHA/EPA supplementation	147
<b>Table S4.2</b>	Sex-dependence of DHA or EPA treatment intervention on lipid panel measured by MSI-NACE-MS and O3L.	147

### List of Abbreviations and Symbols

[M-H] <sup>-</sup>	Deprotonated molecular ion
[M+H] <sup>+</sup>	Protonated molecular ion
[M+Na] <sup>+</sup>	Sodiated molecular ion
ANCOVA	Analysis of covariance
ANOVA	Analysis of variance
APCI	Atmospheric pressure chemical ionization
BGE	Background electrolyte
BMI	Body mass index
CE	Capillary electrophoresis
CID	Collisional induced dissociation
CV	Coefficient of variation
DESI-MS	Desorption electrospray ionization mass-spectrometry
DI-MS	Direct injection-mass spectrometry
EDTA	Ethylenediaminetetraacetic acid
EI	Electron ionization
EOF	Electroosmotic flow
ESI	Electrospray ionization
FC	Fold change
FDR	False discovery rate
FFQ	Food frequency questionnaire
FMOCC	Fluorenylmethoxycarbonyl chloride
FTICR	Fourier-transform ion cyclotron resonance
GC	Gas chromatography
HCA	Hierarchical clustering analysis
HCC	Hepatocellular carcinoma
HILIC	Hydrophilic interaction chromatography
HMDB	Human metabolome database
HP-921	Hexakis (2,2,3,3-tetrafluoropropoxy)phosphazine
KNN	<i>k</i> -nearest neighbour
LAESI-MS	Laser ablation electrospray ionization-mass spectrometry
LC	Liquid chromatography
LC-MS/MS	Liquid chromatography-tandem mass spectrometry
LIPID MAPS	Lipids Metabolites and Pathways Strategy
LOD	Limit of detection
LOQ	Limit of quantification
<i>m/z</i>	Mass to charge ratio
MALDI-MS	Matrix assisted desorption ionization-mass spectrometry
MRM	Multiple reaction monitoring
MS	Mass spectrometry
MS/MS	Tandem mass spectrometry
MSI-CE-MS	Multisegment injection-capillary electrophoresis-mass spectrometry

MSI-CE-MS/MS	Multisegment injection-capillary electrophoresis-tandem mass spectrometry
MSI-NACE-MS	Multisegment injection-nonaqueous capillary electrophoresis-mass spectrometry
MT	Migration time
MUFA	Monounsaturated fatty acids
MWCO	Molecular weight cut off
NACE	Nonaqueous capillary electrophoresis
NAFL	Non-alcoholic fatty liver
NAFLD	Non-alcoholic fatty liver disease
NAS	NAFLD activity score
NASH CRN	NASH clinical research network
NDS	Naphthalene disulfonate
NEFA	Nonesterified fatty acid
NIST	National Institute of Standards and Technology
NMR	Nuclear Magnetic Resonance
O3I	Omega-3 index
oPLS-DA	Orthogonal partial least squares-discriminant analysis
PCA	Principal component analysis
PCDL	Personal Compound Database and Library
PLS-DA	Partial least squares-discriminant analysis
PUFA	Polyunsaturated fatty acids
QA	Quality assurance
QQQ	Triple quadrupole
QC	Quality control
QTOF	Quadrupole time-of-flight
QTOF-MS	Quadrupole time-of-flight-mass spectrometry
R <sup>2</sup>	Coefficient of determination
RF	Random forest
RMT	Relative migration time
ROC	Receiver operating characteristic
RP	Reverse-phase
RPA	Relative peak area
RT	Retention time
S-W	Shapiro-Wilk
S/N	Signal-to-noise ratio
SCFA	Short chain fatty acids
TOF	Time-of-flight
UHPLC	Ultrahigh performance liquid chromatography
UPLC-MS	Ultra performance liquid chromatography-mass Spectrometry
UV	Ultraviolet
VIP	Variables of importance in projection

### **Declaration of Academic Achievement**

The following material has been previously published and is reprinted with written permission:

**Chapter II.** Reprinted and adapted from Ly, R.; Ly, N.; Sasaki, K.; Suzuki, M.; Kami, K.; Ohashi, Y.; Britz-McKibbin, P. Nontargeted Serum Lipid Profiling by Multisegment Injection-Nonaqueous Capillary Electrophoresis-Mass Spectrometry: A Multiplexed Separation Platform for Resolving Ionic Lipids. *J Proteome Res.* **2022**, *21*, 768–777.  
Copyright (2021) American Chemical Society



## **Chapter I**

### **Introduction to Lipidomics and Biomarker Discovery Workflow**

## Chapter I: Introduction

### 1.1. The Advent of Lipidomics

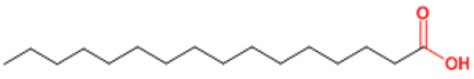
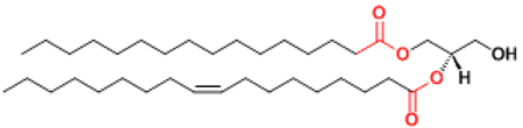
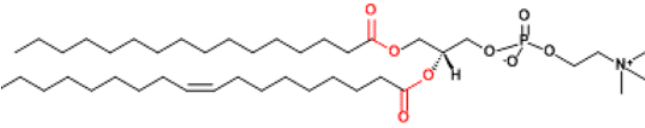
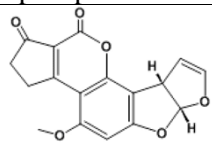
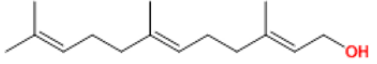
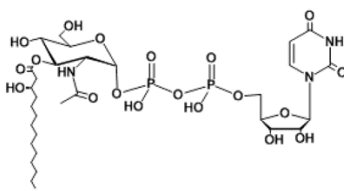
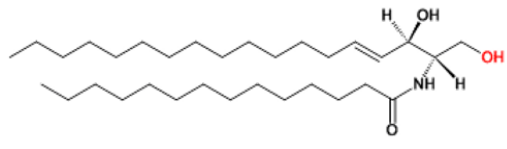
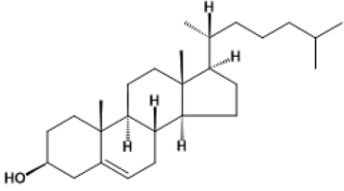
With the ongoing cascade in the -omics fields, the term “lipidomics”, a branch of metabolomics was first put forward in 2003 by Han and Gross.<sup>1</sup> Lipidomics is now defined as the characterization of lipid molecular species and their biological roles with respect to the expression of proteins involved in lipid metabolism and function and gene regulation.<sup>2</sup> Like metabolomics, the approaches to studying lipidomics can largely be divided into two categories targeted lipidomics (*i.e.*, focused lipid analysis/profiling), and untargeted lipidomics (*i.e.*, global lipid profiling).<sup>3</sup> A targeted lipidomics approach aims to analyze a few important lipids or lipid classes that can be carried out by using multiple reaction monitoring (MRM) or selected reaction monitoring (SRM) as the fragmentation patterns of analysis lipids are known. The untargeted lipidomics approach aims to analyze a wide range of lipid species in biological samples and attain as much coverage as reasonably possible. Beyond identifying and quantifying lipids in a system, a major component to lipidomics is the elucidation of individual molecular species in lipid metabolism and its related functions or dysfunction in the context of biological systems.<sup>4</sup> Overall, the field of lipidomics has quickly emerged as a critical component in functional genomic research since lipids function as essential nutrients, structural membrane components and/or bioactive compounds that regulate gene expression. The rise of lipidomics largely parallels the developments in analytical instrumentation separation techniques and mass spectrometry through the years.<sup>5</sup> For example, James and Martin<sup>6</sup> first demonstrated that gas chromatography was a viable platform to separate volatile FAs (C1-C10). This was further

expanded when GC with thermal conductivity was used for analysis of FAs as their methyl esters (FAMES) following an acid catalyzed transesterification.<sup>7</sup> Although LC with UV absorbance offers complementary separation capacity for resolving lipid species, the introduction of electrospray ionization (ESI)-MS was a key advancement that is now the primary ionization source used in modern lipidomic studies.<sup>8</sup> Despite these historic breakthroughs, many analytical challenges still remain in the field due to the sheer chemical complexity of lipid structures, ultimately slowing the translation of validated lipid biomarker candidates into clinical research.

## 1.2. Lipid Classes and Biological Functions

Lipids play diverse and important roles in biological systems such as composition of membrane bilayers, energy storage, contributions to signal transduction and regulating the activity of membrane proteins and their ongoing interactions.<sup>9</sup> The primary difference between lipids, carbohydrates, proteins and nucleic acids is typically their ability to solubilize in different organic solvents. Previously, lipids were defined by these physical properties, specifically solubility in non-polar solvents, or through the presence of long hydrocarbon chains. However, it is clear that not all lipids are able to satisfy the criteria of both definitions. Thus, a new nomenclature system was proposed for lipids based on their biosynthesis and structural motifs. Overall lipids are now classified into eight major categories: fatty acyls, glycerolipids, glycerophospholipids (GPL), polyketides, prenol lipids, saccharolipids, sphingolipids and sterol lipids where the general structures can be seen in **Table 1.1**. Even within these categories, lipids include a broad range of molecular structures such as glycerophospholipids, which include a series of building blocks that give

**Table 1.1:** Structural examples of lipid species. Structures adapted from LIPID MAPS.<sup>10</sup>

<i>Fatty Acyls</i>	 <p>Hexadecenoic acid</p>
<i>Glycerolipids</i>	 <p>1-hexadecanoyl-2-(9Z-octadecenoyl)-<i>sn</i>-glycerol</p>
<i>Glycerophospholipids</i>	 <p>1-hexadecanoyl-2-(9Z-octadecenoyl)-<i>sn</i>-glycerol-3-phosphocholine</p>
<i>Polyketides</i>	 <p>Aflatoxin B1</p>
<i>Prenol lipids</i>	 <p>2E,6E-farnesol</p>
<i>Saccharolipids</i>	 <p>UDP-3-O-(3R-hydroxy-tetradecanoyl)-<math>\alpha</math>-D-N-acetylglucosamine</p>
<i>Sphingolipids</i>	 <p>N-(tetradecanoyl)-sphing-4-enine</p>
<i>Sterol lipids</i>	 <p>Cholest-5-en-3<math>\beta</math>-ol</p>

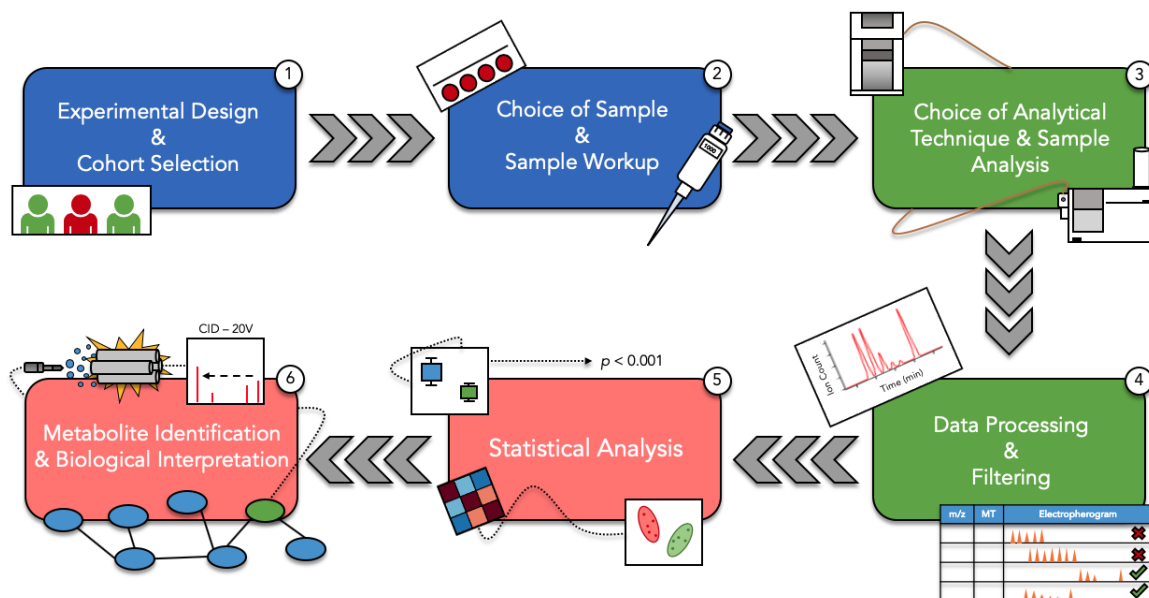


**Figure 1.1.** Overview of typical workflow for metabolomics and lipidomics profiling to uncover differential biomarkers.

rise to many possible combinations. This is apparent through the LIPID MAPS database which houses > 40,000 unique lipid structures, and currently serves the community as a compendium of structures and annotations of biologically relevant lipid species.<sup>10</sup> Thus, new analytical tools are needed to supplement biomarker discovery workflows in lipidomics (**Figure 1.1**) while characterizing unknown lipids of clinical significance.

### 1.3. Challenges in the Biomarker Discovery Workflow for Lipidomics

The analytical challenges that arise in lipidomics occur due to the sheer physicochemical diversity and wide dynamic range of the human lipidome that remains not fully characterized. Although shotgun “MS-only” approaches, using collision-induced dissociation (CID) based fragmentation methods and/or complementary derivatization techniques are often used, they typically restrict levels of annotation to some degree. This

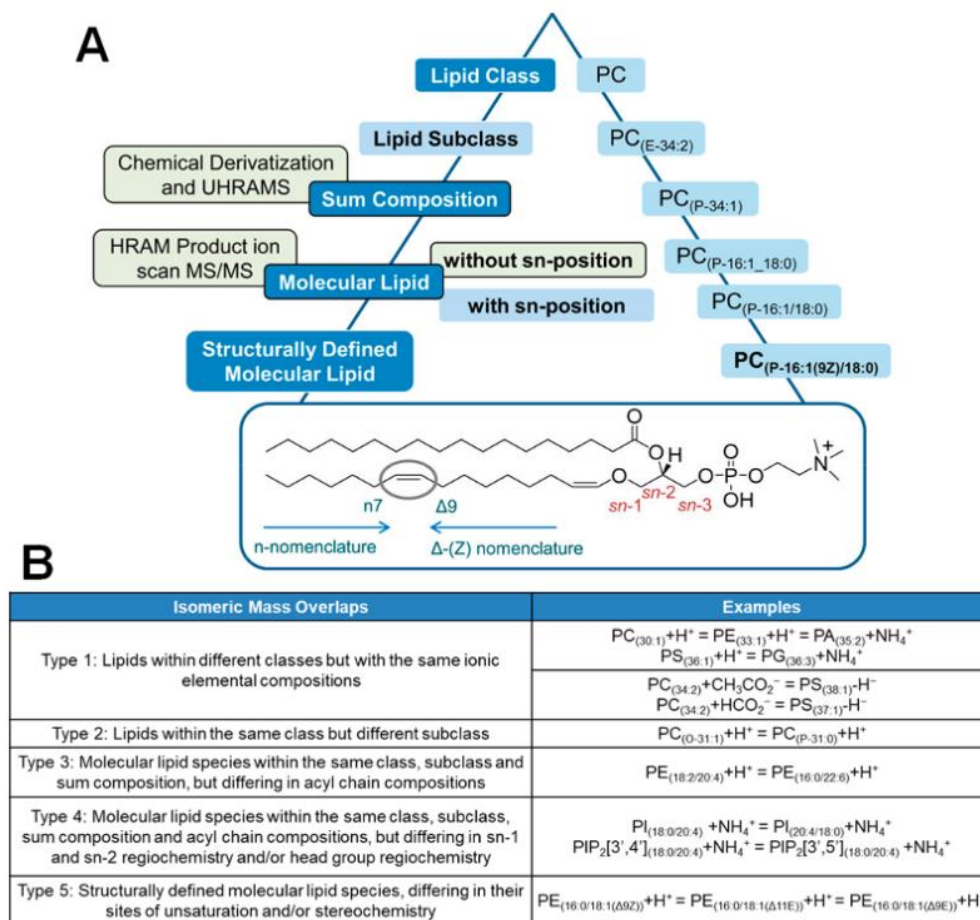


**Figure 1.2.** The lipid annotation hierarchy for lipid identification based on the various structural information that is derived from analytical methods. The types of isomeric mass lipid overlaps that hinder structural characterization at various of these annotation levels. Adapted from Reid *et al.*<sup>27</sup>

annotation hierarchy is summarized in **Figure 1.2**. In most cases, lipid identification can only be made to the “sum composition” or “molecular lipid” levels rather than the more functionally relevant and specific “structurally defined molecular lipid” tier. In the context of a glycerophospholipid, reaching the “structurally defined molecular lipid” level of annotation requires characterization of the lipid head group, the carbon chain length and the configuration of the individual acyl, alkyl or O-alk-1-enyl ether (*i.e.*, plasmalogen)

substituents attached to either the *sn-1* and *sn-2* positions of the glycerol backbone to include the number, location and stereochemistry of any unsaturation (*cis/trans*) and chemical modifications (*i.e.*, branches, cyclization and/or oxidation) within these chains.

#### **1.4. Considerations at the Pre-analytical Phase of Biomarker Discovery**

In the pre-analytical phase of a study, faults can occur, prior to any acquisition of data. This usually involves patient recruitment, study design, sample collection, transportation, sample storage and workup.<sup>11</sup> Often, metabolomic and lipidomic changes can be subtle as there is a high degree of inherent biological variability that can exist in human populations. Thus, care must be taken in these stages to ensure that findings in the study are not subject to bias.<sup>12</sup> Notably, sample size calculations can be challenging as traditional power analyses are not necessarily appropriate for large and untargeted multivariate studies, where in this circumstance *a priori* information about the number of metabolites and/or concentrations is very limited or lacking, as in the case of unknown metabolic or lipidomic features.<sup>13</sup>

Types of sample extraction procedures are critical as they need to adequately accommodate for the various matrices that exist. Biological samples contain many interfering compounds that should ideally be separated/removed before analysis. In the context of lipids, many interfering compounds such as carbohydrates, nucleic acids, proteins and salts need to be considered in the decision-making process. The biospecimen(s) should also be chosen in the context to the research hypothesis that is being explored. An example of this is the analysis of fatty acids, which can encompass the lipid

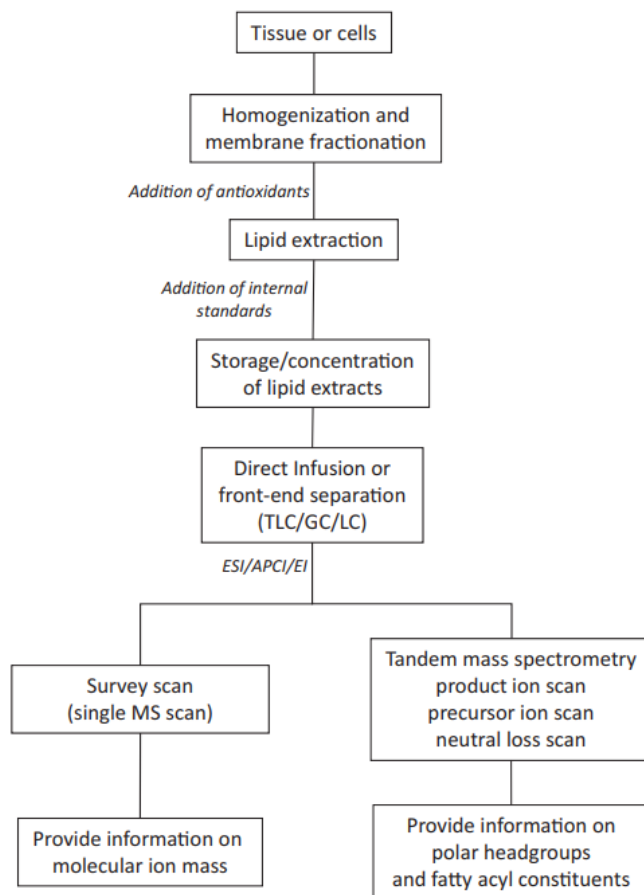


**Figure 1.3.** Overview of general lipidomics approach. Adapted from Khalil et al.<sup>70</sup>

pools from various biospecimens such as adipose tissue, erythrocyte phospholipids and even circulating/protein-bound non-esterified fatty acids (NEFA) which all reflect different stages of turnover time, function, biochemical activity and clinical relevance.<sup>14,15</sup> In lipidomics, the most common approach to extract lipids is using some variation of micro-scale liquid-liquid extraction and it can critically dictate the scope of the work as it occurs early on (**Figure 1.3**). In these approaches, biological samples are homogenized and suspended in aqueous and organic solvent (*e.g.*, chloroform, ethanol, benzene, methyl-*tert* butyl ether) to initially form a monophasic system. After agitation and centrifuging, a



biphasic system is formed due to the intrinsic miscibility and densities of each solvent. In lipidomics, typically, the non-polar layer is removed, containing the various hydrophobic species to which the remaining aqueous layer can be re-extracted with more non-polar solvent or carried forward for analysis using other compatible assays.

One of the most common solvent extraction techniques that makes use of these steps is known as the Bligh and Dyer<sup>16</sup> extraction, to which the resulting extract contains a several different types of lipid species. From here, several variations and modifications have been explored to hone in on specific lipid classes over others to obtain a more simplified sample, such as controlling pH using various buffer systems or altering the ratio of alcohol to water to modulate disruption of lipid-protein complexes. More recently, other solvent systems have been introduced that may have significant advantages over the Bligh and Dyer method as studies aim to provide more comprehensive profiling. The primary disadvantage of the Bligh and Dyer technique is that the lipid rich, chloroform extract settles as the bottom layer and requires piercing through a layer of suspended protein/debris.<sup>17</sup> More recently, two new lipid extraction protocols have gained popularity that make use of methyl *tert*-butyl ether (MTBE) or butanol/heptane/ethyl acetate (BUME).<sup>18</sup> Notably, MTBE has a lower density than water, which enables this organic layer to be present in the top after phase separation, which is much more feasible for high throughput analysis and automation, as well as acquiring both layers. In contrast, the BUME method is able to better discriminate recovery of water-soluble contaminants that likely carry over into the organic phase. Other considerations for sample preparation involve the addition of antioxidants such as butylated hydroxytoluene (BHT) at low concentrations into solvents during the

extraction processes or even purging lipid extracts prior to storage using inert gas bubbling (*e.g.*, nitrogen) to minimize degradation caused by reactive oxygen species.

### **1.5. Considerations of Analytical Platforms for Biomarker Discovery**

Careful considerations must be taken in order to choose analytical platform(s) that will best suit the study objectives. The intrinsic chemical diversity of metabolites and lipids, in terms of their physicochemical properties (*e.g.*, molecular weight, polarity, volatility, stability etc.) and concentration ranges ( $10^7$  to  $10^9$ -fold)<sup>19</sup> coupled to a large fraction of unknown species suggests that a single platform for global metabolic profiling does not exist.<sup>20</sup> Thus, cross- platform metabolomics and lipidomics studies are needed to attain more broader analyte coverage. This in mind, the strength and limitations of each analytical methodology must be considered within the context of study objectives and practical constraints such as budget/costs, sample volume, and acquisition time which is summarized in **Table 1.2**. As such, data from complimentary platforms or multiple targeted studies should ideally be combined to congregate on true global analysis.<sup>20</sup> Indeed, metabolomics and lipidomics represents a range of scopes for analysis, including *fingerprinting* or *footprinting*, targeted metabolic profiling and untargeted metabolomics. Notably, metabolic fingerprinting refers to the analysis of the intracellular metabolome by general, holistic methods.<sup>21</sup> Typically, it is rapid but often qualitative in that it provides a temporal snapshot or “fingerprint” of the metabolome. Targeted profiling is hypothesis-driven to focus on a limited portion of the metabolome, typically for a few specific metabolites or lipids of interest, related in chemical class and/or function with available purified reference standards.

**Table 1.2.** Instrumental platforms used in metabolomics and lipidomics analysis<sup>21–23</sup>

Platform	Advantages	Disadvantages
Nuclear magnetic resonance (NMR)	<ul style="list-style-type: none"> <li>• Non-destructive and minimal sample workup</li> <li>• Fast (2-10 min/sample)</li> <li>• Robust technology</li> </ul>	<ul style="list-style-type: none"> <li>• 10-100x less sensitive than MS platforms</li> <li>• High infrastructure/operating costs</li> <li>• Larger sample volumes needed (&gt;100 µL)</li> <li>• Complex deconvolution required due to spectral overlap in 1D NMR</li> </ul>
Direct Infusion Mass Spectrometry (DI-MS)	<ul style="list-style-type: none"> <li>• Fast (1-3 min/sample)</li> <li>• Low sample volume requirements</li> <li>• High sensitivity</li> <li>• Ideal for targeted analysis</li> <li>• Minimal solvent requirements</li> </ul>	<ul style="list-style-type: none"> <li>• Ion suppression/matrix effects</li> <li>• No separation of isomers/isobaric species</li> <li>• Stable-isotope internal standards are critical for quantification</li> <li>• Limited selectivity</li> </ul>
Liquid Chromatography Mass Spectrometry (LC-MS)	<ul style="list-style-type: none"> <li>• High sensitivity</li> <li>• Good retention time reproducibility (reversed-phase)</li> <li>• Wide selectivity/coverage</li> <li>• Simpler sample workup</li> </ul>	<ul style="list-style-type: none"> <li>• Slow (&gt; 15 min/sample)</li> <li>• High solvent consumption/waste</li> <li>• Less robust, less reproducible retention times using HILIC</li> </ul>
Gas Chromatography Mass Spectrometry (GC-MS)	<ul style="list-style-type: none"> <li>• Extensive EI-MS library, widely validated</li> <li>• High separation efficiency</li> <li>• Reproducible retention times</li> <li>• Ideal for volatile/thermally stable analyte species</li> </ul>	<ul style="list-style-type: none"> <li>• Complicated sample workup</li> <li>• Requirement for thermolability of species</li> <li>• Slow (&gt;20 min/sample)</li> <li>• Limited coverage of species</li> </ul>
Capillary Electrophoresis Mass Spectrometry (CE-MS)	<ul style="list-style-type: none"> <li>• High separation efficiency for ionic species</li> <li>• Effective desalting/minimal ion suppression effects</li> <li>• Low sample volume requirements (&lt; 5 µL)</li> <li>• Simpler sample workup</li> <li>• Minimal solvent use/low operating costs</li> </ul>	<ul style="list-style-type: none"> <li>• Lower sensitivity/limited coverage</li> <li>• Less reproducible migration times to other platforms (i.e. reversed-phase LC)</li> <li>• Technically challenging and less support from vendors</li> <li>• Fewer validated protocols for large-scale studies</li> <li>• Lack of variety in robust CE-MS interfaces</li> </ul>
Ion Mobility Mass Spectrometry (IM-MS)	<ul style="list-style-type: none"> <li>• Ultra-fast</li> <li>• Separation of isobars/isomers</li> <li>• Accurate prediction and annotation using collisional cross-section of species</li> <li>• High reproducibility</li> </ul>	<ul style="list-style-type: none"> <li>• Least mature technology for lipidomic analysis</li> <li>• Limited peak capacity/resolution</li> <li>• Prone to ion suppression</li> </ul>

The direct inject (DI)-ESI-MS or “shotgun” approach offers a high-throughput platform for lipidomic analysis of crude biological extracts that can forgo sample elution and column reconditioning steps that are often a time-hindrance in chromatographic separations.<sup>24</sup> While most platforms only enable characterization of lipid features to their sum composition level,<sup>25</sup> the use of CID experiments for acquisition of MS/MS spectra can provide additional structural information related to length, relative position and degree of unsaturation on fatty acyl chains, especially in the context of glycerophospholipids.<sup>26</sup> Furthermore, developments in ultraviolet photodissociation and ozone-induced dissociation as ion sources for MS/MS can provide distinct information into unsaturated lipid double bond positional isomers.<sup>27</sup> Currently, LC-MS/MS using reversed-phase (RP) and/or hydrophilic interaction chromatography (HILIC) are considered the gold standard for comprehensive lipidomic studies and have been utilized in large-scale clinical studies.<sup>28,29</sup> Furthermore, ion mobility-MS can resolve structurally diverse classes of lipids based on characteristic collisional-cross sectional areas and conformational size using ultra-fast gas phase separations, which has ultimately lead to generation of a Lipid Atlas to supplement annotation of unknown lipid species.<sup>30</sup> Additionally, combining orthogonal separation platforms in multidimensional approaches can further expand lipidome coverage such as in the case with HILIC enabling resolution of lipid classes based on polar head groups prior to spatial resolution via IM-MS.<sup>31</sup>

A promising platform for lipidomics that has remained largely unexplored to date is nonaqueous capillary electrophoresis (NACE), which allows for high efficiency separations using a conductive electrolyte soluble in a compatible organic solvent mixture.

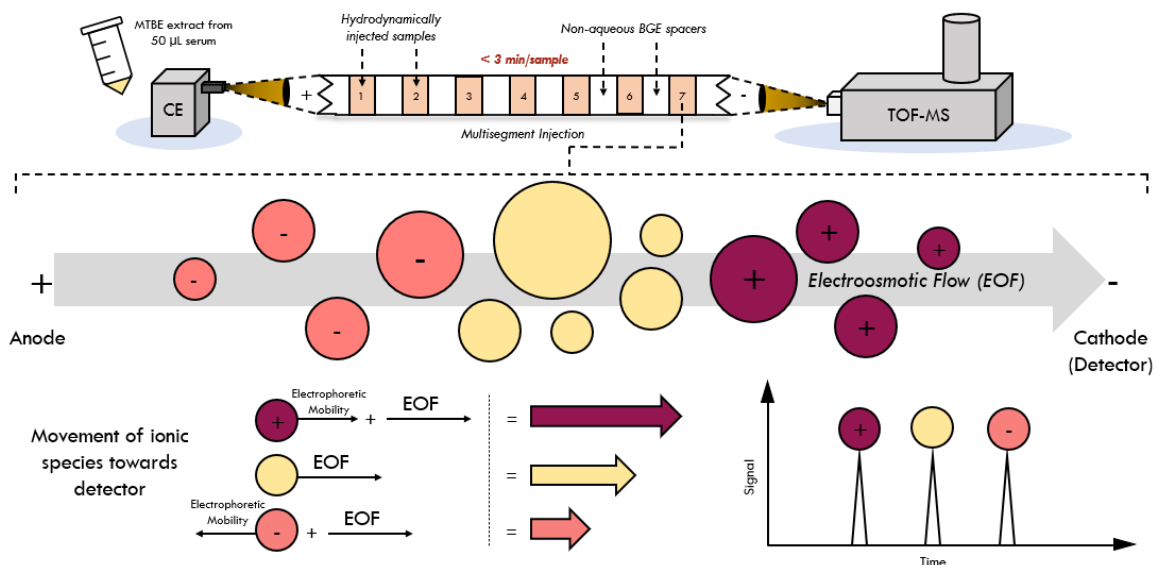


**Figure 1.4.** Schematic depicting phenomenon inducing separation using MSI-NACE-MS. Samples are injected into the capillary separated by non-aqueous BGE spacers, followed by the application of current inducing the differential movement of ions under a magnetic field. A secondary force known as the electroosmotic flow (EOF) is generated from the movement of cations in the buffer, generating another vector in the direction of the detector. As a result, cations exhibit the fastest migration speed while anions are the slowest. The order of detection begins with cations, followed by neutrals, and ending with anions.

When coupling to ESI-MS, the solvent mixtures typically comprise methanol, acetonitrile and/or isopropyl alcohol due to their volatility and miscibility. What differentiates NACE from conventional CE separations is that it offers unique selectivity when separating ionic lipids by modulating their ionization properties (*i.e.*, apparent  $pK_a$ ) due to varying solvent physicochemical properties (*i.e.*, relative permittivity/dielectric constant). The two primary electrokinetic principles that drive CE separations are the electroosmotic flow (EOF) and the apparent electrophoretic mobility ( $\mu_{ep}$ ) of an ion as described in **Figure 1.4**. Briefly, the silanol groups on the inner wall of fused-silica capillaries are deprotonated at  $pH > 2$ . This forms an overall negative surface charge as the background electrolyte (BGE) is flushed

through the capillary. An inner fixed layer (Stern layer) is strongly adsorbed while an outer diffuse layer (Helmholtz) of electrolytes generates a potential difference (*i.e.*, zeta potential) from the capillary surface to the bulk solution. Upon application of voltage, transport of bulk solution moves towards the cathode due to the movement of the diffuse layer, generating a natural pumping mechanism (*i.e.*, EOF). This is typically mediated by properties of the buffer solution such as pH, ionic strength, and viscosity. Additionally, the electrophoretic mobility directly impacts the selectivity of separation and is dependent on differences in the intrinsic physicochemical properties of an ion, namely  $pK_a$  and molecular volume (*i.e.*, effective charge density). Under normal polarity, smaller electrolytes/salts will migrate first due to their high positive mobility, acting as an effective desalting mechanism prior to slightly bulkier/minimally charged metabolites and lipids. Neutral compounds are unresolved and co-migrate with the EOF, whereas acidic/anionic metabolites migrate towards the anode in the opposite direction. However, they are still transported to the detector due to the higher velocity of the EOF under most buffer conditions. Overall, there have only been a small handful of NACE-MS methods that feature targeted analysis of specific lipid classes for proof of concept, including FAs, glycerophospholipids or lipid A isomers.<sup>32,33</sup> This likely reflects the many technical challenges in NACE-MS related to generating stable spray formation with low viscosity solvents using the coaxial sheath liquid interface (*i.e.*, suctioning effects of the nebulizer) as well as incidental capillary fractures that occur from organic solvent-induced swelling of the outer polyimide coatings of the fused-silica capillary.<sup>34</sup> More recently, our group sought to overcome these issues and introduced a multiplexed separation method referred

to as multisegment injection-nonaqueous capillary electrophoresis-mass spectrometry (MSI-NACE-MS) as a high-throughput screening method for total (hydrolyzed) or NEFAs from serum extracts.<sup>35</sup> With rigorous optimization and method development, this overcame several of the aforementioned technical issues using an alkaline nonaqueous BGE system to resolve anionic FAs (< 3.5 min/sample) under negative ion detection without the need for pre-column chemical derivatization. Nevertheless, despite the successful introduction and applications of this platform from our group,<sup>36–38</sup> its usage primarily focused on targeted analysis of FAs and has yet to be explored in a more nontargeted fashion.

Rustam and Reid<sup>27</sup> summarized two primary analytical challenges of lipidomics that continue to act as barriers in further advancement of the field. These can be defined in terms of their ability to (1) achieve complete analytical coverage and precise structural characterization of all the lipids that are present in a given sample, as well as (2) determining the accurate concentrations of each of these lipids, including defining their spatial distributions within an organ, tissue, cell or subcellular region of interest. The first issue is due to the fact that there exists an extreme complexity of lipids structures and their physicochemical properties that is difficult to fully resolve and detect from several thousands of individual molecular species, including numerous isobaric (same nominal mass) and isomeric (same exact mass) lipids. As a result, ion suppression and/or dynamic range limitations during ionization are further exacerbated, especially if the decision is to move forward with a workflow that uses little to no separation prior to MS analysis. Furthermore, there is limited structural information that is generated from “MS-only” measurements which typically restrict the level of annotation to the sum

composition/molecular lipid level.<sup>39</sup> The second challenge involving accurate quantification of lipid species, occurs due to the wide dynamic range of concentrations > 6 to 8 orders of magnitude. Most ionization methods used in lipidomics are “soft” in nature (*i.e.*, ESI) so they are not inherently quantitative. Thus, accurate quantitation can be difficult given the differential ionization efficiencies and/or ion suppression effects that result from lipid classes and/or individual lipid structures that elute at different times in a LC separation with gradient elution. As a result, external calibration is used with internal standards that are isotopically labelled. However, purified lipid standards (including isotopically labelled variants) are often difficult to obtain and quite costly. Nevertheless, the fidelity of the data ultimately relies on the control of variances that are introduced during sample preparation protocols to ensure that internal standards are incorporated in such a way that yields ionization responses that are similar to endogenous species.

## **1.6. Chemical Derivatization Strategies in Lipidomics**

Indeed, chemical derivatization of lipids is another approach to increase sensitivity, separate isobaric masses, or even probe the location of double bonds. This is summarized nicely by Rustam and Reid<sup>27</sup> in that there are four primary purposes for chemical derivatization to occur in lipidomic analysis. These include (1) improving sensitivity via incorporation of a highly efficient ionizable group to the lipid molecules, (2) the resolution of certain types of isomeric lipid species as a result of mass shifts induced via the derivatization process, (3) enhancing structural information from MS/MS due to alteration of the chemical structure of the lipid following derivatization and (4) multiplexed quantitation via the introduction of stable isotope-labels as part of the derivatization



chemistry.<sup>27</sup> One of the earliest methods that continues to widely be used is the methylation of fatty acids followed by GC-MS analysis, which can be achieved through acid-catalyzed esterification that relies on excess methanol to shift equilibrium to completion. A modern example of its usage in application to a large-scale study is the EPIC-InterACT project to profile total fatty acids in plasma ( $n > 20,000$ ) and their association with type 2 diabetes.<sup>40,41</sup> While GC remains the gold standard platform for fatty acid analysis when coupled to this derivatization strategy, this required substantial infrastructure with several automated systems to aid in sample preparation. Furthermore, this required a team of dedicated, trained researchers to operate multiple GC systems to complete the study in 24 months.<sup>40</sup> Although the study generated incredible amounts of data to interpret and correlate to type 2 diabetes, it is evident that more practical, cost-efficient workflows are needed to continue towards this direction in accelerating biomarker discovery. A couple examples of “charge switch” derivatization techniques have been used to improve ionization efficiency in a particular mode. For example, the use of *N*-(4-amino-methylphenyl) pyridinium (AMPP) was used to introduce a permanent charge on lipid species that contained carboxylic acid functional groups, more specifically, FAs involved in inflammatory signalling processes. more informative MS/MS fragmentation pathway to provide information about double bond positions through charge-remote fragmentation in positive mode. Another example of “charge-switch” derivatization was reported by the Smith group known as trimethylation enhancement using diazomethane (TrEnDi), which aimed to enhance lipid ionization of zwitterionic species as well as mass-resolving isobaric and isomeric lipids. Not only did this enhance ionization sensitivity and signal to noise ratios but provided a shotgun

approach via the use of a  $^{13}\text{C}$  labelled isotope of diazomethane.<sup>42–45</sup> Another example of a derivatization strategy for shotgun lipidomics approaches focuses on PEs. In 2012, the Reid group proposed d<sub>6</sub>-dimethylthiobutanoylhydroxysuccinimide ester (d<sub>6</sub>-DMBNHS), which harbors a fixed positive charge via a sulfonium ion as seen in **Figure 1.5**. When d<sub>6</sub>-DMBNHS reacts with PE, a new amide bond is formed, adding another moiety that increases ionization efficiency greatly.<sup>46</sup> This approach is useful as it increases the sensitivity of lower abundance PE species as well as separating isobaric lipid species due to a unique mass shift of the d<sub>6</sub>-DMB moiety (+136 Da) as seen in **Figure 1.6**.

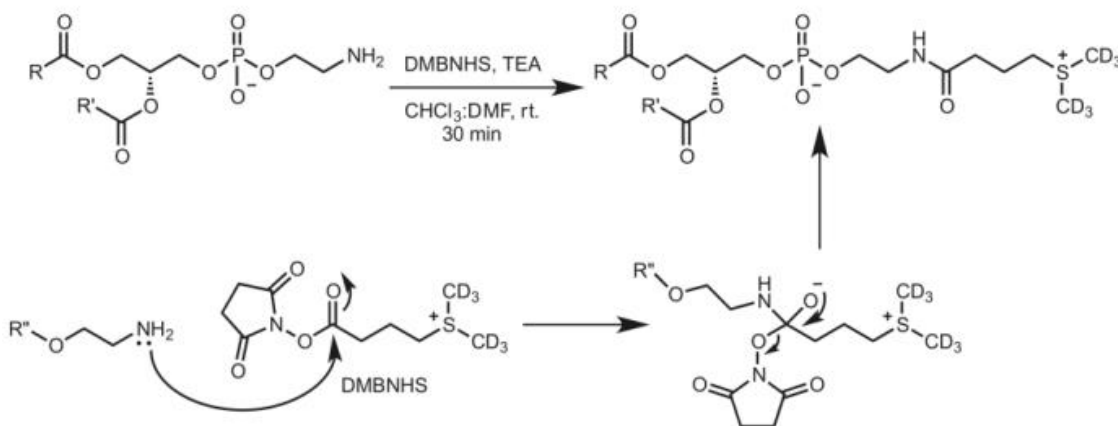


**Figure 1.5.** Overview of chemical derivatization scheme involving PEs with d<sub>6</sub>-DMBNHS. Figure adapted from Phaner *et al.*<sup>46</sup>

### 1.7. Considerations at the Post-analytical Phase for Biomarker Discovery

Post-analytical stages of biomarker discovery typically involve pre-processing of data following acquisition. This usually incorporates operations such as peak picking or binning, spectral deconvolution, filtering/smoothing, time alignment, normalization, and/or

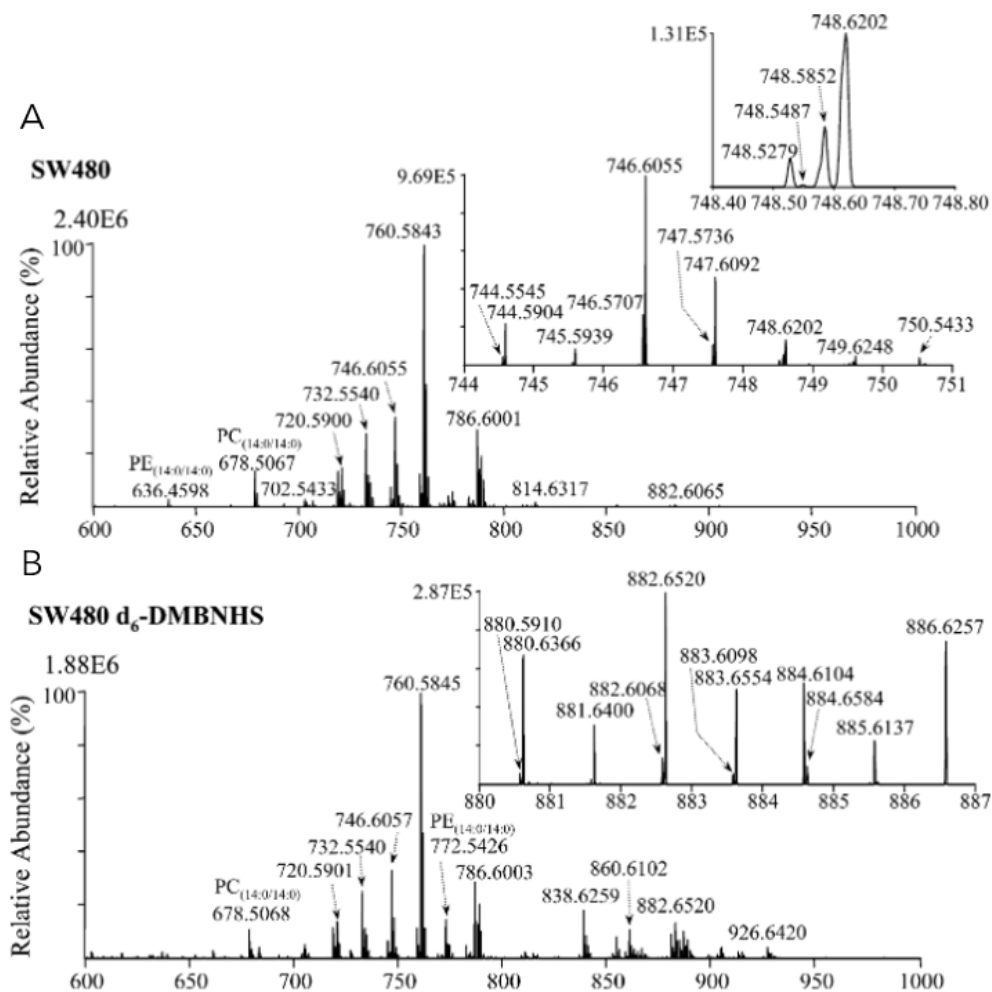


**Figure 1.6.** Unmodified lipid extract (top trace) and derivatized lipid extracted with  $d_6$ -DMB (bottom). Note the mass shift in PE (14:0/14:0) before and after derivatization via a characteristic mass shift (+136 Da). Figure adapted from Phaner e al.<sup>46</sup>

appropriate data transformation and scaling techniques. Given the instrumental platform that is selected, the generated datasets and the population where the samples were drawn, not all of the aforementioned steps may be necessary. Nevertheless, a slew of bioinformatics tools are available to handle data, even in the context of lipidomics alone as highlighted in **Figure 1.7**. Generally in MS-based metabolomic and lipidomic studies,

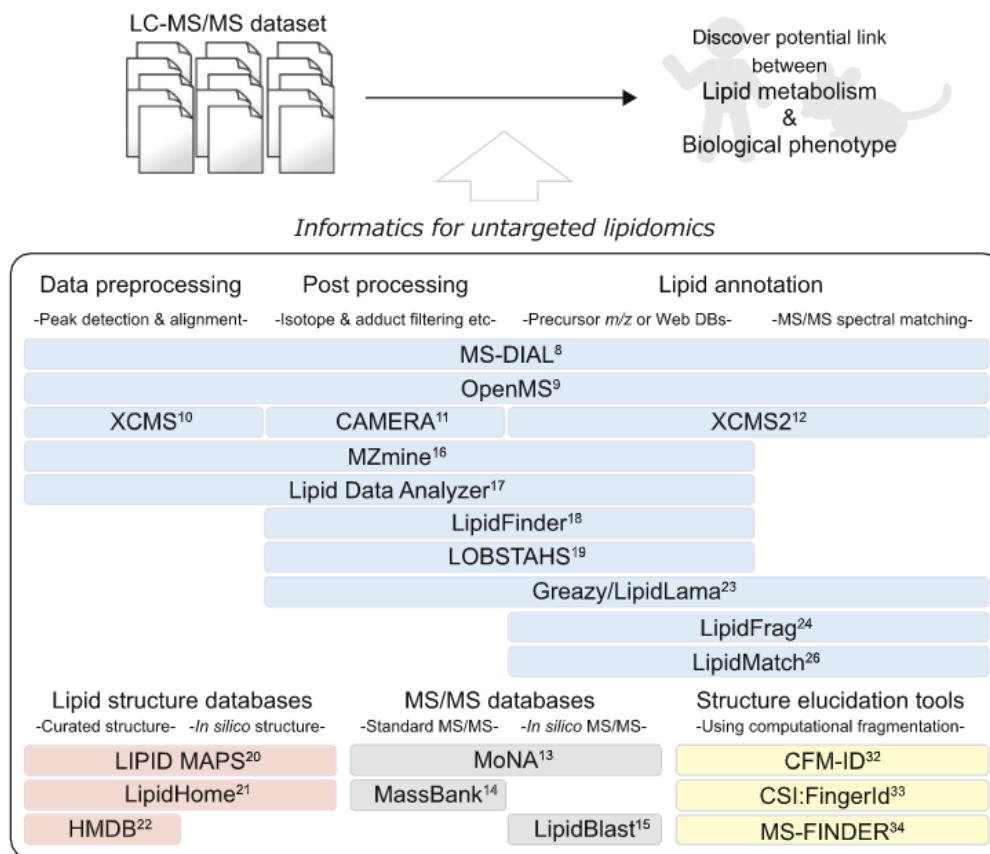


**Figure 1.7.** Overview of various software tools and databases available for handling of lipidomics datasets. Figure adapted from Tsugawa et al.<sup>71</sup>

signal conversion may refer more to the transformation of the detector output of continuous data (e.g. chromatogram or electropherogram of retention/migration time against ion counts against *m/z*) to a smaller dataset that consists of discrete molecular features that are defined by information such as accurate mass, retention/migration time and/or fragmentation patterns (MS/MS) where responses are determined by their integrated peak area that is often normalized to an internal standard. Data filtering then typically occurs afterwards where signals that can correspond to random or instrumental noise are removed from the data. parameters that are defined by the user as being an “authentic peak” (*i.e.*, Gaussian).<sup>47</sup> An

alternative method to eliminate spurious signals in electrophoretic separations is using dilution trend filtering based on a pooled quality control sample. In this context, multisegment injection (MSI)-CE-MS is extorted by performing a series of injections of a QC sample which include a set of triplicate injections, a blank and three injections that serially dilute. An authentic yet reliably measurable metabolite is one decided based on acceptable precision ( $CV < 30\%$ ,  $n = 3$ ), no signal in the blank and adequate linearity upon serial dilution ( $R^2 > 0.90$ ).<sup>48-50</sup> Other techniques involve time-aligning the filtered data sets. One filtration method removes chromatographic peaks that do not match the shape to account for instrumental drift that can occur in separations when coupled to MS. This ensures that features are consistently identified across multiple samples, with various algorithms available (*e.g.*, mapping of time axes from raw chromatograms [TICs], clustering of detected features to correct for drift, time-warping) from either a proprietary vendor, such as Agilent MassHunter or Waters MassLynx, or open-source software, such as XCMS,<sup>47,51</sup> MZmine,<sup>52</sup> or metAlign.<sup>53</sup> Given that electrospray ionization (ESI) is commonly used as an ionization technique in metabolomic and lipidomic studies, multiple adducts are prone to form from a single compound (*e.g.*,  $[M+H]^+$  and  $[M+Na]^+$ ), and/or multiple charge states ( $[M+H_2]^{2+}$ ). Thus, these adducts, as well as dimers, isotopes should be removed to eliminate data redundancy and narrow focus in subsequent statistical analyses. This ability is provided for lipidomics through LipidFinder<sup>54</sup> and LOBSTAHS<sup>55</sup>, having access to locally customizable databases as well as on-line structural databases such as LIPID MAPS,<sup>10</sup> LipidHome,<sup>56</sup> and HMDB.<sup>57</sup> Even for more specific lipid classes exist bioinformatics tools such as for annotation of phospholipid species with matching MS/MS

data using Greazy/LipidLama.<sup>58</sup> Nevertheless, several other MS/MS libraries exist for use such as MoNA or MassBank<sup>59</sup> to compare against a reference compound or against an *in silico* MS/MS spectral library such as LipidBlast. Despite the existence of automated software for peak detection and filtering to tackle these tasks, care must be taken to manually inspect the data to determine the presence of redundancies that can contribute to bias and/or overfitting. This is especially the case as these tools are still limited in their ability to distinguish and trace adducts, solvent background, in-source fragment ions as well as other artifact signals.<sup>60</sup>

### **1.8. Thesis Motivations & Objectives: Strategies for Accelerated Screening of Lipid Based Biomarkers Using MSI-NACE-MS**

For applications in clinical context and public health, screening relies on rapid, yet reliable measurements of one or more biomarkers that are associated with disease risk. Researchers must be consistent, thorough, and provide sufficient tools at the most critical stages of discovery to ensure that the community is equipped to take full advantage in harnessing the power of metabolomics and lipidomics for advancing precision medicine and population health. Whilst the lipidomics community makes strides towards standardization of protocols and approaches,<sup>61,62</sup> many technical issues continue to exist that are further exacerbated in large-scale and/or nontargeted applications that can deter the community wide goal for integrating lipidomics with the other-omics fields. Thus, the work in this thesis aims to tackle these issues by expanding and demonstrating the capabilities of multisegment-injection-nonaqueous capillary electrophoresis-mass spectrometry (MSI-NACE-MS), an underutilized separation platform that can expansively profile several polar

lipid classes in a cost-effective, high-throughput manner while providing extensive strategies for accelerating biomarker discovery.

### **1.8.1 Establishing a Structured Nontargeted Data Workflow for MSI-NACE-MS**

Despite the successful introduction of MSI-NACE-MS for profiling of free and total fatty acids<sup>35</sup>, several other lipid classes exist that have yet to be explored by the platform. While new methods are needed for global lipid profiling due to their complex chemical structures and diverse physicochemical properties, it can be difficult to effectively identify and annotate unambiguously without exploring other orthogonal technologies. Thus, *Chapter II* presents a robust data workflow for this case, in unambiguously selecting lipid features from serum ether extracts using MSI-NACE-MS. This discusses an iterative three-stage screening strategy that is developed for nontargeted analyses when using multiplexed electrophoretic separations that are coupled to an Orbitrap mass analyzer under negative ion acquisition mode. This approach enabled credentialing of 270 serum lipid features based on their accurate mass and relative migration time, with 128 ionic lipids reliably measured in most serum samples from a cohort of Japanese non-alcoholic steatohepatitis (NASH) patients. Notably, we discuss the use of an expansive mobility map to classify charged lipid classes over a wide polarity range with selectivity complementary to chromatographic separations, including lysophosphatidic acids, phosphatidylcholines, phosphatidylinositols, phosphatidylethanolamines and non-esterified fatty acids (NEFAs). This approach was used to stratify high and low-risk NASH patients using their serum lipidome profiles where elevated circulating NEFAs were associated with increased glucose intolerance, more severe liver fibrosis and greater disease burden.

### **1.8.2. Expanding Coverage of MSI-NACE-MS Using a Convenient Derivatization Strategy for Zwitterionic Lipid Species**

After successful introduction of MSI-NACE-MS for profiling in negative ion mode, this piqued interest in its capabilities to profile other lipid species. The previous chapter discussed the ability to detect phosphatidylcholines in negative ion mode as an acetate adduct. However, the basic buffer conditions and strong EOF do not allow for sufficient separation of PC species, resulting in substantial overlap with each other as well as with other neutral species where they are subject to increased ion suppression effects. Thus, positive ion mode using acidic BGE conditions should provide a better platform for analysis of these lipids as well as many other zwitterionic/cationic lipid species. A derivatization approach is required to fix a permanent positive charge on phosphatidylcholine species by neutralizing the phosphoric acid residue. However, current approaches make use of dangerous reagents that are not amenable to be applied for larger scale studies. In *Chapter III*, a new derivatization scheme is discussed to approach these issues to enable analysis in MSI-NACE-MS using positive ion mode acquisition. An underutilized reagent, 3-methyl-1-p-tolyl triazene is rigorously validated to achieve quantitative yields in methylating PC species. Additionally, we introduce FMOC in this derivatization scheme to cap phosphatidylethanolamines, to prevent their reaction and conversion into PCs through methylation. Furthermore, the apparent mobility of various classes of lipids was examined to facilitate identification and is complementary to high resolution MS/MS. The lipidome performance of MSI-NACE-MS is compared to various other methodologies using a standard reference material (NIST SRM-1950) that was subject to an international round-



robin trial.<sup>61</sup> Overall, this work strives to expand the conventional aqueous-based CE-MS analyses to encompass a wide range of ionic lipids from volume-restricted biospecimens with improved sample throughput, robustness and data fidelity, especially when applied to larger scale studies.

### **1.8.3. Screening for Circulating *n*-3 Phospholipids as Surrogate Markers for Routine Screening of Omega-3 Status**

Currently, many nutritional studies rely on various biological specimens for FA determination, yet it is still unclear how levels of serum NEFAs correlate with other circulating lipid pools. The accurate assessment of dietary fat intake remains a methodological challenge, reflecting decades of conflicting evidence regarding the benefits of a low-fat diet for public health.<sup>63</sup> Typically, semi-quantitative food-frequency questionnaires (FFQs) are used as tools for dietary assessment in large-scale observational studies as they reliably differentiate habitual dietary patterns and estimate micro- and macronutrient intake in a cost-effective manner. Despite this, FFQs are prone to recall bias, errors in estimation of true proportion sizes and selective reporting.<sup>64</sup> Furthermore, this does not take into account the large variation of FA species in diet. Recent findings from the PURE study report that total fat is correlated with lower total mortality and increased saturated fat or total dairy consumption with a lower risk of cardiovascular events.<sup>65</sup> Nevertheless, many of these studies heavily rely on intake estimates of FAs from FFQs. Furthermore, various biospecimens reflect different time intervals associated with dietary fat intake. Additionally, it has been reported that the regulation of EPA alone is not easy to monitor (likely due to faster metabolism) or faster incorporation in erythrocytes, which

results in the appearance of nonadherence.<sup>66</sup> The omega-3 index (O3I) presents as a metric useful for this and already has history of being associated with various cardiovascular events.<sup>67,68</sup> However, this involves fatty acid measurement from red blood cell erythrocytes that are prone to hemolysis during processing and long-term storage, as well as not being available in most biobank repositories, unlike serum and plasma.<sup>69</sup> Thus, surrogate markers for O3I may provide a solution in rapid screening to objectively monitor dietary fat intake. In *Chapter IV*, we investigate this phenomenon by applying signal pattern recognition strategies discussed in *Chapter II* as well as the validated method described in *Chapter III* to profile phospholipids in two different cohorts through a collaborative study with Dr. Stuart Philips (McMaster University) and Dr. David Mutch (University of Guelph). A high-dose oral omega-3 FA supplementation regime was provided to both cohorts. However, in one female comprising cohort, a mixed dosage of EPA/DHA from a fish oil supplement was provided to the treatment group. This study was used to quickly screen for serum phospholipids in an untargeted fashion that underwent a treatment response relative to placebo and blank extract that could be serve as circulating biomarkers for O3I. These results were then subsequently validated in an independent cohort comprising a larger age and sex-balanced number of participants in a randomized placebo-controlled study comprising either DHA, EPA, or olive oil (control) supplementation over a 12-week period. An accelerated workflow for lipidomics using MSI-NACE-MS uncovered a panel of omega-3 containing phosphatidylcholines (PC 36:5 and PC 38:6) that demonstrated a strong correlation to O3I derived from erythrocyte membranes ( $r = 0.764$ ,  $p = 3.0E-33$ ). Overall, serum biomarkers of omega-3 status enable for a more convenient, yet rapid

screening approach for dietary fat intake in large-scale nutritional epidemiological studies, as well as risk assessment of cardiac events and sudden cardiac death in high-risk patients.

## 1.9. References

- (1) Han, X.; Gross, R. W. *J Lipid Res* 2003, *44* (6), 1071–1079.
- (2) Spener, F.; Lagarde, M.; G elo en, A.; Record, M. *Eur J Lipid Sci Tech* 2003, *105* (9), 481–482.
- (3) Lee, H.-C.; Yokomizo, T. *Biochem Bioph Res Co* 2018, *504* (3), 576–581.
- (4) Yang, K.; Han, X. *Trends Biochem Sci* 2016, *41* (11), 954–969.
- (5) Gross, R. W. *Biochimica Et Biophysica Acta Bba - Mol Cell Biology Lipids* 2017, *1862* (8), 731–739.
- (6) James, A. T.; Martin, A. J. P. *Biochem J* 1952, *50* (5), 679–690.
- (7) Abel, K.; deSchmertzing, H.; Peterson, J. I. *J Bacteriol* 1963, *85* (5), 1039–1044.
- (8) Fenn, J. B.; Mann, M.; Meng, C. K.; Wong, S. F.; Whitehouse, C. M. *Science* 1989, *246* (4926), 64–71.
- (9) Subramaniam, S.; Fahy, E.; Gupta, S.; Sud, M.; Byrnes, R. W.; Cotter, D.; Dinasarapu, A. R.; Maurya, M. R. *Chem Rev* 2011, *111* (10), 6452–6490.
- (10) Sud, M.; Fahy, E.; Cotter, D.; Brown, A.; Dennis, E. A.; Glass, C. K.; Merrill, A. H.; Murphy, R. C.; Raetz, C. R. H.; Russell, D. W.; et al. *Nucleic Acids Res* 2007, *35* (suppl\_1), D527–D532.
- (11) Plebani, M. *Clin Biochem Rev* 2012, *33* (3), 85–88.
- (12) Consortium, T. H. S. M. (HUSERMET); Dunn, W. B.; Broadhurst, D.; Begley, P.; Zelena, E.; Francis-McIntyre, S.; Anderson, N.; Brown, M.; Knowles, J. D.; Halsall, A.; et al. *Nat Protoc* 2011, *6* (7), 1060–1083.
- (13) Vinaixa, M.; Samino, S.; Saez, I.; Duran, J.; Guinovart, J. J.; Yanes, O. *Metabolites* 2012, *2* (4), 775–795.

- (14) Saoi, M.; Li, A.; McGlory, C.; Stokes, T.; Allmen, M. T. von; Phillips, S. M.; Britz-McKibbin, P. *Metabolites* 2019, 9 (7), 134.
- (15) Wild, J.; Shanmuganathan, M.; Hayashi, M.; Potter, M.; Britz-McKibbin, P. *Analyst* 2019, 144 (22), 6595–6608.
- (16) Bligh, E. G.; Dyer, W. J. *Can J Biochem Phys* 1959, 37 (8), 911–917.
- (17) Saini, R. K.; Prasad, P.; Shang, X.; Keum, Y.-S. *Int J Mol Sci* 2021, 22 (24), 13643.
- (18) Matyash, V.; Liebisch, G.; Kurzchalia, T. V.; Shevchenko, A.; Schwudke, D. *J Lipid Res* 2008, 49 (5), 1137–1146.
- (19) Dunn, W. B.; Ellis, David. I. *Trac Trends Anal Chem* 2005, 24 (4), 285–294.
- (20) Psychogios, N.; Hau, D. D.; Peng, J.; Guo, A. C.; Mandal, R.; Bouatra, S.; Sinelnikov, I.; Krishnamurthy, R.; Eisner, R.; Gautam, B.; et al. *Plos One* 2011, 6 (2), e16957.
- (21) Dunn, W. B.; Broadhurst, D. I.; Atherton, H. J.; Goodacre, R.; Griffin, J. L. *Chem Soc Rev* 2010, 40 (1), 387–426.
- (22) Cajka, T.; Fiehn, O. *Anal Chem* 2016, 88 (1), 524–545.
- (23) Wishart, D. S. *Nat Rev Drug Discov* 2016, 15 (7), 473–484.
- (24) Han, X.; Gross, R. W. *Mass Spectrom Rev* 2005, 24 (3), 367–412.
- (25) Ekroos, K.; Chernushevich, I. V.; Simons, K.; Shevchenko, A. *Anal Chem* 2002, 74 (5), 941–949.
- (26) Claes, B. S. R.; Bowman, A. P.; Poad, B. L. J.; Young, R. S. E.; Heeren, R. M. A.; Blanksby, S. J.; Ellis, S. R. *Anal Chem* 2021, 93 (28), 9826–9834.
- (27) Rustam, Y. H.; Reid, G. E. *Anal Chem* 2017, 90 (1), 374–397.
- (28) Chew, W. S.; Torta, F.; Ji, S.; Choi, H.; Begum, H.; Sim, X.; Khoo, C. M.; Khoo, E. Y. H.; Ong, W.-Y.; Dam, R. M. V.; et al. *Jci Insight* 2019, 4 (13).
- (29) Huynh, K.; Barlow, C. K.; Jayawardana, K. S.; Weir, J. M.; Mellett, N. A.; Cinel, M.; Magliano, D. J.; Shaw, J. E.; Drew, B. G.; Meikle, P. J. *Cell Chem Biol* 2019, 26 (1), 71-84.e4.

- (30) Leaptrot, K. L.; May, J. C.; Dodds, J. N.; McLean, J. A. *Nat Commun* 2019, 10 (1), 985.
- (31) Li, A.; Hines, K. M.; Xu, L. *Methods Mol Biology* 2019, 2084, 119–132.
- (32) Gao, F.; Zhang, Z.; Fu, X.; Li, W.; Wang, T.; Liu, H. *Electrophoresis* 2007, 28 (9), 1418–1425.
- (33) Sándor, V.; Berkics, B. V.; Kilár, A.; Kocsis, B.; Kilár, F.; Dörnyei, Á. *Electrophoresis* 2020, 41 (13–14), 1178–1188.
- (34) Yamamoto, M.; Ly, R.; Gill, B.; Zhu, Y.; Moran-Mirabal, J.; Britz-McKibbin, P. *Anal Chem* 2016, 88 (21), 10710–10719.
- (35) Azab, S.; Ly, R.; Britz-McKibbin, P. *Anal Chem* 2019, 91 (3), 2329–2336.
- (36) Saoi, M.; Kennedy, K. M.; Gohir, W.; Sloboda, D. M.; Britz-McKibbin, P. *Sci Rep-uk* 2020, 10 (1), 9399.
- (37) Azab, S. M.; Zamzam, A.; Syed, M. H.; Abdin, R.; Qadura, M.; Britz-McKibbin, P. *J Clin Medicine* 2020, 9 (6), 1877.
- (38) Azab, S. M.; Souza, R. J. de; Teo, K. K.; investigators), (for the FAMILY; Anand, S. S.; Williams, N. C.; Holzschuher, J.; McGlory, C.; Philips, S. M.; Britz-McKibbin, P. *J Lipid Res* 2020, 61 (6), 933–944.
- (39) Liebisch, G.; Vizcaíno, J. A.; Köfeler, H.; Trötz Müller, M.; Griffiths, W. J.; Schmitz, G.; Spener, F.; Wakelam, M. J. O. *J Lipid Res* 2013, 54 (6), 1523–1530.
- (40) Imamura, F.; Sharp, S. J.; Koulman, A.; Schulze, M. B.; Kröger, J.; Griffin, J. L.; Huerta, J. M.; Guevara, M.; Sluijs, I.; Agudo, A.; et al. *Plos Med* 2017, 14 (10), e1002409.
- (41) Forouhi, N. G.; Wareham, N. J. *Curr Nutrition Reports* 2014, 3 (4), 355–363.
- (42) Canez, C. R.; Shields, S. W. J.; Bugno, M.; Wasslen, K. V.; Weinert, H. P.; Willmore, W. G.; Manthorpe, J. M.; Smith, J. C. *Anal Chem* 2016, 88 (14), 6996–7004.
- (43) Betancourt, S. K.; Canez, C. R.; Shields, S. W. J.; Manthorpe, J. M.; Smith, J. C.; McLuckey, S. A. *Anal Chem* 2017, 89 (17), 9452–9458.
- (44) Wasslen, K. V.; Canez, C. R.; Lee, H.; Manthorpe, J. M.; Smith, J. C. *Anal Chem* 2014, 86 (19), 9523–9532.

- (45) Wasslen, K. V.; Tan, L. H.; Manthorpe, J. M.; Smith, J. C. *Anal Chem* 2014, 86 (7), 3291–3299.
- (46) Phaner, C. J.; Liu, S.; Ji, H.; Simpson, R. J.; Reid, G. E. *Anal Chem* 2012, 84 (21), 8917–8926.
- (47) Smith, C. A.; Want, E. J.; O’Maille, G.; Abagyan, R.; Siuzdak, G. *Anal Chem* 2006, 78 (3), 779–787.
- (48) Ly, R.; Ly, N.; Sasaki, K.; Suzuki, M.; Kami, K.; Ohashi, Y.; Britz-McKibbin, P. *J Proteome Res* 2022, 21 (3), 768–777.
- (49) Kuehnbaum, N. L.; Kormendi, A.; Britz-McKibbin, P. *Anal Chem* 2013, 85 (22), 10664–10669.
- (50) DiBattista, A.; McIntosh, N.; Lamoureux, M.; Al-Dirbashi, O. Y.; Chakraborty, P.; Britz-McKibbin, P. *Anal Chem* 2017, 89 (15), 8112–8121.
- (51) Tautenhahn, R.; Patti, G. J.; Rinehart, D.; Siuzdak, G. *Anal Chem* 2012, 84 (11), 5035–5039.
- (52) Pluskal, T.; Castillo, S.; Villar-Briones, A.; Orešič, M. *Bmc Bioinformatics* 2010, 11 (1), 395.
- (53) Lommen, A. *Anal Chem* 2009, 81 (8), 3079–3086.
- (54) O’Connor, A.; Brasher, C. J.; Slatter, D. A.; Meckelmann, S. W.; Hawksworth, J. I.; Allen, S. M.; O’Donnell, V. B. *Jci Insight* 2017, 2 (7), e91634.
- (55) Collins, J. R.; Edwards, B. R.; Fredricks, H. F.; Mooy, B. A. S. V. *Anal Chem* 2016, 88 (14), 7154–7162.
- (56) Foster, J. M.; Moreno, P.; Fabregat, A.; Hermjakob, H.; Steinbeck, C.; Apweiler, R.; Wakelam, M. J. O.; Vizcaíno, J. A. *Plos One* 2013, 8 (5), e61951.
- (57) Wishart, D. S.; Tzur, D.; Knox, C.; Eisner, R.; Guo, A. C.; Young, N.; Cheng, D.; Jewell, K.; Arndt, D.; Sawhney, S.; et al. *Nucleic Acids Res* 2007, 35 (suppl\_1), D521–D526.
- (58) Kochen, M. A.; Chambers, M. C.; Holman, J. D.; Nesvizhskii, A. I.; Weintraub, S. T.; Belisle, J. T.; Islam, M. N.; Griss, J.; Tabb, D. L. *Anal Chem* 2016, 88 (11), 5733–5741.

- (59) Horai, H.; Arita, M.; Kanaya, S.; Nihei, Y.; Ikeda, T.; Suwa, K.; Ojima, Y.; Tanaka, K.; Tanaka, S.; Aoshima, K.; et al. *J Mass Spectrom* 2010, 45 (7), 703–714.
- (60) Tsugawa, H.; Ikeda, K.; Arita, M. *Biochimica Et Biophysica Acta Bba - Mol Cell Biology Lipids* 2017, 1862 (8), 762–765.
- (61) Bowden, J. A.; Heckert, A.; Ulmer, C. Z.; Jones, C. M.; Koelmel, J. P.; Abdullah, L.; Ahonen, L.; Alnouti, Y.; Armando, A. M.; Asara, J. M.; et al. *J Lipid Res* 2017, 58 (12), 2275–2288.
- (62) McDonald, J. G.; Ejsing, C. S.; Kopeczynski, D.; Holčapek, M.; Aoki, J.; Arita, M.; Arita, M.; Baker, E. S.; Bertrand-Michel, J.; Bowden, J. A.; et al. *Nat Metabolism* 2022, 1–3.
- (63) Committee, A. H. A. N.; Lichtenstein, A. H.; Appel, L. J.; Brands, M.; Carnethon, M.; Daniels, S.; Franch, H. A.; Franklin, B.; Kris-Etherton, P.; Harris, W. S.; et al. *Circulation* 2006, 114 (1), 82–96.
- (64) Andersen, L. F.; Solvoll, K.; Johansson, L. R. K.; Salminen, I.; Aro, A.; Drevon, C. A. *Am J Epidemiol* 1999, 150 (1), 75–87.
- (65) Poli, A. *Eur Heart J Suppl* 2020, 22 (Supplement\_E), E113–E115.
- (66) Brenna, J. T.; Plourde, M.; Stark, K. D.; Jones, P. J.; Lin, Y.-H. *Am J Clin Nutrition* 2018, 108 (2), 211–227.
- (67) Harris, W. S. *Am J Clin Nutrition* 2008, 87 (6), 1997S-2002S.
- (68) Harris, W. S.; Schacky, C. von. *Prev Med* 2004, 39 (1), 212–220.
- (69) Stark, K. *Lipid Technology* 2008, 20 (8), 177–179.
- (70) Khalil, M. B.; Hou, W.; Zhou, H.; Elisma, F.; Swayne, L. A.; Blanchard, A. P.; Yao, Z.; Bennett, S. A. L.; Figeys, D. *Mass Spectrom Rev* 2010, 29 (6), 877–929.
- (71) Tsugawa, H.; Ikeda, K.; Takahashi, M.; Satoh, A.; Mori, Y.; Uchino, H.; Okahashi, N.; Yamada, Y.; Tada, I.; Bonini, P.; et al. *Nat Biotechnol* 2020, 38 (10), 1159–1163.

## Chapter II

### **Nontargeted Serum Lipid Profiling by Multisegment Injection-Nonaqueous Capillary Electrophoresis-Mass Spectrometry: A Multiplexed Separation Platform for Resolving Ionic Lipids**

*Ritchie Ly,<sup>1</sup> Nicholas Ly,<sup>1</sup> Kazunori Sasaki,<sup>2</sup> Makoto Suzuki,<sup>2</sup> Kenjiro Kami,<sup>2</sup> Yoshiaki Ohashi,<sup>2</sup> Philip Britz-McKibbin<sup>1</sup>*

*<sup>1</sup>Department of Chemistry and Chemical Biology, McMaster University, Hamilton, Canada L8S 4M1*

*<sup>2</sup>Human Metabolome Technologies Inc., Tsuruoka, Yamagata, 997-0052, Japan*

R.L performed all the experiments including sample preparation, data acquisition using MSI-NACE-MS, data processing, interpretation, statistical analysis and wrote the initial draft for publication. N.L assisted in data processing and interpretation. K.S. conducted MS/MS experiments. K.S. M.S. K.K. and Y.O. provided feedback on the manuscript. P.B.M wrote and provided feedback on the manuscript draft.



## 2.1. Abstract

New methods are needed for global lipid profiling due to their complex chemical structures and diverse physicochemical properties. Current mass spectrometry-based lipidomic protocols are also hampered by complicated data pre-processing, low sample throughput, and/or inadequate resolution that may contribute to false discoveries. Herein, we introduce a robust data workflow to unambiguously select lipid features from serum ether extracts by multisegment injection-nonaqueous capillary electrophoresis-mass spectrometry (MSI-NACE-MS). An iterative three-stage screening strategy is developed for nontargeted lipid analyses to rigorously filter spurious signals and dataset redundancy when using multiplexed electrophoretic separations coupled to an Orbitrap mass analyzer with full-scan data acquisition under negative ion mode. This approach allows for the credentialing of 270 serum lipid features annotated based on their accurate mass and relative migration time, including 128 ionic lipids reliably measured (median CV ~ 13%) in most serum samples (> 75%) from a cohort of non-alcoholic steatohepatitis (NASH) patients ( $n=85$ ). A mobility map is introduced to classify charged lipid classes/sub-classes over a wide polarity range with selectivity complementary to chromatographic separations, including lysophosphatidic acids, phosphatidylcholines, phosphatidylinositols, phosphatidylethanolamines, and non-esterified fatty acids (NEFAs). Serum lipidome profiles were also used to differentiate high-risk from low-risk NASH patients following a  $k$ -means clustering algorithm, where elevated circulating NEFAs (*e.g.*, palmitic acid) were associated with increased glucose intolerance, more severe liver fibrosis, and greater disease burden/co-morbidity. MSI-NACE-MS greatly expands the metabolome coverage

of conventional aqueous-based CE-MS protocols that is optimal for large-scale lipidomic studies requiring higher sample throughput, lower operating costs, and greater data fidelity while also supporting lipid identification in conjunction with MS/MS.

## 2.2. Introduction

Lipids play vital roles in biological processes to maintain homeostasis while regulating normal growth and development ranging from energy storage, cellular structure, and chemical signalling. Perturbations in lipid metabolism (*i.e.*, dyslipidemia) are implicated in the etiology of chronic diseases, including cardiorespiratory diseases<sup>70</sup> neurodegenerative disorders<sup>71</sup> and an alarming rise in nonalcoholic fatty liver disease (NAFLD) prevalence worldwide.<sup>72</sup> For these reasons, there is growing interest in developing new analytical methods in lipidomics for biomarker discovery beyond standard lipid blood panels in clinical medicine, which may provide new insights into disease mechanisms. However, the diverse structural properties of lipids prevents their comprehensive analysis since a major fraction of the human lipidome comprise unknown compounds lacking chemical standards and/or reference MS/MS spectra.<sup>72</sup> Although shotgun lipidomics using direct infusion-MS (DI-MS) enables rapid profiling of lipid extracts, it is prone to isobaric and isomeric interferences, as well as ion suppression effects and artifact signal generation when performing nontargeted analyses.<sup>73</sup> As a result, chromatographic separations based on reversed-phase, normal-phase and/or hydrophilic interaction (HILIC) in LC-MS are needed to improve the resolution, quantification and identification of lipids and their isomers, including over 100,000 curated and

computationally derived lipid structures in the LIPID MAPS database.<sup>10</sup> Ion mobility spectrometry (IMS), supercritical chromatography and multidimensional separations have also been explored as alternative separation techniques to further enhance separation speed, selectivity, and/or peak capacity in MS-based lipidomic studies.<sup>74,75</sup> Nevertheless, various lipidomic methodologies are used across different laboratories that require better harmonization to assess performance based on evolving consensus guidelines.<sup>74,75</sup>

Nonaqueous capillary electrophoresis-mass spectrometry (NACE-MS) remains largely an unrecognized separation technique in lipidomics despite its high separation efficiency, fast analysis times and unique selectivity for resolving complex mixtures of water-insoluble peptides, drugs, and natural products.<sup>76,77</sup> Yet, there have been few lipidomic studies reported using NACE-MS, which have been limited to the targeted analysis of ionic lipids, such as glycerophospholipids,<sup>32,78</sup> saturated fatty acids<sup>79</sup> and lipid A isomers<sup>16</sup> in small pilot studies. This trend likely reflects a lack of robust NACE-MS protocols applicable for high throughput lipid profiling<sup>80</sup> due to deleterious acetonitrile-induced polyimide coating swelling and siphoning effects when using low viscosity organic solvents in the background electrolyte (BGE).<sup>80</sup> These processes contribute to frequent capillary fractures and current drops,<sup>80</sup> as well as corona discharge under negative ion mode conditions.<sup>81</sup>

Recently, we have overcome these technical barriers when optimizing multisegment injection-nonaqueous capillary electrophoresis-mass spectrometry (MSI-NACE-MS) for the determination of fatty acids with good mutual agreement as compared to GC-MS.<sup>35</sup> To date, MSI-NACE-MS offers a multiplexed separation platform for the

rapid analysis of total hydrolyzed or non-esterified FAs (NEFAs) in serum and tissue extracts,<sup>35</sup> however its feasibility for nontargeted screening a much broader range of complex lipids in blood specimens has yet to be explored. For the first time, we introduce a standardized MSI-NACE-MS data workflow for lipidomics that enables the classification of various classes of polar/ionic lipids from serum extracts. This method was also used to differentiate a heterogenous cohort of nonalcoholic steatohepatitis (NASH) patients based on differences in their serum lipid profiles as required for improved risk assessment of NAFLD progression.<sup>35</sup>

## **2.3. Experimental**

### **2.3.1. Chemicals and Reagents.**

Ultra LC-MS grade methanol, acetonitrile, water and 2-propanol were used to prepare sheath liquid and background electrolyte (BGE). Ammonium acetate, ammonium hydroxide, myristic acid-d27 (14:0-d27), stearic acid-d3 (18:0-d3) and all other chemical standards were purchased from Sigma-Aldrich Inc. (Tokyo, Japan). All stock solutions were prepared in methanol or BGE and stored at 4°C, unless otherwise stated.

### **2.3.2. Lipid Serum Extract Preparation.**

The sample workup procedure for lipid extraction from serum samples using methyl-*tert*-butyl ether (MTBE) is based on a validated protocol previously reported for NEFA determination when using MSI-NACE-MS.<sup>17,18</sup> Extractions were carried out in glass GC vials that were pre-rinsed with dichloromethane and all pipette tips used during this procedure were pre-rinsed with methanol. First, 100 µL of 0.01% *vol* butylated hydroxytoluene (BHT) in methanol was mixed with a 50 µL aliquot of serum. Next, 250

$\mu\text{L}$  of 50  $\mu\text{M}$  14:0-d27 (recovery standard) in MTBE and 12.5  $\mu\text{L}$  of 1.0 M HCl were added to the mixture followed by vigorous shaking for 30 min at room temperature. Phase separation was then induced by addition of 100  $\mu\text{L}$  of deionized water, and samples were then centrifuged at 3000  $g$  at +4  $^{\circ}\text{C}$  for 30 min to sediment protein at bottom of vial followed by a biphasic water and ether (top) layer. A fixed volume (200  $\mu\text{L}$ ) was collected from the upper MTBE layer into a new vial then dried under a gentle stream of nitrogen gas at room temperature. Serum extracts from NASH patients were then stored dry at -80  $^{\circ}\text{C}$  prior to analysis when they were reconstituted in 25  $\mu\text{L}$  of acetonitrile/isopropanol/water (70:20:10) with 10 mM ammonium acetate and 50  $\mu\text{M}$  18:0-d3 as internal standard. Further details on the recruitment of NASH patients, blood collection/storage protocols, as well as standard clinical blood tests and histopathology used for staging of liver fibrosis severity (F score) and NASH activity score (NAS)<sup>35</sup> are described in the **Supplemental Experimental**.

### 2.3.3. CE-MS Instrumentation and Serial Injection Configuration

Separation using capillary electrophoresis (CE) was carried out using an Agilent 7100 series (Agilent Technologies Inc., Santa Clara, CA) that was coupled to a Q-Exactive Plus Orbitrap-MS (ThermoFisher Scientific Inc., Waltham, MA, USA) using a customized coaxial sheath liquid interface as described by Sasaki *et al.*<sup>35</sup> CE separations were performed with 30 kV of applied voltage at 25  $^{\circ}\text{C}$  using uncoated fused-silica capillaries (Polymicro Technologies Inc., AZ, USA) with 50  $\mu\text{m}$  ID and a total length of 95 cm. A background electrolyte (BGE) consisting of 35 mM ammonium acetate in 70% *vol* acetonitrile, 15% *vol* methanol, 10% *vol* H<sub>2</sub>O, and 5% *vol* 2-propanol at an apparent pH 9.5

that was adjusted by addition of 30% *vol* ammonium hydroxide was used for the separation of complex lipids and NEFAs from serum extracts. The capillary was flushed with BGE at 950 mbar for 5 min between each run. Multiplexed electrophoretic separations were performed based on a serial hydrodynamic injection at 50 mbar alternating between a 5 s injection of sample (or QC) and a 40 s injection of BGE for a total of seven discrete samples analyzed within a single run.<sup>35</sup> An Agilent 1260 isopump module with degasser was used to deliver a sheath liquid consisting of 80:20 methanol and deionized water with 0.5% *vol* ammonium hydroxide supplied at a rate of 10  $\mu\text{L}/\text{min}$ . For internal reference mass correction, hexakis(1H,1H,2H-difluoroethoxy)phosphazene (HDFEP) was spiked into the sheath liquid at 0.02% *vol* to provide a reference ion at  $m/z$  680.0355 as its acetate adduct. For analysis of all individual serum samples, the Orbitrap-MS was operated under full scan data acquisition in negative ion mode with 140,000 full-width-at-half-maximum (FWHM) resolution and a scan speed of 1.5 Hz. The source parameters used during analysis were set to 4 units for the auxiliary gas, sheath gas and dry gas flow rates, while the external modules for the customized coaxial sheath liquid interface<sup>25</sup> were set to operate at 3.5 and 3.0 kV for the primary and secondary electrodes respectively, and the temperature of the MS inlet capillary was set to 100 °C. The magnitude of the S-lens RF level was set to 90 while operating in negative ion mode. Agilent MassHunter B 08.00 and Thermo Fischer Scientific Xcalibur 3.1 were used for control of CE and Orbitrap MS instruments, respectively while using an Agilent 1200 Universal Interface Box for communication between vendor-specific workstation platforms. Full-scan data acquisition was performed from  $m/z$  90 to 1000 for nontargeted lipid profiling, whereas collision-induced dissociation

experiments were acquired at different collision energies (10, 20 and 40V) by MS/MS for structural elucidation of representative serum lipid sub-classes to support their classification in the mobility map. The Orbitrap-MS was mass calibrated daily and the CE inlet electrode was cleaned with 2-propanol/water (50:50) to prevent sample carryover. Evaporation of lipid serum extracts during MSI-NACE-MS was prevented using sealed sample vial containers together with data normalization of all integrated lipid signals and apparent migration times to an internal standard (18:0-d3). A neutral marker (BHT) was used for calculation of the apparent electrophoretic mobility of ionic lipids from the same injection position as described elsewhere.<sup>20</sup> Most ionic serum lipids were putatively identified based on their sum composition (level 3) with the exception serum NEFAs that were confirmed by spiking with commercial standards, and certain serum lipid sub-classes whose structure were characterized by MS/MS (level 2) following a 5 level annotation hierarchy for structurally defined molecular lipids.<sup>4</sup>

#### **2.3.4. Data Processing and Statistical Analysis.**

All serum lipid ion responses were normalized to a single deuterated recovery standard, 14:0-d27 using Thermo Fisher Xcalibur software and Microsoft Excel. For the nontargeted workflow in MSI-CE-MS, datafiles were converted to mzXML format using MSconvert (Proteowizard)<sup>27</sup> prior to importing into MZmine 2.<sup>28</sup> For spectra generation, settings were set to molecular features by exact mass with a minimum signal intensity of 300 counts. Generation of extracted ion electropherograms were conducted using a minimum signal intensity of 300 counts, a minimum time span of 0.01 min and a  $m/z$  tolerance of 5 ppm. Adduct filtering was applied using MZmine's built-in molecular feature

module with a migration time tolerance of 1.0 %,  $m/z$  tolerance of 10 ppm and a maximum relative adduct peak height of 50%. CAMERA<sup>29</sup> was also used dataset redundancy from isotope and multiple charge states with the following settings: a FWHM sigma at 0.20, FWHM percentage at 1.0%, and isotopes maximum charge and max charge per cluster set to 3 and 4 respectively. The correlation threshold was set to 0.70 and correlation  $p$ -value was set to 0.05 under negative ion mode conditions. The package was set to perform shape correlation before isotope search as well prior to database search for serum lipid annotation using LIPID MAPS.<sup>30</sup> Prior to any multivariate and univariate statistical analysis, normality testing was performed on SPSS (IBM SPSS Statistics for Windows, Version 20.0. Armonk, NY, USA) using a Shapiro-Wilk's test for normality ( $p < 0.05$ ). Complementary multivariate statistical analysis methods were performed using MetaboAnalyst 5.0,<sup>31</sup> including principal component analysis (PCA), partial least squares-discriminant analysis (PLS-DA), 2D heat map with hierarchal clustering analysis (HCA), as well as a  $k$ -means clustering algorithm using generalized  $\log$ -transformed and autoscaled data. The  $k$ -means cluster analysis for differentiation of NASH patient sub-groups was determined as optimal when  $k = 2$  based on their lipid serum profiles, since  $k > 2$  had greater inter-cluster deviation in the median lines between groups. Univariate statistical tests were performed on all patient clinical data on SPSS while an analysis of covariance (ANCOVA) was applied where  $p$ -values were adjusted for sex, age, BMI and NASH patient co-morbidities (*i.e.*, diabetes, hypertension, hyperlipidemia) as covariates. A Bonferroni correction was used to correct for multiple hypothesis testing when rank ordering serum lipids associated with NASH patient sub-group differentiation.



## 2.4. Results and Discussion.

### 2.4.1 NASH Cohort and Serum Lipidomic Workflow in MSI-NACE-MS.

**Table 2.1** summarizes the clinical characteristics of a cohort of NASH patients ( $n=85$ ) who were overweight Japanese adults (mean age 51 years) having moderate stages of liver fibrosis as confirmed from histopathology examination with mean fibrosis (F score = 1-4) and NASH activity score (NAS = 1-8) of 2.6 and 6.0, respectively. As expected, NASH patients also had a high incidence of diabetes, hypertension and/or hyperlipidemia as co-morbidities reflecting underlying metabolic syndrome (**Supporting Table S1**). **Figure 2.1** illustrates a three-tiered strategy for global lipid profiling of human serum extracts by MSI-NACE-MS when using an alkaline nonaqueous BGE system<sup>20</sup> with full-scan data acquisition under negative ion mode. This iterative approach was developed to rigorously select, filter, and authenticate non-artifactual serum lipid signals consistently detected in NASH patients.<sup>24</sup> In this case, a pooled serum sample served as an internal reference or quality control (QC) that was used for nontargeted lipid screening and method precision monitoring. A dilution trend filter run<sup>26,32</sup> based on a serial introduction of 6 pooled serum ether extracts along with a blank extract was first applied for peak picking when using multiplexed separations in MSI-NACE-MS after rejecting spurious peaks, background ions, and dataset redundancy in MS-based lipidomics.<sup>52</sup> This process allows for credentialing<sup>34</sup> serum-derived lipid features by ultra-high resolution MS while minimizing false discoveries and data overfitting, which is distinct from data-dependent or independent MS/MS workflows in lipidomics.<sup>35</sup> Structural elucidation of unknown lipids by MS/MS is thus prioritized to authenticated features of clinical or biological significance

**Table 2.1.** Clinical characteristics and grading score of Japanese NASH patients from the full cohort and sub-group of patients identified after a k-mean clustering algorithm of their serum lipid profiles.

Clinical Parameter <sup>a</sup>	Full Cohort (n = 85)	Cluster A (n = 26)	Cluster B (n = 59)	p-value <sup>b</sup>	Mean FC <sup>c</sup>	Effect Size <sup>d</sup>
Age (years)	51 ± 14	46 ± 3	53 ± 2	-	-	-
Sex (M:F)	38:48	13:13	25:34	-	-	-
BMI (kg/m <sup>2</sup> )	27 ± 5	27.1 ± 0.8	26.8 ± 0.8	0.896	0.98	0.000222
Albumin (g/dL)	4.5 ± 0.4	4.4 ± 0.1	4.5 ± 0.1	0.341	1.02	0.0123
ALP (µmmol/min)	270 ± 100	242 ± 15	283 ± 15	0.565	1.17	0.00467
ALT (µmmol/min)	97 ± 68	91 ± 13	98 ± 9	0.508	1.08	0.00577
AST (µmmol/min)	59 ± 35	51 ± 6	61 ± 5	0.204	1.20	0.0211
HbA1c (%)	6.3 ± 1.3	5.7 ± 0.2	6.5 ± 0.2	<b>0.00492</b>	<b>1.14</b>	<b>0.102</b>
F score (1-4)	2.60 ± 0.70	2.22 ± 0.14	2.76 ± 0.09	0.0693*	1.25	0.0455
I score (1-4)	2.35 ± 0.50	2.28 ± 0.12	2.40 ± 0.06	0.579	1.05	0.00423
S score (1-4)	2.56 ± 0.60	2.63 ± 0.11	2.53 ± 0.08	0.572	0.96	0.00435
Ballooning (1-3)	1.36 ± 0.50	1.3 ± 0.1	1.4 ± 0.1	0.876	1.07	0.000348
NAS (1-8) <sup>e</sup>	6.0 ± 1.6	6.2 ± 1.3	6.3 ± 1.1	0.778	1.02	0.00114
PLT (× 10 <sup>9</sup> /L)	31 ± 46.7	22 ± 2	38 ± 8	0.265	1.72	0.0167
PT (%)	90 ± 16	90 ± 4	91 ± 2	0.914	1.01	0.000161
TBil (mg/dL)	0.86 ± 0.4	0.98 ± 0.10	0.81 ± 0.5	0.180	0.83	0.0256
TChol (mg/dL)	202 ± 36	202 ± 8	203 ± 6	0.162	1.00	0.00380
TG (mg/dL)	172 ± 88	150 ± 16	181 ± 12	0.603	1.21	0.00363
Diabetes <sup>f</sup>	44 (52%)	11 (42%)	33 (56%)	-	-	-
Hypertension <sup>f</sup>	44 (52%)	12 (46%)	41 (81%)	-	-	-
Hyperlipidemia <sup>f</sup>	62 (73%)	14 (54%)	48 (81%)	-	-	-

<sup>a</sup> Clinical data expressed as mean ± 1 SD. Abbreviations refer to ALP, alkaline phosphatase; ALT, alanine aminotransferase; AST, aspartate aminotransferase; F score, fibrosis score; I score, inflammation score; S score, steatosis score; NAS, non-alcoholic fatty liver disease score, PLT, platelet count; PT, prothrombin time; TBil, total bilirubin; TChol, total cholesterol; TG, triacylglycerides.

<sup>b</sup> p-values obtained using ANCOVA were adjusted for age, sex, BMI, diabetes, hypertension and hyperlipidemia as covariates with significance at  $p < 0.05$  (bold). \*  $p < 0.05$  if excluding hyperlipidemia or diabetes as a covariate adjustment.

<sup>c</sup> Average fold-changes (FC) based on ratio of clinical parameters in clusters of patients (B/A).

<sup>d</sup> Effect sizes calculated using partial ETA square where small effects > 0.01, medium effects > 0.06 and large effects > 0.14

<sup>e</sup> NAS determined with sum of steatosis, inflammation and ballooning score

<sup>f</sup> Patients with one condition (21/85), two conditions: hyperlipidemia and hypertension (11/85), diabetes and hyperlipidemia (12/85) or diabetes and hypertension (6/85), and with all three conditions (21/85).

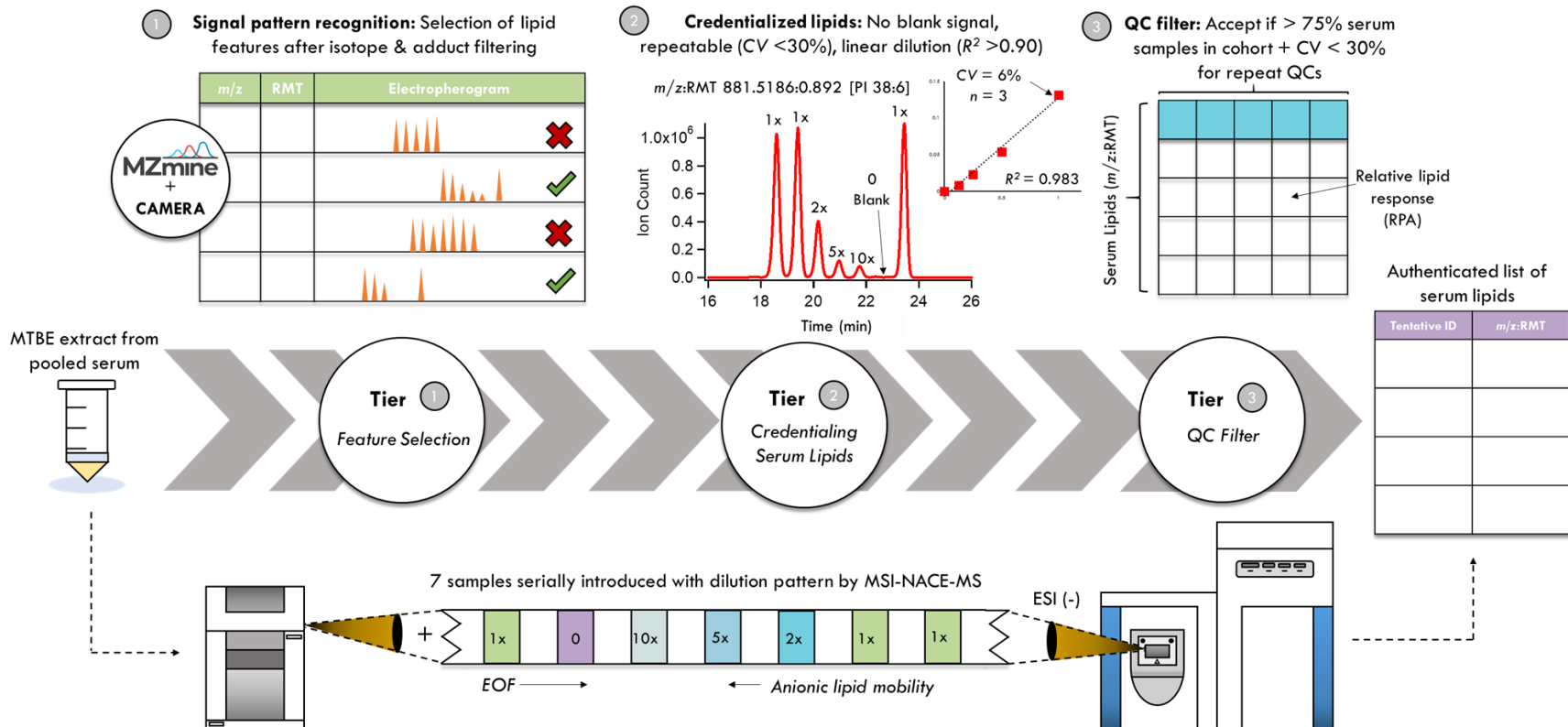


**Figure 2.1.** Lipidomics data workflow using a 3-tiered strategy when performing nontargeted lipid profiling from serum ether extracts by MSI-NACE-MS with a 7 sample plug serial injection format. These steps include molecular feature selection and filtering via signal pattern recognition, followed by lipid authentication based on repeatability, lack of blank signal and linear dilution. The third stage of lipid verification includes a frequency filter with quality control following analysis of all serum samples from NASH patients ( $n=85$ ).

after appropriate statistical analyses.<sup>23</sup>

A first-tier nontargeted screen using MZmine 2.0 with CAMERA as open-source software tools was used to filter isotopic and adduct ions following a visual review of extracted ion electropherograms (**Figure 2.1, step 1**). Over 83,000 total molecular features were initially detected in pooled serum extracts. However, only about 270 lipid features annotated by their accurate mass and relative migration time ( $m/z$ :RMT) were subsequently credentialized via temporal signal pattern recognition<sup>32</sup> in MSI-NACE-MS based on a distinctive 3, 4 or 5 signal pattern depending on ion abundance (*step 2*). This second-tier confirmatory screen formally integrates selected lipid features that are measured with adequate repeatability ( $CV < 30\%$ ,  $n=3$ ) and linearity ( $R^2 > 0.90$ ) upon serial dilution, yet have no blank signal contribution (*i.e.*, background ion) as shown for a representative serum phosphatidylinositol (**Figure 2.1**). A single stable-isotope internal standard (18:0-d3) was used for data normalization to improve the precision of lipid migration times (*i.e.*, RMTs) and their data integration (*i.e.*, relative peak area, RPA) due to differences in electroosmotic flow (EOF) between runs, and sample volumes introduced in-capillary when using serial hydrodynamic injections in CE, respectively.<sup>35</sup>

A third-tier screen (*step 3*) was next implemented following targeted analysis of a list of 270 known and unknown lipid features from all individual NASH serum samples ( $n=85$ ). Unlike gradient elution chromatographic programs in lipidomics, isocratic conditions are used in MSI-NACE-MS for the resolution and ionization of serum lipids under steady-state conditions from 7 different samples introduced on-capillary within a single run. In this case, each MSI-NACE-MS run was comprised of a QC sample together

with 6 serum extracts from individual NASH patients introduced in random sequence.<sup>24</sup> Serum lipids satisfying this final stage of screening corresponded to frequently detected features in most serum samples (> 75% of cohort) that were measured with adequate technical precision (CV for QC < 30%). Overall, 128 ionic lipids from serum extracts were reliably measured following this iterative data workflow after removing neutral lipids (*e.g.*, triacylglycerides) co-migrating with the EOF as they were prone to ion suppression and isobaric interferences, as well as low abundance ionic lipids with high data variance. Further evidence of acceptable reproducibility was demonstrated by a control chart for a recovery standard (14:0-d27) added to all serum/QC samples prior to MTBE extraction (mean CV = 9.5%,  $n=100$ ). Also, a 2D PCA scores plot comprising 128 ionic lipids were measured in repeat QC samples throughout this study (median CV = 13%,  $n=17$ ) as shown in **Supporting Figure S2.1**. All NASH patient serum extracts, QC samples, dilution trend filter, and calibrant checks/equilibration runs were analyzed within 8 h by MSI-NACE-MS with an effective throughput ~ 4.5 min/sample, which compares favorably to high throughput LC-MS lipidomic platforms (~ 15 min/sample).<sup>17</sup>

#### 2.4.2. Serum Lipidome Coverage and Lipid Classification in Mobility Maps.

**Figure 2.2A** depicts a total ion electropherogram in MSI-NACE-MS under negative ion mode, where most anionic lipids were detected as their intact deprotonated molecular ion,  $[M-H]^-$  except for cationic phosphatidylcholines as their acetate adduct,  $[M+CH_3COO]^-$ . Also, a reference mass (HDFEP) added to the sheath liquid and infused continuously into the ion source provides a convenient way to monitor for potential matrix-induced signal suppression as reflected by regions of reduced ion counts (*i.e.*, signal dips)

that occur primarily for neutral lipids co-migrating within the EOF. Overall, 6 major sub-classes of ionic lipids were resolved by MSI-NACE-MS as summarized in **Figure 2.2B**, namely glycerophospholipids (~ 34%, including phosphatidylcholine: PCs, phosphatidylinositols: PIs, phosphatidylethanolamines: PEs, and lysophosphatidic acids: LPAs), fatty acids (~ 30%), including a wide range of saturated (from 6:0 to 26:0) and mono-/polyunsaturated NEFAs, as well as other classes of anionic serum lipids (*e.g.*, bile acids, prostaglandins, fatty acyl derivatives) together with unknown lipids (~ 36%) with no likely candidate after a database search. Overall, serum-derived lipid features were tentatively identified by their accurate mass when using LIPID MAPS, and they were further deemed plausible based on their characteristic electrophoretic mobility and relative migration order. For instance, cationic and anionic classes of serum lipids migrate over a wide separation window ranging from lysophosphatidylcholines (*e.g.*, LPC 16:0) relative to slower migrating lysophosphatidic acid (*e.g.*, LPA 16:0) and medium-chain NEFAs (*e.g.*, 6:0) reflecting differences in their fundamental physicochemical properties (*i.e.*, charge density) in solution. A series of tables summarize the 128 ionic lipids measured consistently from NASH patients in this study, including their putative identification mainly based on their sum composition (level 3),  $m/z$ :RMT, mass error, mobility, relative abundance, and technical precision from repeat QC analyses (**Supporting Tables S2-S8**).

Similar to the use of collisional-cross section areas for classifying and predicting lipid structures based on their drift times in ion mobility spectrometry (IMS),<sup>30</sup> **Figure 2B** depicts an (electrophoretic) mobility map over a wide mass range (100-900  $m/z$ ) for a diverse array of ionic lipids from serum extracts. In this case, serum lipids were readily

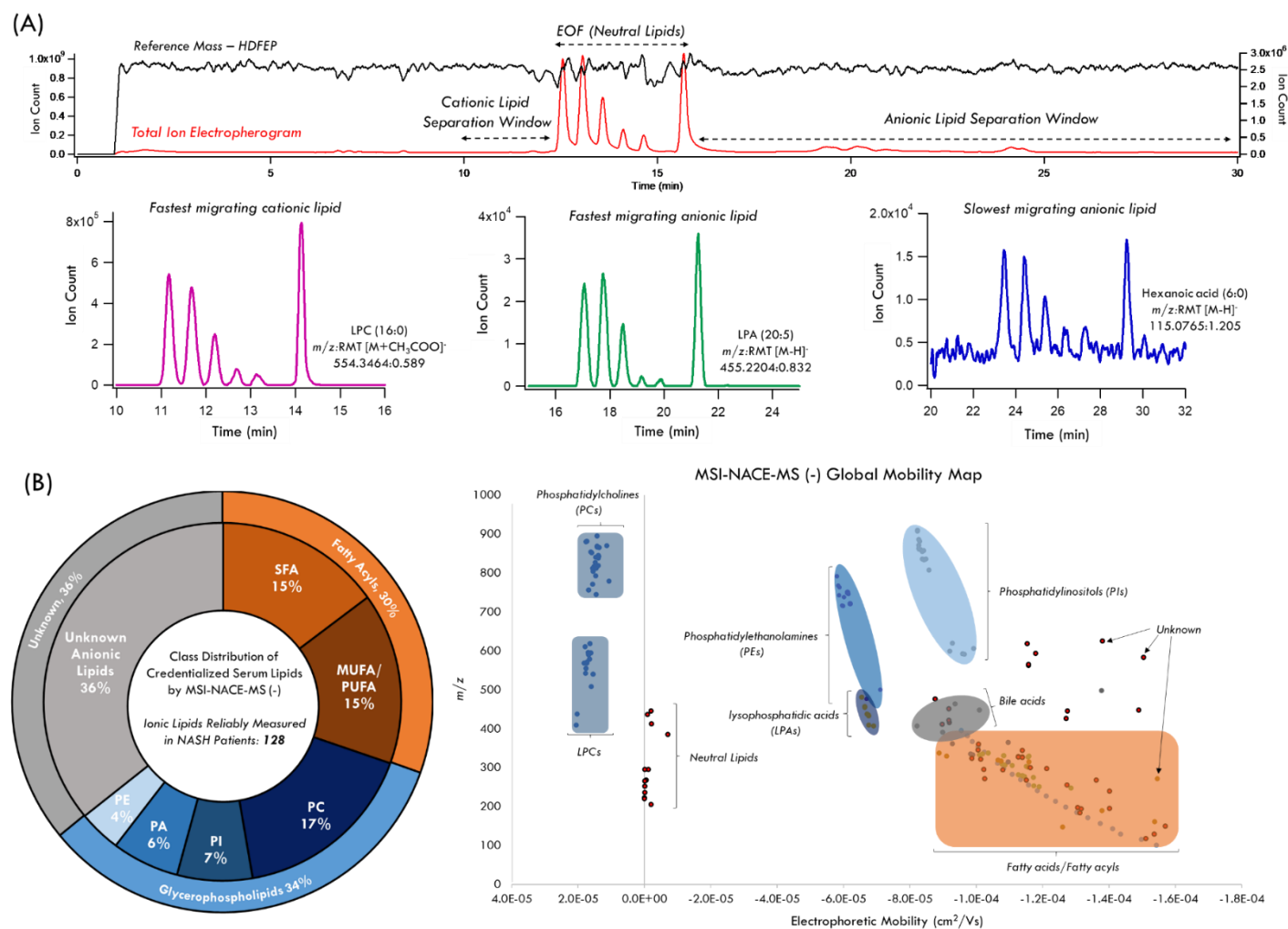


**Figure 2.2.** (A) Representative total and extracted ion electropherograms highlighting the unique selectivity of MSI-NACE-MS for resolving a diverse range of ionic lipids having different polarity. (B) Overall, 128 ionic lipids were credentialized in serum extracts from NASH patients forming distinct clusters in the mobility plot, including major lipid sub-classes ranging from nonesterified fatty acids, phosphatidylinositols, phosphatidylethanolamines, lyophosphatidic acids, and phosphatidylcholines.

classified based on their group cluster since their mobility is dependent on their effective charge and conformational size due to differences in specific polar head groups, number of acyl chains, total carbon chain length, and degree of unsaturation. This strategy also facilitates putative identification of unknown lipids based on their overlap within well characterized lipid sub-classes, whereas unknown lipids typically had mobilities distinct from the major lipid clusters. For instance, **Figure 2.3A** depicts a mobility plot for a series of serum PIs showing consistent linear trends ( $R^2 > 0.80$ ) as a function of structural changes in total carbon number and degree of unsaturation. Additionally, MS/MS was used to confirm the likely identity of select ionic lipids from the mobility map in the absence of commercial standards. A MS/MS spectrum acquired for PI 38:6 (**Figure 2.1**) confirms its lipid sub-structure as PI 16:0/22:6 based on diagnostic products ions detected for the polar inositol head group (241.1017  $m/z$ ), as well as two fatty acid acyl groups from *sn*-1 (16:0, 255.2330  $m/z$ ) and *sn*-2 (22:6, 327.230  $m/z$ ) positions annotated based on their relative ion abundance. Also, **Figure 2.3B** depicts a homologous series of LPAs that have a linear change in mobility determined by their total chain length and degree of unsaturation with shorter and more highly unsaturated LPAs adopting more compact conformations and thus larger negative mobilities. This is consistent with trends previously reported when modeling the mobility of serum NEFAs<sup>35</sup>

Annotation of the MS/MS spectrum for LPA 20:4 in **Figure 2.3B** is also confirmed by diagnostic product ions for its polar phosphate head group (152.995  $m/z$ ; 78.9588  $m/z$ ), and polyunsaturated fatty acid acyl group consistent with arachidonic acid (20:4, 303.2330  $m/z$ ). As expected, the greatest change in mobility reflects structural changes in the number



of acyl chains as highlighted for serum PCs and LPCs in the mobility map (**Figure 2.2B**), as well as serum PEs and LPEs (*e.g.*, LPE 20:4) as shown in **Supporting Figure S2.2**. Interestingly, lipid selectivity in MSI-NACE-MS represents a hybrid of reversed-phase (*i.e.*, acyl/carbon chain length and degree of unsaturation) and HILIC (*i.e.*, polar head group and effective charge) modes of chromatography. Although selectivity is more analogous to gas-phase lipid separations in IMS, unique advantages of MSI-NACE-MS include higher peak capacity notably for smaller/hydrophilic lipid sub-classes (*e.g.*, LPAs, LPCs, LPEs), novel lipidomic data workflows to reduce false discoveries, and higher sample throughput with robust batch correction adjustment as required in large-scale epidemiological studies.<sup>37</sup>

#### **2.4.3. Differential Risk Assessment of NASH Patients from Serum Lipid Profiles.**

Aberrant lipid metabolism and insulin resistance has long been associated in the pathophysiology of NAFLD and severe liver fibrosis progression in NASH notably among overweight/obese individuals with metabolic syndrome.<sup>38</sup> **Figure 2.4A** provides an 2D heat map of the serum lipidome from NASH patients ( $n=85$ ) by MSI-NACE-MS following data exploration using a  $k$ -means clustering algorithm, which revealed two distinct sub-groups of patients (**Supporting Figure S2.3**) corresponding to cluster A ( $n=26$ ) and cluster B ( $n=59$ ). Supervised multivariate data analysis using PLS-DA of assigned NASH patient sub-groups having differential lipid profiles are shown in **Figure 2.4B**. Also, a VIP scores plot (**Figure 2.4C**) highlights that credentialized serum lipids ( $VIP > 1.6$ ) annotated by their  $m/z$ :RMT were consistently elevated in NASH patients from cluster B as compared to cluster A as shown in box plots (**Figure 2.4D**) for 3 top-ranked serum NEFAs. Univariate

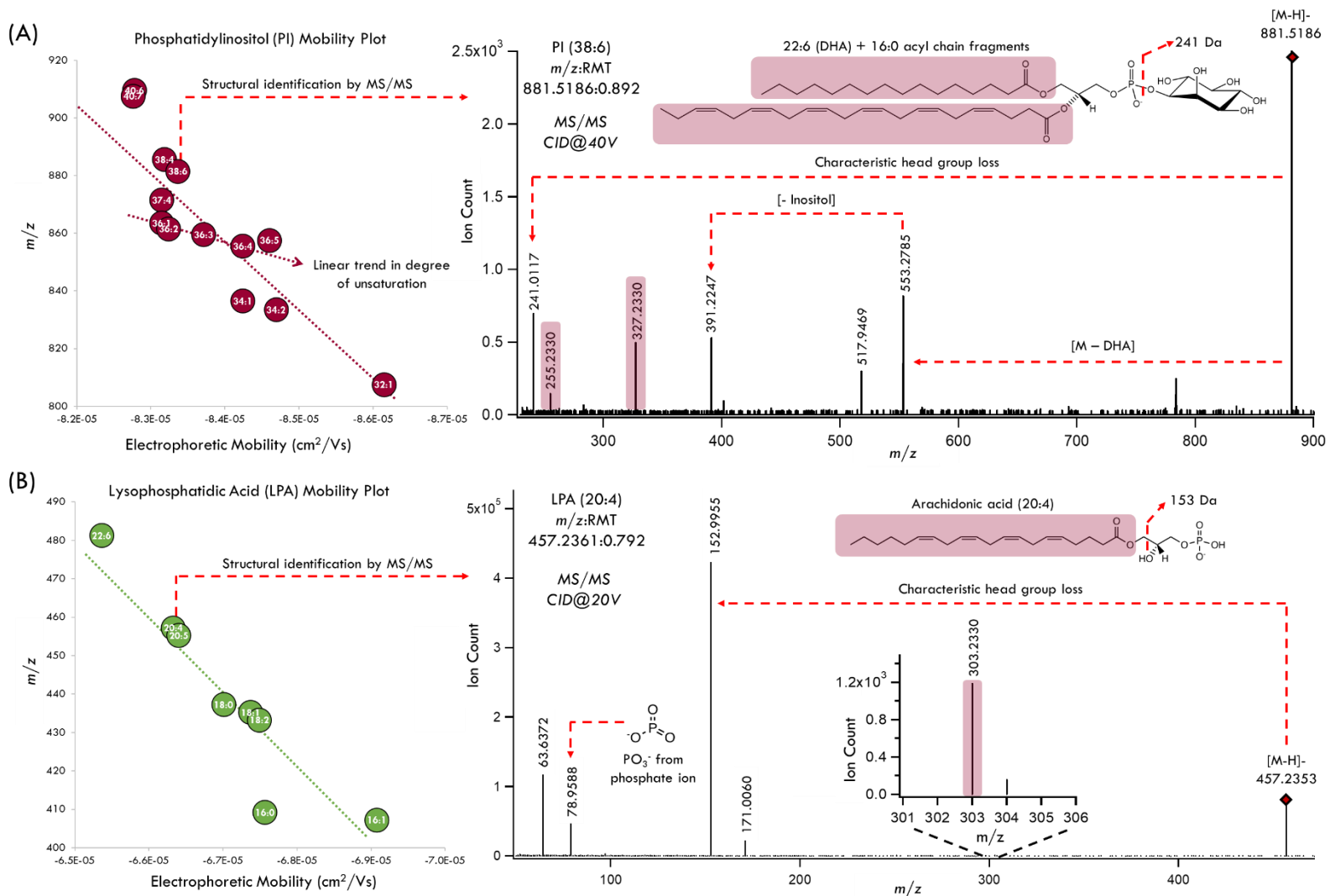


**Figure 2.3.** MS/MS spectra from collisional-induced dissociation experiments at an optimal collision energy under negative ion mode for structural elucidation of select anionic lipids by MSI-NACE-MS, including (A) phosphatidylinositol (PI 16:0, 22:6) and (B) lysophosphatidic acid (LPA 20:4). The mobility plots highlight that the effective charge and conformational size of ionic lipids influence their apparent electrophoretic mobility, including the specific polar head group, number of acyl chains, total number of carbons, and degree of unsaturation.

statistical analysis of serum lipids between NASH patient sub-groups using ANCOVA after covariate adjustments (BMI, sex, age, co-morbidities) confirmed 29 differentiating serum lipids satisfying a Bonferroni correction (adjusted  $p < 3.90 \times 10^{-4}$ ) as listed in **Supporting Table S2.9**. These lipids were predominately circulating NEFAs, such as palmitic acid (16:0) which was elevated on average 1.95-fold in NASH patients in cluster B relative to cluster A ( $p = 3.43 \times 10^{-10}$ , effect size = 0.411) similar to other saturated (*e.g.*, 15:0, 17:0, 14:0) and mono-/polyunsaturated (*e.g.*, 18:2, 22:6, 16:1) NEFAs. Indeed, palmitic acid has been shown to elicit inflammation of hepatic stellate cells with reduced autophagy, which are associated with fibrogenic progression in NASH.<sup>39</sup>

**Table 2.1** highlights that although NASH patient sub-groups had similar clinical characteristics, including classic liver enzyme, blood lipid and histopathology results (*e.g.*, ALT, TG, NAS), patients corresponding to cluster B ( $n=59$ ) had elevated glycated hemoglobin (HbA1c,  $p = 0.00492$ , effect size = 0.102) as compared to cluster A ( $n=26$ ) after adjusting for sex, age, BMI, and co-morbidity prevalence (diabetes, hypertension, hyperlipidemia). In addition, liver fibrosis severity (F score) was modestly elevated in NASH patients from cluster B as compared to cluster A; however this outcome was statistically significant ( $p < 0.05$ ) only if diabetes or hyperlipidemia status were excluded as covariates. For these reasons, cluster B was inferred as high-risk NASH patients (relative to low-risk NASH patients in cluster A) given their elevated circulating NEFA profiles, greater glucose intolerance, and higher overall disease burden with 31% having all 3 co-morbidities, and only 5% having no other co-morbidities (**Supporting Table S2.1**). **Figure 2.4D** demonstrates that high-risk NASH patients (cluster B) had greater Hb1Ac (> 6.5%)

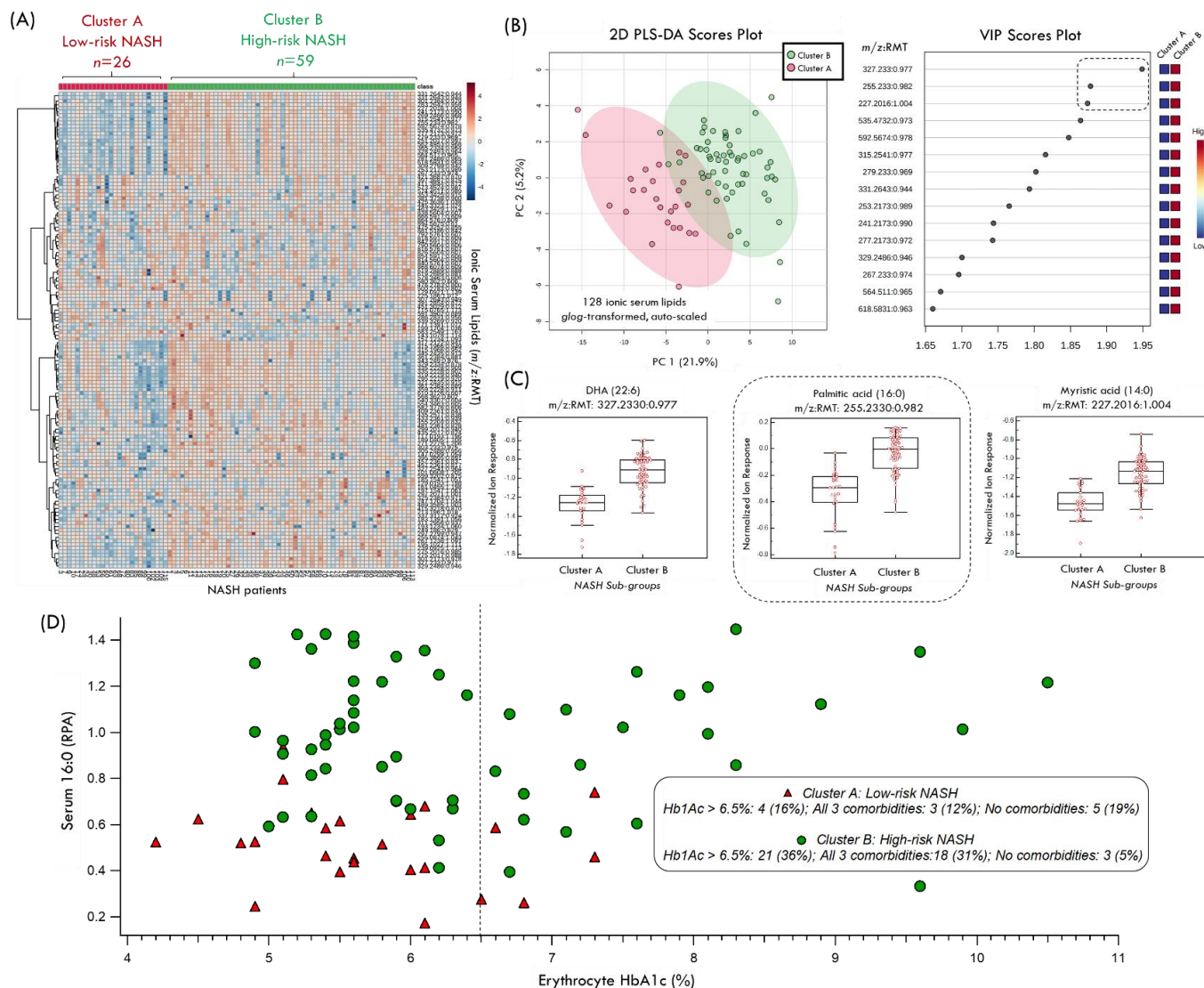


**Figure 2.4.** (A) A 2D heat map depicting the ionic serum lipidome from a cohort of NASH patients (n=85) classified into two sub-groups (cluster A, n=26; cluster B, n=59) following a k-means clustering algorithm. (B) PLS-DA confirms serum lipid profile differences between assigned NASH patient sub-groups, with lipids ranked ordered in terms of their VIP scores (VIP > 1.6) with cluster B having higher serum lipid levels than cluster B with good model performance after 10-fold cross-validation ( $R^2 = 0.746$ ,  $Q^2 = 0.388$ ). (C) Box-whisker plots for the top 3 ranked NEFAs from the PLS-DA model that were also confirmed after ANCOVA with covariate adjustments. (D) Scatter plot highlights that serum palmitic acid (16:0) was elevated in high-risk (cluster B) as compared to low-risk (cluster A) NASH patients, which also coincided with higher glycated hemoglobin (Hb1Ac), modestly elevated fibrosis (F score), and greater overall disease burden.

and serum 16:0 levels as compared to the low-risk NASH patients (cluster A). These results are consistent with recent studies demonstrating that advanced liver fibrosis is independently associated with elevated palmitic acid and insulin levels in NAFLD patients underlying aberrant regulation of fatty acid metabolism.<sup>40</sup>

## 2.5. Conclusion

In summary, an integrative data workflow for lipidomics is developed for unambiguous credentialing of serum lipid features by MSI-NACE-MS. This work represents the first nontargeted lipid profiling study using a multiplexed NACE-MS platform that enables the resolution of ionic/polar classes of lipids complementary to existing chromatographic methods. A mobility map is also introduced to classify diverse sub-classes of ionic lipids, which may support their structural identification in conjunction with MS/MS. This method greatly expands CE-MS metabolome coverage beyond hydrophilic metabolites, and is ideal for large-scale lipidomic studies requiring higher sample throughput (< 4.5 min/sample) and lower sample volume requirements (*i.e.*, < 5  $\mu$ L). Overall, acceptable technical precision (CV < 15%) was achieved when resolving 128 different anionic (*e.g.*, lysophosphatidic acids) and cationic (*e.g.*, lysophosphatidylcholines) lipids consistently analyzed in a cohort of NASH patients. MSI-NACE-MS was applied for risk assessment of NASH patients with advanced liver fibrosis based on their serum lipid profiles. In this case, high-risk NASH patients with likely poor clinical outcomes were associated with elevated palmitic acid and other circulating NEFAs that also coincided with greater glucose intolerance and metabolic disease burden. Limitations of MSI-NACE-MS include that electrically neutral lipid classes and certain

positional or geometric lipid isomers are not resolved, whereas peak capacity is limited for zwitter-ionic phosphatidylcholines that migrate close to the EOF. Current work is underway to further validate MSI-NACE-MS and expand its performance for resolving cationic lipids in positive ion mode when using pre-column chemical derivatization. Future work will also focus on absolute lipid quantification using reference serum samples together with multiple stable-isotope internal standards for improved data harmonization.

## 2.6 References

1. X. Han, *Nat. Rev. Endocrinol.* **2016**, *12*, 668–679.
2. C. D. Calvano, F. Palmisano, and T. R. Cataldi, *Bioanalysis* **2018**, *10*, 787–790.
3. G. Musso, M. Cassader, E. Paschetta, and R. Gambino, *Gastroenterol.* **2018**, *155*, 282–302.
4. Y. H. Rustam and G. E. Reid, *Anal. Chem.* **2017**, *90*, 374–397.
5. T. Xu, C. Hu, Q. Xuan, and G. Xu, *Anal. Chim. Acta* **2020**, *1137*, 156–159.
6. M. Sud, E. Fahy, D. Cotter, A. Brown, E. A. Dennis, C. K. Glass, A. H. Merrill, R. C. Murphy, C. R. H. Raetz, D. W. Russell, and S. Subramaniam, *Nucleic Acids Res.* **2007**, *35*, D527–D532.
7. A. Baglai, A. F. G. Gargano, J. Jordens, Y. Mengerink, M. Honing, S. van der Wal, and P. J. Schoenmakers, *J. Chromatogr. A* **2017**, *1530*, 90. 13868–13884.
8. T. Züllig, M. Trötz Müller, and H.C. Köfeler *Anal. Bioanal. Chem.* **2020**, *412*, 2191–2209.
9. J. A. Bowden, A. Heckert, C. Z. Ulmer, C. M. Jones, J. P. Koelmel, L. Abdullah, L. Ahonen Y. Alnouti, A. M. Armando, J. M. Asara *et al. J. Lipid Res.* **2017**, *58*, 2275–2288.
10. B. Burla, M. Arita, M. Arita, A. K. Bendt, A. Cazenave-Gassiot, E. A. Dennis, K. Ekroos, X. Han, K. Ikeda, G. Liebisch, *et al. J. Lipid Res.* **2018** *59*, 2001–2017.
11. E. Kenndler, *J. Chromatogr. A* **2014**, *1335*, 16–30.

12. E. Kenndler, *J. Chromatogr. A* **2014**, 1335, 31–41.
13. F. Gao, Z. Zhang, X. Fu, W. Li, T. Wang, and H. Liu, *Electrophoresis* **2007**, 28, 1418–1425.
14. C. Montealegre, L. Sánchez-Hernández, A. L. Crego, and M. L. Marina, *J. Agr. Food Chem.* **2013**, 61, 1823–1832.
15. J.-H. Lee, S.-J. Kim, S. Lee, J.-K. Rhee, S. Y. Lee, and Y.-C. Na, *Anal. Chim. Acta* **2017**, 984, 223–231.
16. V. Sándor, B. Viktor Berkics, A. Kilar, B. Kocsis, F. Kilar, and Á. Dörnyei, *Electrophoresis* **2020**, 41, 1178–1188.
17. K. Huynh, C. K. Barlow, K. S. Jayawardana, J. M. Weir, N. A. Mellett, M. Cinel, D. J. Magliano, J. E. Shaw, B. G. Drew, and P. J. Meikle. *Cell Chem. Biol.* **2019** 26, 71–84.
18. M. Yamamoto, R. Ly, B. Gill, Y. Zhu, J. Moran-Mirabal, and P. Britz-McKibbin, *Anal. Chem.* **2016**, 88, 10710–10719.
19. W. Zhang, F. Guled, T. Hankemeier, and R. Ramautar, *Electrophoresis* **2020**, 41, 360–369.
20. S. M. Azab, R. Ly, and P. Britz-McKibbin, *Anal. Chem.* **2019**, 91, 2329–2336.
21. S. M. Azab, R. J. de Souza, K. K. Teo, S. S. Anand, N. C. Williams, J. Holzschuher, C. McGlory, S. M. Philips, and P. Britz-McKibbin, *J. Lipid Res.* **2020**, 61, 933–944.
22. S. M. Azab, A. Zamzam, M. H. Syed, R. Abdin, M. Qadura, and P. Britz-McKibbin, *J. Clin. Med.* **2020**, 9, 1877.
23. M. Saoi, K. M. Kennedy, W. Gohir, D. M. Sloboda, and P. Britz-McKibbin, *Sci. Rep.* **2020**, 10, 9399.
24. M. Saoi, K. Sasaki, H. Sagawa, K. Abe, T. Kogiso, K. Tokushige, E. Hashimoto, Y. Ohashi, and P. Britz-McKibbin *P. J. Proteome Res.* **2020**, 19, 2689–2699.
25. K. Sasaki, H. Sagawa, M. Suzuki, H. Yamamoto, M. Tomita, T. Soga, and Y. Ohashi, *Anal. Chem.* **2018**, 91, 1295–1301.
26. N. L. Kuehnbaum, A. Kormendi, and P. Britz-McKibbin, *Anal. Chem.* **2013**, 85, 10664–10669
27. R. Adusumilli and P. Mallick, *Methods Mol. Biology*, **2017**, 1550, 339–368.

28. T. Pluskal, S. Castillo, A. Villar-Briones, and M. Orešič, *BMC Bioinformatics* **2010**, *11*, 395.
29. C. Kuhl, R. Tautenhahn, C. Böttcher, T. R. Larson, and S. Neumann, *Anal. Chem.* **2012**, *84*, 283–289.
30. E. Fahy, D. Cotter, M. Sud, and S. Subramaniam S. *Biochim. Biophys. Acta.* **2011**, *1811*, 637–647.
31. Z. Pang, J. Chong, G. Zhou, D. Anderson de Lima Morais, L. Chang, M. Barrette, C. Gauthier, P.-É. Jacques, S. Li, and J. Xia, *Nucleic Acids Res.* **2021**, *49*, W388–W396.
32. A. DiBattista, N. McIntosh, M. Lamoureux, O. Y. Al-Dirbashi, P. Chakraborty, and P. Britz-McKibbin P. *Anal. Chem.* **2017**, *89*, 8112–8121.
33. P.D. Hutchins, J. D. Russell, and J. J. Coon *Cell Syst.* **2018**, *6*, 621–625.
34. N. G. Mahieu, X. Huang, Y. J. Chen, and G. J. Patti, *Anal. Chem.* **2014**, *86*, 9583–9589.
35. J. P. Koelmel, X. Li, S. M. Stow, M. J. Sartain, A. Murali, R. Kemperman, H. Tsugawa, M. Takahashi, V. Vasiliou, J. A. Bowden, R. A. Yost, T. J. Garrett, and N. Kitagawa, *Metabolites* **2020** *10*, 101.
36. K. L. Leaptrot, J. C. May, J. N. Dodds, and J. A. McLean, *Nat. Commun.* **2019**, *10*, 985.
37. M. Shanmuganathan, Z. Kroezen, B. Gill, S. Azab, R. J. de Souza, K. K. Teo, S. Atkinson, P. Subbarao, D. Desai, S. S. Anand, and P. Britz-McKibbin *Nat. Prot.* **2021** *16*, 1966–1994.
38. G. Firneisz, *World J Gastroenterol.* **2014**, *20*, 9072–9089.
39. N. N. Duan, X. J. Liu, and J. Wu, *Life Sci.* 2017, *176*, 42–53.
40. K. Cansanção, L. Silva Monteiro, N. Carvalho Leite, A. Dávalos, M. D. G. Tavares do Carmo, and W. Arantes Ferreira Peres, *Nutrients* **2018**, *10*, 1586.



## 2.7. Supporting Information

### Chapter II

#### **Nontargeted Serum Lipid Profiling by Multisegment Injection-Nonaqueous Capillary Electrophoresis-Mass Spectrometry: A Multiplexed Separation Platform for Resolving Ionic Lipids**

*Ritchie Ly<sup>1</sup>, Nicholas Ly<sup>1</sup>, Kazunori Sasaki<sup>2</sup>, Makoto Suzuki<sup>2</sup>, Kenjiro Kami<sup>2</sup>, Yoshiaki Ohashi<sup>2</sup>,  
Philip Britz-McKibbin<sup>1</sup>*

<sup>1</sup> Department of Chemistry and Chemical Biology, McMaster University, Hamilton, Canada

<sup>2</sup> Human Metabolome Technologies Inc., Tsuruoka, Yamagata, Japan

## Supporting Experimental.

**Sample Collection and Study Cohort.** Fasting serum samples were collected from a cohort of adult Japanese patients ( $n=85$ ) at Tokyo Women's Medical University who were diagnosed with probable (NAS = 3–4, 14%) or definitive NASH (NAS  $\geq$  5.0, 86%) with a median NAS of 6.0 (ranging from 3.0 to 7.5) following standardized histopathology grading and exclusion of excessive alcohol intake or other chronic liver diseases. Written informed consent was acquired from all the patients, and the study design followed the ethical guidelines of the 1975 Declaration of Helsinki. Standard liver enzyme and blood protein tests were performed at the Tokyo Women's Medical University using serum aliquots stored at  $-20\text{ }^{\circ}\text{C}$ , which were previously used for targeted analysis of serum  $\gamma$ -glutamyl dipeptides when using MSI-CE-MS/MS [*J. Proteome Res.* **2020**, 19, 2689-2699]. **Table S2.1** summarizes all patient characteristics and clinical information from the NASH cohort ( $n=85$ ), including histopathology grading based on the NASH clinical research network's (NASH CRN) scoring system for non-alcoholic fatty liver disease (NAFLD). **Table S2.1** also highlights the prevalence of comorbidities among the full cohort of NASH patients, as well as two major NASH sub-groups having distinctive serum lipid profiles identified following cluster analysis.

(A)

Run Number	Injection Position						
	1	2	3	4	5	6	7
<i>i</i>	Standard mixture to check instrument performance						
<i>ii</i>	Pooled QC run to check instrument performance for biofluid						
1	QC	N4-25	N4-19	N4-115	N4-71	N4-58	N4-38
2	N4-5	N4-106	N4-95	N4-20	N4-85	QC	N4-24
3	N4-55	N4-63	N4-84	N4-27	QC	N4-72	N4-81
4	N4-14	N4-98	N4-34	N4-30	N4-93	N4-33	QC
5	N4-32	N4-50	QC	N4-87	N4-45	N4-1	N4-16
6	N4-96	N4-61	N4-29	QC	N4-11	N4-39	N4-23
7	N4-100	N4-82	N4-54	N4-91	QC	N4-52	N4-80
8	QC	N4-7	N4-113	N4-9	N4-59	N4-48	N4-66
9	N4-13	N4-12	QC	N4-83	N4-70	N4-36	N4-15
10	N4-73	N4-41	N4-99	QC	N4-88	N4-75	N4-68
11	N4-78	N4-109	N4-57	N4-94	N4-103	QC	N4-2
12	N4-53	N4-92	N4-89	N4-6	QC	N4-60	N4-44
13	N4-18	QC	N4-37	N4-43	N4-110	N4-17	N4-102
14	N4-56	QC	N4-74	N4-10	N4-4	N4-35	N4-46
15	N4-90	N4-3	N4-97	N4-28	QC	QC	QC
<i>iii</i>	Pooled QC run to check instrument performance for biofluid						
<i>iv</i>	Dilution trend filter pattern for untargeted analysis						

Analysis of all serum ( $n=85$ ), QCs ( $n=17$ ) & control runs ( $n=28$ ) completed < 8 hours using MSI-NACE-MS ( $n=128$ )

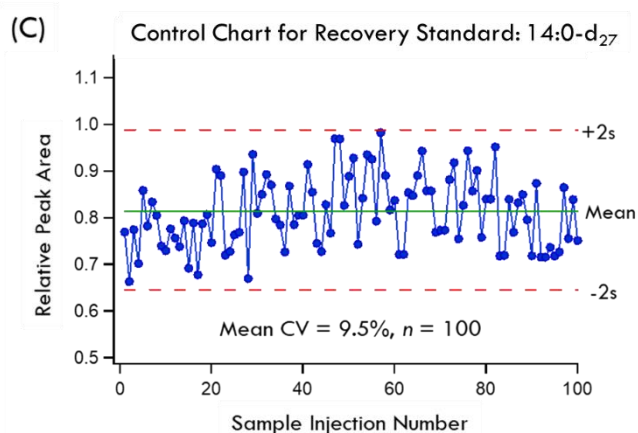
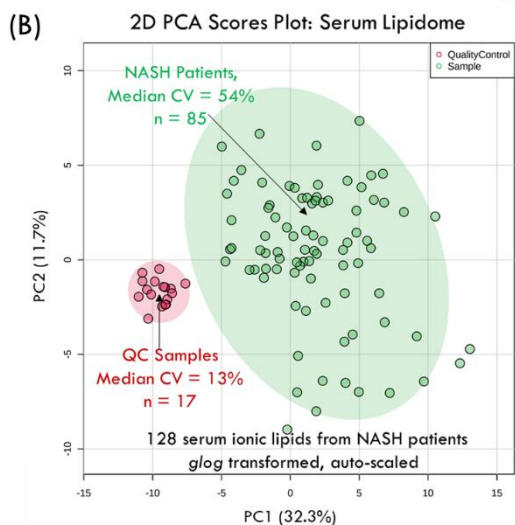


**Figure S2.1.** (A) Schematic of the serial injection configuration for ionic lipids by MSI-NACE-MS, including six serum extracts from NASH patients ( $n=86$ ) and a pooled sample as quality control (QC,  $n=17$ ). (B) Overall, there was good technical precision (median CV = 13%,  $n=17$ ) as shown in the 2D scores plot when using PCA based on the analysis of 128 ionic lipids consistently measured in the NASH patient cohort (CV < 30%, > 75% all samples) reflecting underlying biological variability (median CV = 54%). (C) Also a control chart for the recovery standard is shown for every serum and QC sample (mean CV = 9.5%,  $n=100$ ) in this study.

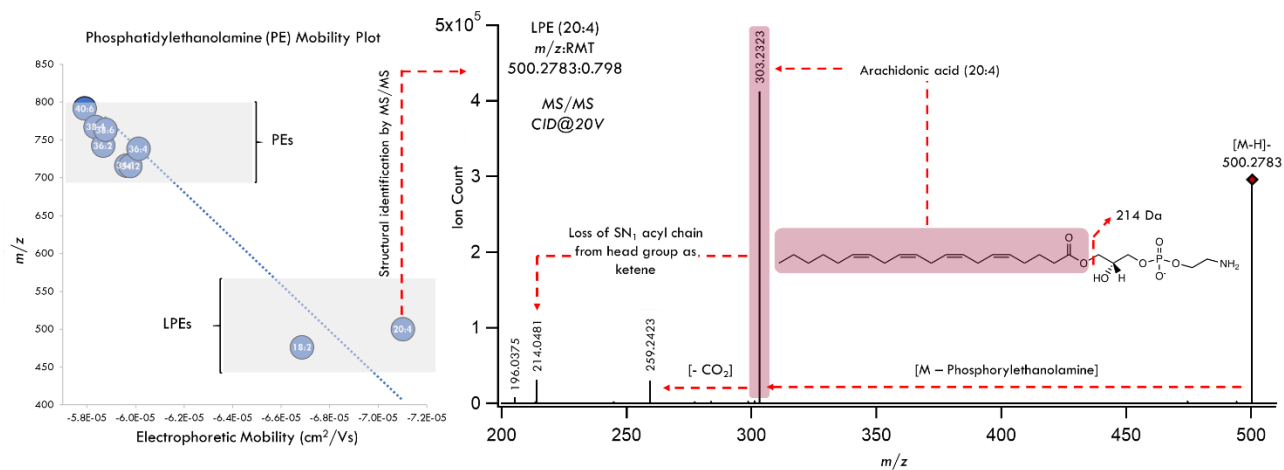


**Figure S2.2.** Representative MS/MS spectra from collisional-induced dissociation experiments at an optimal collision energy under negative ion mode for confirming the structural identity of a lysophosphatidylethanolamine (LPE 20:4). The mobility plot for PIs highlights the distinct changes in lipid sub-class mobility reflecting differences in the number of acyl chains, total chain length, and degrees of unsaturation.

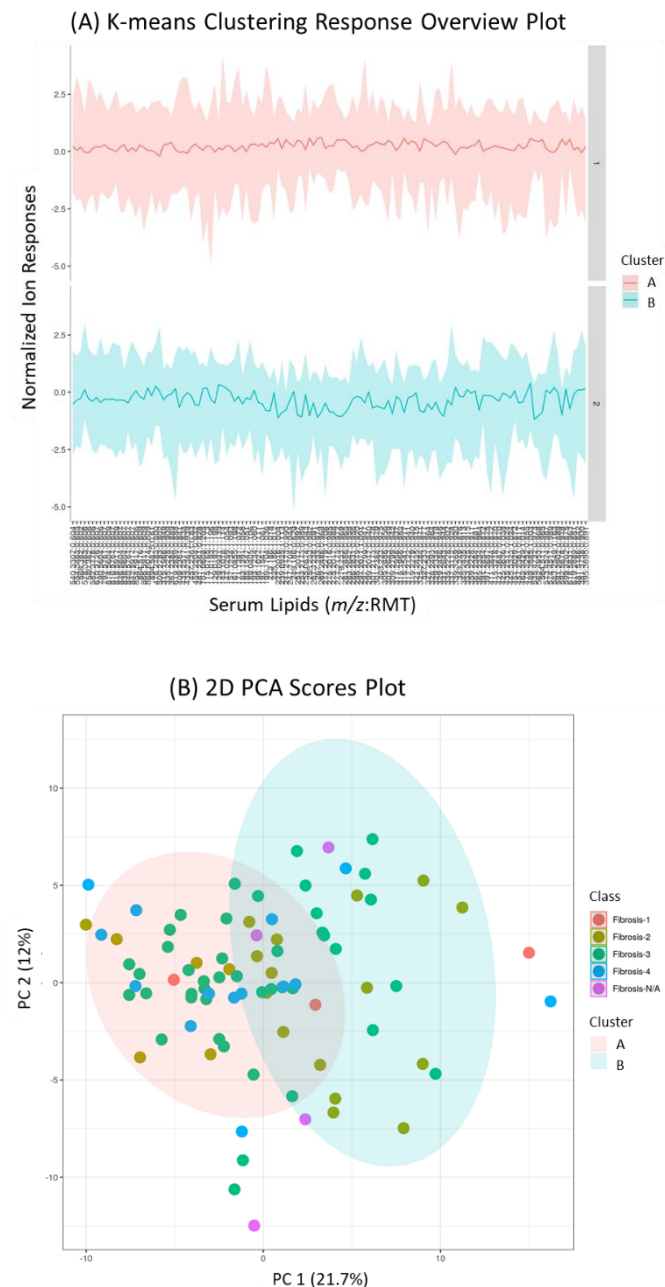


**Figure S2.3.** Results of partitional clustering of Japanese NASH patients ( $n=85$ ), labelled by their reported clinical fibrosis scores ( $F=1-4$ ), using a  $k$ -means clustering algorithm ( $k=2$ ) based on 128 ionic lipids measured by MSI-NACE-MS. **(A)** The median intensities represented by the bold lines in the overview of serum lipidome demonstrate strong fit of re-categorized samples within each cluster. **(B)** NASH patients classified to each cluster (cluster A,  $n=26$ ; cluster B,  $n=59$ ) were then projected on a 2D PCA scores plot highlighting two distinct NASH patient sub-groups in the cohort. Overall,  $k > 2$  demonstrated larger inter-cluster deviation in the median lines as confirmed by overlapping ellipses for assigned NASH patient sub-groups in a 2D PCA scores plot.

**Table S2.1.** Summary of clinical characteristics of a Japanese patient cohort diagnosed with NASH.

<b>Clinical Parameter</b>	<b>Cluster A: <i>Low Risk</i> NASH (n=26)</b>	<b>Cluster B: <i>High Risk</i> NASH (n=59)</b>
Diabetes [total]	11 (42%)	33 (56%)
Hb1Ac > 6.5%	4 (16%)	21 (36%)
No comorbidities	5 (19%)	3 (5%)
Diabetes [only]	1 (4%)	3 (5%)
Hypertension [only]	2 (8%)	3 (5%)
Hyperlipidemia [only]	5 (19%)	12 (20%)
Diabetes + Hyperlipidemia	3 (12%)	9 (15%)
Diabetes + Hypertension	4 (15%)	2 (3%)
Hyperlipidemia + Hypertension	3 (12%)	8 (14%)
All 3 Comorbidities	3 (12%)	18 (31%)

**Table S2.2** List of credentialized saturated fatty acids detected in pooled NASH serum sample.

Tentative ID	<i>m/z</i> :RMT	Mass Error (ppm)	Electrophoretic Mobility (cm <sup>2</sup> /Vs)	Molecular Formula	Relative Abundance (%) <sup>a</sup>	Mean CV (%) (n=17) <sup>b</sup>
Cerotic Acid (26:0)	395.3895:0.893	1.26	-9.544E-05	C <sub>26</sub> H <sub>52</sub> O <sub>2</sub>	0.11%	8.5%
Hyenic Acid (25:0)	381.3738:0.901	0.79	-9.734E-05	C <sub>25</sub> H <sub>50</sub> O <sub>2</sub>	0.13%	8.9%
Lignoceric Acid (24:0)	367.3582:0.906	1.09	-9.871E-05	C <sub>24</sub> H <sub>48</sub> O <sub>2</sub>	0.06%	8.4%
Tricosylic acid (23:0)	353.3425:0.914	0.85	-1.006E-04	C <sub>23</sub> H <sub>46</sub> O <sub>2</sub>	0.12%	13.0%
Docosanoic acid (22:0)	339.3269:0.921	1.77	-1.024E-04	C <sub>22</sub> H <sub>44</sub> O <sub>2</sub>	0.05%	28.1%
Arachidic acid (20:0)	311.2956:0.938	0.96	-1.063E-04	C <sub>20</sub> H <sub>40</sub> O <sub>2</sub>	0.21%	14.0%
Nonadecylic Acid (19:0)	297.2799:0.946	1.68	-1.082E-04	C <sub>19</sub> H <sub>38</sub> O <sub>2</sub>	0.10%	6.7%
Stearic acid (18:0)	283.2642:0.958	1.06	-1.108E-04	C <sub>18</sub> H <sub>36</sub> O <sub>2</sub>	25.11%	15.1%
Margaric acid (17:0)	269.2486:0.969	0.74	-1.133E-04	C <sub>17</sub> H <sub>34</sub> O <sub>2</sub>	1.82%	9.5%
Palmitic acid (16:0)	255.2330:0.981	1.18	-1.157E-04	C <sub>16</sub> H <sub>32</sub> O <sub>2</sub>	100.00%	14.7%
Pentadecylic acid (15:0)	241.2173:0.993	0.83	-1.183E-04	C <sub>15</sub> H <sub>30</sub> O <sub>2</sub>	0.93%	12.6%
Myristic acid (14:0)	227.2016:1.006	0.44	-1.210E-04	C <sub>14</sub> H <sub>28</sub> O <sub>2</sub>	5.94%	5.5%
Tridecylic acid (13:0)	213.1860:1.020	0.94	-1.238E-04	C <sub>13</sub> H <sub>26</sub> O <sub>2</sub>	0.21%	6.3%
Lauric acid (12:0)	199.1704:1.037	1.51	-1.269E-04	C <sub>12</sub> H <sub>24</sub> O <sub>2</sub>	1.24%	8.5%
Undecylic acid (11:0)	185.1547:1.055	1.62	-1.303E-04	C <sub>11</sub> H <sub>22</sub> O <sub>2</sub>	0.11%	11.3%
Capric acid (10:0)	171.1391:1.073	1.17	-1.335E-04	C <sub>10</sub> H <sub>20</sub> O <sub>2</sub>	0.41%	6.3%
Pelargonic Acid (9:0)	157.1234:1.094	1.27	-1.372E-04	C <sub>9</sub> H <sub>18</sub> O <sub>2</sub>	0.30%	9.2%
Caprylic Acid (8:0)	143.1078:1.117	1.40	-1.410E-04	C <sub>8</sub> H <sub>16</sub> O <sub>2</sub>	0.69%	20.8%
Heptanoic Acid (7:0)	129.0921:1.142	0.00	-1.434E-04	C <sub>7</sub> H <sub>14</sub> O <sub>2</sub>	0.07%	9.5%
Caproic Acid (6:0)	115.0765:1.173	1.74	-1.497E-04	C <sub>6</sub> H <sub>12</sub> O <sub>2</sub>	0.08%	14.3%

<sup>a</sup> Normalized ion relative peak area ratio to most abundant lipid within class in pooled serum from NASH patients.

<sup>b</sup> Technical precision based on repeat analysis of pooled serum extracts from NASH patients as QC.

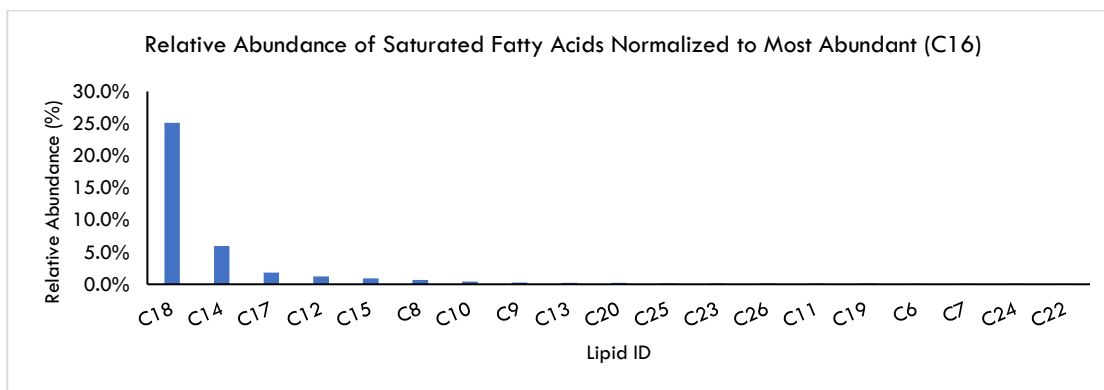


**Table S2.3.** List of credentialized mono-/polyunsaturated fatty acids detected in pooled NASH serum sample.

Tentative ID	<i>m/z</i> :RMT	Mass Error (ppm)	Electrophoretic Mobility (cm <sup>2</sup> /Vs)	Molecular Formula	Relative Abundance (%) <sup>a</sup>	Mean CV (%) (n=17) <sup>b</sup>
16:1	253.2173:0.986	0.39	-1.17E-04	C <sub>16</sub> H <sub>30</sub> O <sub>2</sub>	11.22%	5.0%
16:2	251.2017:0.998	0.80	-1.19E-04	C <sub>16</sub> H <sub>28</sub> O <sub>2</sub>	0.18%	21.3%
16:4	247.1704:1.045	1.62	-1.29E-04	C <sub>16</sub> H <sub>24</sub> O <sub>2</sub>	0.04%	10.4%
18:1	281.2486:0.965	1.42	-1.13E-04	C <sub>18</sub> H <sub>34</sub> O <sub>2</sub>	44.65%	24.0%
18:2	279.2330:0.970	1.07	-1.14E-04	C <sub>18</sub> H <sub>32</sub> O <sub>2</sub>	4.26%	5.3%
18:3	277.2173:0.985	0.36	-1.14E-04	C <sub>18</sub> H <sub>30</sub> O <sub>2</sub>	0.10%	12.8%
18:4	275.2017:0.986	0.73	-1.17E-04	C <sub>18</sub> H <sub>28</sub> O <sub>2</sub>	1.04%	6.5%
20:1	309.2799:0.942	0.65	-1.11E-04	C <sub>20</sub> H <sub>38</sub> O <sub>2</sub>	1.34%	16.2%
20:2	307.2643:0.946	0.98	-1.09E-04	C <sub>20</sub> H <sub>36</sub> O <sub>2</sub>	7.91%	13.5%
20:3	305.2486:0.957	0.98	-1.11E-04	C <sub>20</sub> H <sub>34</sub> O <sub>2</sub>	3.42%	7.8%
20:4	303.2330:0.976	0.99	-1.15E-04	C <sub>20</sub> H <sub>32</sub> O <sub>2</sub>	0.09%	10.2%
20:5	301.2173:0.979	1.00	-1.16E-04	C <sub>20</sub> H <sub>30</sub> O <sub>2</sub>	0.01%	28.4%
22:1	337.3112:0.926	0.30	-1.01E-04	C <sub>22</sub> H <sub>42</sub> O <sub>2</sub>	0.23%	11.8%
22:2	335.2956:0.927	0.60	-1.02E-04	C <sub>22</sub> H <sub>40</sub> O <sub>2</sub>	11.22%	5.6%
22:3	333.2799:0.934	0.30	-1.04E-04	C <sub>22</sub> H <sub>38</sub> O <sub>2</sub>	0.18%	9.4%
22:6	327.2330:0.977	0.85	-1.16E-04	C <sub>22</sub> H <sub>32</sub> O <sub>2</sub>	0.44%	8.7%

<sup>a</sup> Normalized ion relative peak area ratio to most abundant lipid within class in pooled serum from NASH patients.

<sup>b</sup> Technical precision based on repeat analysis of pooled serum extracts from NASH patients as QC.

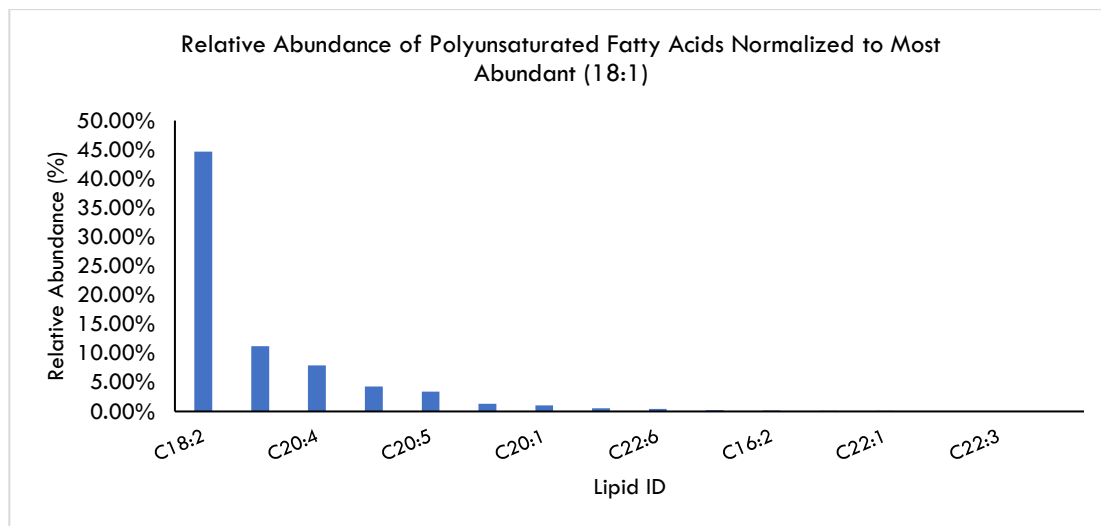




**Table S2.4.** List of credentialized phosphatidylcholines (PC) detected in pooled NASH serum.

Tentative ID	<i>m/z</i> :RMT	Mass Error (ppm)	Electrophoretic Mobility (cm <sup>2</sup> /Vs)	Molecular Formula	Relative Abundance (%) <sup>a</sup>	Mean CV (%) (n=17) <sup>b</sup>
LPC 14:0	540.3307:0.604	0.37	1.55E-05	C <sub>22</sub> H <sub>44</sub> NO <sub>8</sub> P	16.7%	16.2%
LPC 16:0	554.3463:0.605	0.18	1.77E-05	C <sub>24</sub> H <sub>50</sub> NO <sub>7</sub> P	100.0%	14.0%
LPC 17:1	566.3463:0.605	0.18	1.77E-05	C <sub>25</sub> H <sub>50</sub> NO <sub>7</sub> P	2.0%	15.6%
LPC 17:0	568.3620:0.602	0.88	1.82E-05	C <sub>25</sub> H <sub>52</sub> NO <sub>7</sub> P	15.6%	24.2%
LPC 18:2	578.3463:0.606	0.69	1.62E-05	C <sub>26</sub> H <sub>50</sub> NO <sub>7</sub> P	13.7%	13.7%
LPC 18:1	580.3620:0.606	0.86	1.68E-05	C <sub>26</sub> H <sub>52</sub> NO <sub>7</sub> P	11.6%	11.2%
LPC 18:0	582.3776:0.606	0.86	1.64E-05	C <sub>26</sub> H <sub>54</sub> NO <sub>7</sub> P	23.9%	12.9%
LPC 19:0	610.3726:0.607	0.33	1.79E-05	C <sub>27</sub> H <sub>54</sub> NO <sub>8</sub> P	1.1%	29.5%
PC 32:1	790.5604:0.606	2.15	1.48E-05	C <sub>40</sub> H <sub>78</sub> NO <sub>8</sub> P	9.5%	15.0%
PC 32:0	792.5761:0.607	5.05	1.47E-05	C <sub>40</sub> H <sub>80</sub> NO <sub>8</sub> P	3.7%	27.9%
PC 33:1	804.5761:0.608	0.12	1.55E-05	C <sub>41</sub> H <sub>80</sub> NO <sub>8</sub> P	1.6%	22.3%
PC 34:2	816.5761:0.605	0.86	1.52E-05	C <sub>42</sub> H <sub>80</sub> NO <sub>8</sub> P	1.6%	12.0%
PC 34:1	818.5917:0.609	0.12	1.39E-05	C <sub>42</sub> H <sub>82</sub> NO <sub>8</sub> P	9.1%	15.7%
PC 35:4	826.5604:0.607	0.24	1.48E-05	C <sub>43</sub> H <sub>78</sub> NO <sub>8</sub> P	0.4%	22.9%
PC 36:5	838.5604:0.607	0.72	1.40E-05	C <sub>44</sub> H <sub>78</sub> NO <sub>8</sub> P	1.8%	14.1%
PC 36:4	840.5761:0.607	0.71	1.47E-05	C <sub>44</sub> H <sub>80</sub> NO <sub>8</sub> P	4.5%	11.9%
PC 36:3	842.5917:0.607	1.54	1.37E-05	C <sub>44</sub> H <sub>82</sub> NO <sub>8</sub> P	7.0%	11.2%
PC 37:4	854.5917:0.606	1.29	1.62E-05	C <sub>45</sub> H <sub>82</sub> NO <sub>8</sub> P	4.6%	28.1%
PC 38:6	864.5760:0.609	1.85	1.37E-05	C <sub>46</sub> H <sub>80</sub> NO <sub>8</sub> P	5.5%	10.7%
PC 38:5	866.5917:0.609	1.38	1.43E-05	C <sub>46</sub> H <sub>82</sub> NO <sub>8</sub> P	1.6%	14.8%
PC 38:4	868.6074:0.609	0.35	1.43E-05	C <sub>46</sub> H <sub>84</sub> NO <sub>8</sub> P	3.9%	13.0%
PC 40:5	894.5875:0.610	2.01	1.43E-05	C <sub>48</sub> H <sub>86</sub> NO <sub>8</sub> P	2.3%	13.9%

<sup>a</sup> Normalized ion relative peak area ratio to most abundant lipid within class in pooled serum from NASH patients.

<sup>b</sup> Technical precision based on repeat analysis of pooled serum extracts from NASH patients as QC.

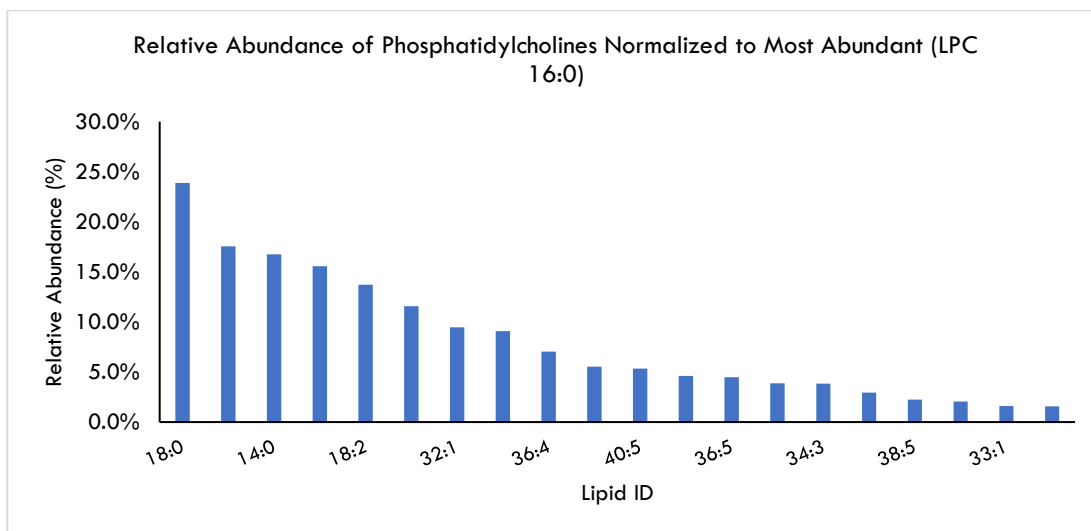


**Table S2.5.** List of credentialized phosphatidylethanolamines (PE) in pooled NASH serum.

Tentative ID	<i>m/z</i> :RMT	Mass Error (ppm)	Electrophoretic Mobility (cm <sup>2</sup> /Vs)	Molecular Formula	Relative Abundance (%) <sup>a</sup>	Mean CV (%) (n=17) <sup>b</sup>
LPE 18:2	476.2783:0.789	0.84	-6.69E-05	C <sub>23</sub> H <sub>43</sub> NO <sub>7</sub> P	41.0%	11.5%
LPE 20:4	500.2783:0.802	0.80	-7.10E-05	C <sub>25</sub> H <sub>43</sub> NO <sub>7</sub> P	100.0%	11.1%
PE 34:1	716.5236:0.769	1.12	-5.96E-05	C <sub>39</sub> H <sub>76</sub> NO <sub>8</sub> P	2.3%	23.5%
PE 35:6	720.4894:0.770	8.47	-6.20E-05	C <sub>40</sub> H <sub>70</sub> NO <sub>8</sub> P	2.9%	18.7%
PE 36:4	738.5079:0.767	3.52	-6.01E-05	C <sub>44</sub> H <sub>81</sub> NO <sub>8</sub> P	11.9%	19.2%

<sup>a</sup> Normalized ion relative peak area ratio to most abundant lipid within class in pooled serum from NASH patients.

<sup>b</sup> Technical precision based on repeat analysis of pooled serum extracts from NASH patients as QC.

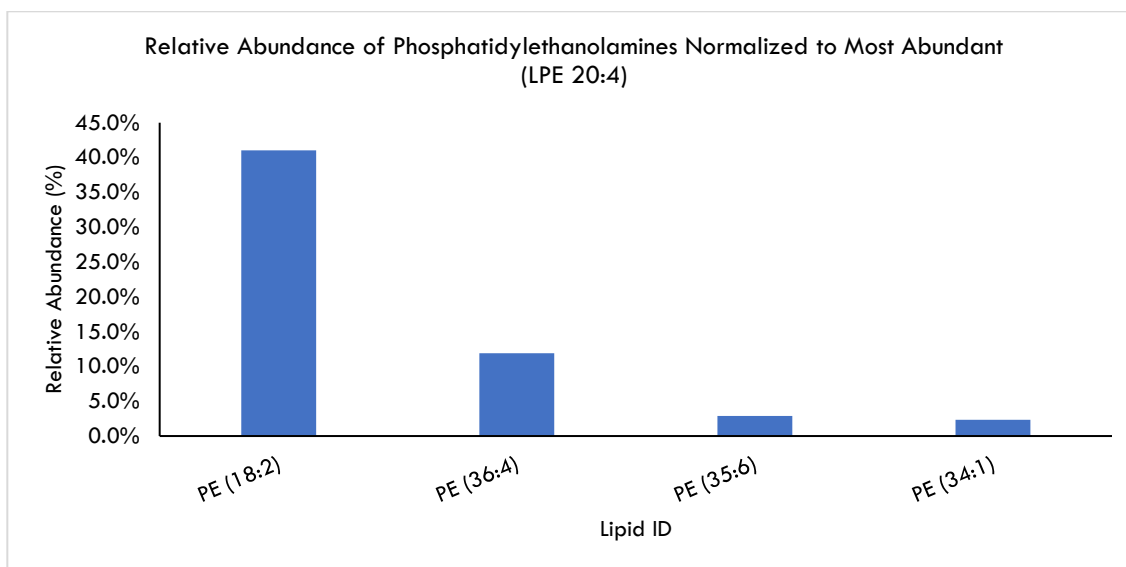


**Table S2.6.** List of credentialized lysophosphatidic acids (LPA) in pooled NASH serum.

Tentative ID	<i>m/z</i> :RMT	Mass Error (ppm)	Electrophoretic Mobility (cm <sup>2</sup> /Vs)	Molecular Formula	Relative Abundance (%) <sup>a</sup>	Mean CV (%) ( <i>n</i> =17) <sup>b</sup>
LPA 16:0	409.2361:0.841	1.47	-6.54E-05	C <sub>19</sub> H <sub>39</sub> O <sub>7</sub> P	36.2%	30.0%
LPA 16:1	407.2204:0.842	1.72	-6.63E-05	C <sub>19</sub> H <sub>37</sub> O <sub>7</sub> P	7.3%	23.8%
LPA 18:1	435.2517:0.838	0.69	-6.64E-05	C <sub>21</sub> H <sub>41</sub> O <sub>7</sub> P	26.9	16.9%
LPA 18:2	433.2361:0.939	0.92	-6.70E-05	C <sub>21</sub> H <sub>39</sub> O <sub>7</sub> P	100%	14.0%
LPA 20:4	457.2361:0.830	1.09	-6.75E-05	C <sub>23</sub> H <sub>39</sub> O <sub>7</sub> P	98.8%	12.3%
LPA 20:5	455.2204:0.832	0.44	-6.76E-05	C <sub>23</sub> H <sub>37</sub> O <sub>7</sub> P	17.0%	9.7%
LPA 22:6	481.2361:0.828	1.04	-6.91E-05	C <sub>25</sub> H <sub>39</sub> O <sub>7</sub> P	28.4%	12.4%

<sup>a</sup> Normalized ion relative peak area ratio to most abundant lipid within class in pooled serum from NASH patients.

<sup>b</sup> Technical precision based on repeat analysis of pooled serum extracts from NASH patients as QC.

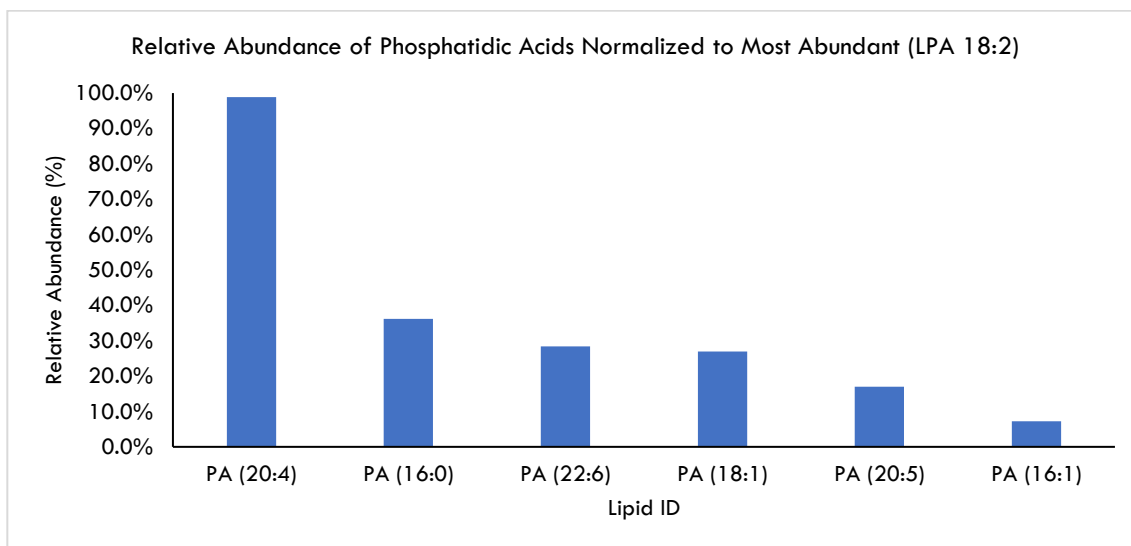


**Table S2.7** List of credentialized phosphatidylinositols (PI) in pooled NASH serum sample.

Tentative ID	<i>m/z</i> :RMT	Mass Error (ppm)	Electrophoretic Mobility (cm <sup>2</sup> /Vs)	Molecular Formula	Relative Abundance (%) <sup>a</sup>	Mean CV (%) (n=17) <sup>b</sup>
LPI 18:0	599.3202:0.875	0.73	-9.19E-05	C <sub>27</sub> H <sub>52</sub> O <sub>12</sub> P	5.7%	11.3%
LPI 20:4	619.2889:0.888	0.48	-9.27E-05	C <sub>29</sub> H <sub>49</sub> O <sub>12</sub> P	9.8%	7.7%
PI 34:2	833.5186:0.853	0.84	-8.42E-05	C <sub>43</sub> H <sub>79</sub> O <sub>13</sub> P	10.6%	9.9%
PI 34:1	835.5342:0.851	0.60	-8.48E-05	C <sub>43</sub> H <sub>81</sub> O <sub>13</sub> P	4.3%	10.2%
PI 36:4	857.5186:0.854	1.40	-8.41E-05	C <sub>45</sub> H <sub>79</sub> O <sub>13</sub> P	20.9%	16.5%
PI 36:3	859.5342:0.850	2.91	-8.32E-05	C <sub>45</sub> H <sub>81</sub> O <sub>13</sub> P	6.0%	13.4%
PI 36:2	861.5499:0.847	1.97	-8.27E-05	C <sub>45</sub> H <sub>83</sub> O <sub>13</sub> P	15.3%	10.2%
PI 38:6	881.5186:0.850	2.38	-8.29E-05	C <sub>47</sub> H <sub>79</sub> O <sub>13</sub> P	0.5%	7.0%
PI 38:4	885.5499:0.849	0.23	-8.27E-05	C <sub>47</sub> H <sub>83</sub> O <sub>13</sub> P	100.0%	12.0%
PI 40:7	907.5342:0.847	0.66	-8.23E-05	C <sub>49</sub> H <sub>81</sub> O <sub>13</sub> P	3.0%	14.5%
PI 40:6	909.5499:0.845	1.23	-8.23E-05	C <sub>49</sub> H <sub>83</sub> O <sub>13</sub> P	11.0%	18.3%

<sup>a</sup> Normalized ion relative peak area ratio to most abundant lipid within class in pooled serum from NASH patients.

<sup>b</sup> Technical precision based on repeat analysis of pooled serum extracts from NASH patients as QC.

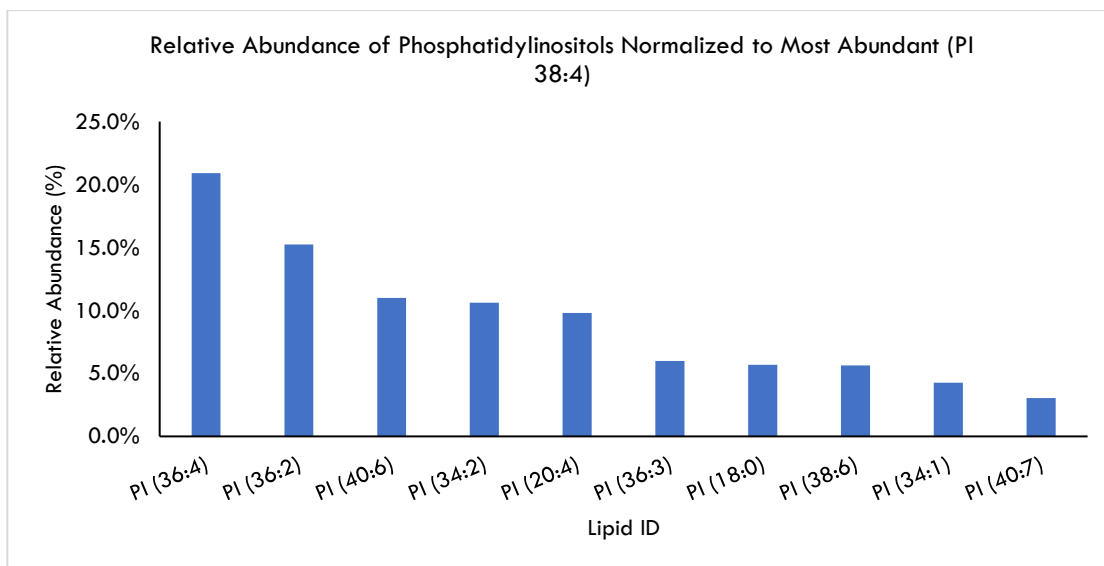


**Table S2.8.** Unknown serum lipid features that satisfied the three-tiered screening criteria in MSI-NACE-MS. Putative lipid classification assigned for anionic lipids within distinct clusters evident in the mobility map.

Molecular Formula	m/z:RMT	Tentative Classification	Electrophoretic Mobility (cm <sup>2</sup> /Vs)	Mean CV (%) <sup>a</sup>
C <sub>4</sub> H <sub>6</sub> O <sub>4</sub>	117.0193:1.196	Short-chain fatty acid	-1.51E-04	15.3%
C <sub>5</sub> H <sub>6</sub> O <sub>4</sub>	129.0193:1.198	Short-chain fatty acid	-1.54E-04	9.5%
C <sub>5</sub> H <sub>8</sub> O <sub>5</sub>	147.0299:1.054	Short-chain fatty acid	-1.26E-04	11.2%
C <sub>6</sub> H <sub>10</sub> O <sub>5</sub>	161.0455:1.197	Fatty acid derivative	-1.54E-04	5.1%
C <sub>11</sub> H <sub>20</sub> O <sub>2</sub>	183.1391:1.056	Fatty acid derivative	-1.31E-04	7.3%
C <sub>7</sub> H <sub>10</sub> O <sub>6</sub>	189.0405:1.092	Fatty acid derivative	-1.38E-04	5.3%
C <sub>12</sub> H <sub>18</sub> O <sub>2</sub>	193.1234:1.060	Unknown	-1.32E-04	7.7%
C <sub>11</sub> H <sub>16</sub> O <sub>3</sub>	195.1027:1.111	Fatty acid derivative	-1.40E-04	7.0%
C <sub>12</sub> H <sub>22</sub> O <sub>2</sub>	197.1547:1.061	Fatty acid derivative	-1.31E-04	8.9%
C <sub>14</sub> H <sub>26</sub> O <sub>2</sub>	225.1860:1.012	Fatty acid derivative	-1.24E-04	4.0%
C <sub>12</sub> H <sub>16</sub> O <sub>5</sub>	239.0925:1.113	Fatty acid derivative	-1.40E-04	6.5%
C <sub>12</sub> H <sub>16</sub> O <sub>6</sub>	255.0874:1.043	Fatty acid derivative	-1.27E-04	14.7%
C <sub>14</sub> H <sub>20</sub> O <sub>5</sub>	267.1238:1.091	Fatty acid derivative	-1.36E-04	4.1%
C <sub>17</sub> H <sub>32</sub> O <sub>2</sub>	267.2330:0.974	Fatty acid derivative	-1.15E-04	10.6%
C <sub>16</sub> H <sub>32</sub> O <sub>3</sub>	271.2279:1.202	Fatty acid derivative	-1.55E-04	6.8%
C <sub>18</sub> H <sub>32</sub> O <sub>3</sub>	295.2279:0.920	Fatty acid derivative	-1.02E-04	5.6%
C <sub>17</sub> H <sub>30</sub> O <sub>4</sub>	297.2071:1.001	Fatty acid derivative	-1.21E-04	6.7%
C <sub>17</sub> H <sub>34</sub> O <sub>4</sub>	301.2384:0.980	Fatty acid derivative	-1.16E-04	28.4%
C <sub>20</sub> H <sub>28</sub> O <sub>3</sub>	315.1966:0.949	Unknown	-1.10E-04	24.2%
C <sub>18</sub> H <sub>36</sub> O <sub>4</sub>	315.2541:0.980	Fatty acid derivative	-1.16E-04	13.7%
C <sub>20</sub> H <sub>30</sub> O <sub>3</sub>	317.2122:0.941	Fatty acid derivative	-1.07E-04	11.2%
C <sub>20</sub> H <sub>32</sub> O <sub>3</sub>	319.2279:0.936	Fatty acid derivative	-1.07E-04	12.9%
C <sub>20</sub> H <sub>34</sub> O <sub>3</sub>	321.2435:0.915	Fatty acid derivative	-1.01E-04	29.9%
C <sub>19</sub> H <sub>34</sub> O <sub>4</sub>	325.2384:0.971	Unknown	-1.14E-04	15.0%
C <sub>18</sub> H <sub>34</sub> NO <sub>4</sub>	328.2493:0.964	Unknown	-1.13E-04	12.0%
C <sub>18</sub> H <sub>34</sub> O <sub>5</sub>	329.2334:0.874	Fatty acid derivative	-9.10E-05	15.7%
C <sub>20</sub> H <sub>32</sub> O <sub>4</sub>	335.2228:0.902	Fatty acid derivative	-9.82E-05	11.9%
C <sub>19</sub> H <sub>36</sub> O <sub>5</sub>	343.2490:0.876	Unknown	-9.10E-05	10.7%
C <sub>22</sub> H <sub>34</sub> O <sub>3</sub>	345.2435:0.913	Unknown	-1.01E-04	14.8%
C <sub>22</sub> H <sub>32</sub> O <sub>4</sub>	359.2228:0.911	Unknown	-1.01E-04	13.9%
C <sub>22</sub> H <sub>34</sub> O <sub>4</sub>	361.2384:0.889	Unknown	-9.28E-05	11.5%
C <sub>24</sub> H <sub>40</sub> O <sub>4</sub>	391.2854:0.872	Bile acid	-8.98E-05	11.1%
C <sub>27</sub> H <sub>44</sub> O <sub>3</sub>	415.3218:0.870	Unknown	-9.20E-05	10.2%
C <sub>27</sub> H <sub>49</sub> O <sub>3</sub>	421.3687:0.870	Unknown	-9.18E-05	30.0%
C <sub>28</sub> H <sub>45</sub> O <sub>4</sub>	445.3323:1.024	Unknown	-1.28E-04	12.3%
C <sub>21</sub> H <sub>44</sub> N <sub>2</sub> O <sub>8</sub>	451.3029:0.872	Unknown	-9.18E-05	9.7%
C <sub>28</sub> H <sub>48</sub> O <sub>5</sub>	463.3429:1.014	Fatty acid derivative	-9.54E-05	13.0%
C <sub>31</sub> H <sub>45</sub> N <sub>2</sub> P	475.3252:0.855	Unknown	-8.76E-05	14.3%
C <sub>30</sub> H <sub>49</sub> O <sub>5</sub>	489.3585:1.003	Unknown	-1.21E-04	15.3%
C <sub>34</sub> H <sub>64</sub> O <sub>4</sub>	535.4732:0.973	Fatty acid derivative	-1.16E-04	9.5%
C <sub>34</sub> H <sub>65</sub> N <sub>3</sub> O <sub>3</sub>	562.4953:0.968	Unknown	-1.16E-04	18.8%
C <sub>34</sub> H <sub>67</sub> N <sub>3</sub> O <sub>3</sub>	564.5110:0.965	Unknown	-1.16E-04	20.8%
C <sub>36</sub> H <sub>62</sub> O <sub>5</sub>	573.4524:0.987	Unknown	-1.16E-04	11.2%
C <sub>32</sub> H <sub>65</sub> NO <sub>5</sub> S	574.4511:0.992	Unknown	-6.74E-05	9.2%
C <sub>32</sub> H <sub>40</sub> O <sub>10</sub>	583.2549:1.163	Unknown	-1.51E-04	5.1%
C <sub>34</sub> H <sub>55</sub> O <sub>8</sub>	591.3902:0.889	Unknown	-9.64E-05	6.3%
C <sub>38</sub> H <sub>75</sub> NO <sub>3</sub>	592.5674:0.978	Unknown	-1.18E-04	7.5%
C <sub>40</sub> H <sub>77</sub> NO <sub>3</sub>	618.5831:0.963	Unknown	-1.15E-04	5.3%

<sup>a</sup> Technical precision based on repeat analysis of pooled serum extracts from NASH patients as QC

**Table S2.9.** Top-ranked serum lipids differentially expressed in NASH patient sub-groups following cluster analysis that satisfied Bonferroni correction ( $p < 3.90 \times 10^{-4}$ ) and covariate adjustment.

Tentative ID <sup>a</sup>	Lipid Classification <sup>a</sup>	m/z:RMT	p-value <sup>b</sup>	Effect Size <sup>c</sup>	FC <sup>d</sup>
Palmitic acid (16:0)	Fatty acid	255.2330:0.982	$3.43 \times 10^{-10}$	0.411	1.95
C <sub>38</sub> H <sub>75</sub> NO <sub>3</sub>	Unknown	592.5674:0.978	$1.23 \times 10^{-9}$	0.391	1.75
C <sub>18</sub> H <sub>36</sub> O <sub>4</sub>	Fatty acid derivative	315.2541:0.977	$1.53 \times 10^{-9}$	0.387	2.07
C <sub>40</sub> H <sub>77</sub> NO <sub>3</sub>	Unknown	618.5831:0.963	$7.39 \times 10^{-9}$	0.362	2.29
22:4	Fatty acid	331.2643:0.944	$9.03 \times 10^{-9}$	0.358	1.87
Margaric acid (17:0)	Fatty acid	269.2486:0.968	$1.04 \times 10^{-8}$	0.356	1.46
Pentadecanoic acid (15:0)	Fatty acid	241.2173:0.990	$1.30 \times 10^{-8}$	0.352	1.82
Myristic acid (14:0)	Fatty acid	227.2016:1.004	$1.39 \times 10^{-8}$	0.351	2.07
Linoleic acid (18:2)	Fatty acid	279.2330:0.969	$1.42 \times 10^{-8}$	0.351	1.77
C <sub>21</sub> H <sub>34</sub> O <sub>5</sub>	Prostaglandin	365.2334:0.964	$2.18 \times 10^{-8}$	0.343	2.43
Oleic acid (18:1)	Fatty acid	281.2486:0.965	$4.49 \times 10^{-8}$	0.331	1.88
C <sub>17</sub> H <sub>32</sub> O <sub>2</sub>	Fatty acid derivative	267.2330:0.974	$6.12 \times 10^{-8}$	0.325	1.85
DHA (22:6)	Fatty acid	327.2330:0.977	$6.87 \times 10^{-8}$	0.323	2.22
C <sub>34</sub> H <sub>67</sub> N <sub>3</sub> O <sub>3</sub>	Unknown	564.5110:0.965	$1.41 \times 10^{-7}$	0.311	3.66
C <sub>34</sub> H <sub>63</sub> O <sub>4</sub>	Unknown	535.4732:0.973	$1.81 \times 10^{-7}$	0.306	2.84
Palmitoleic acid (16:1)	Fatty acid	253.2173:0.989	$1.97 \times 10^{-7}$	0.305	2.17
C <sub>34</sub> H <sub>65</sub> N <sub>3</sub> O <sub>3</sub>	Unknown	562.4953:0.968	$5.80 \times 10^{-7}$	0.285	3.08
$\alpha$ -Linoleic acid (18:3)	Fatty acid	277.2173:0.972	$1.40 \times 10^{-6}$	0.268	1.85
16:2	Fatty acid	251.2017:0.997	$1.86 \times 10^{-6}$	0.263	1.64
C <sub>17</sub> H <sub>34</sub> O <sub>4</sub>	Fatty acid derivative	301.2384:0.979	$6.23 \times 10^{-6}$	0.240	1.52
20:1	Fatty acid	309.2799:0.942	$9.55 \times 10^{-6}$	0.231	1.84
Stearic acid (18:0)	Fatty acid	283.2642:0.958	$1.28 \times 10^{-5}$	0.225	1.37
C <sub>18</sub> H <sub>35</sub> NO <sub>4</sub>	Unknown	328.2493:0.964	$1.49 \times 10^{-5}$	0.222	2.32
Tridecanoic acid (13:0)	Fatty acid	213.1860:1.018	$2.33 \times 10^{-5}$	0.214	1.37
Arachidonic acid (20:4)	Fatty acid	303.2330:0.975	$2.91 \times 10^{-5}$	0.209	1.57
Mead acid (C20:3)	Fatty acid	305.2486:0.956	$4.12 \times 10^{-5}$	0.202	1.51
DPA (22:5)	Fatty acid	329.2486:0.946	$8.93 \times 10^{-5}$	0.186	1.94
C <sub>19</sub> H <sub>36</sub> O <sub>4</sub>	Fatty acid derivative	327.2541:0.964	$1.45 \times 10^{-4}$	0.176	1.72
20:2	Fatty acid	307.2643:0.949	$2.86 \times 10^{-4}$	0.162	1.59

<sup>a</sup> Tentative IDs assigned after LIPIDMAPS database search using mobility map to cross-reference, whereas molecular formulas were assigned for unknowns without ambiguous classification in mobility map.

<sup>b</sup> p-values obtained using ANCOVA and adjusted for age, sex, BMI, diabetes, hyperlipidemia and hypertension as covariates.

<sup>c</sup> Effect sizes calculated using partial eta square where small effects > 0.001, medium effects > 0.060 and large effects > 0.14.

<sup>d</sup> Mean fold change (FC) is calculated as the ratio of Cluster B/Cluster A

### **Chapter III**

## **Expanding Lipidomic Coverage in Multisegment Injection-Nonaqueous Capillary Electrophoresis-Mass Spectrometry via a Convenient and Quantitative Methylation Strategy**

*Ritchie Ly, Lucas Christian Torres, Nicholas Ly, Philip Britz-McKibbin*

*Department of Chemistry and Chemical Biology, McMaster University, Hamilton,  
Canada L8S 4M1*

R.L performed all the experiments including sample preparation, data acquisition using MSI-NACE-MS, data processing, interpretation, statistical analysis and wrote the initial draft for publication. L.C.T and N.L assisted in the method development, sample preparation, data processing and interpretation. P.B.M wrote and provided feedback on the manuscript draft.

### 3.1. Abstract

Orthogonal separation techniques coupled to high-resolution mass spectrometry (MS) are required for characterization of the human lipidome given its inherent chemical and structural complexity. Although various chromatographic and ion mobility methods are used to resolve diverse lipid molecular species, electrophoretic separations remain largely unrecognized in untargeted lipidomics research. Herein, we introduce a novel two-step derivatization strategy using 3-methyl-1-*p*-tolyltriazene (MTT) as a safer alternative to diazomethane for quantitative phospholipid methylation (~ 90%), which enables the rapid analysis of cationic lipids by multisegment injection-nonaqueous capillary electrophoresis-mass spectrometry (MSI-NACE-MS). Isobaric interferences and ion suppression effects were minimized by performing an initial reaction using 9-fluorenylmethoxycarbonyl chloride on methyl-*tert*-butyl ether lipid extracts with a subsequent back extraction in hexane. This charge-switch derivatization strategy and sample workup procedure expands lipidome coverage when using MSI-NACE-MS under positive ion mode detection with improved resolution, greater sensitivity and higher throughput (~ 3.5 min/sample), notably for zwitterionic phospholipids that otherwise co-migrate close to the electroosmotic flow. Our method was optimized and validated by analyzing lipid ether extracts from a Standard Reference Material (SRM)-1950 human plasma, which allowed for a direct comparison of 53 phosphatidylcholine and 30 sphingomyelin species consistently reported from an inter-laboratory lipidomics harmonization study. The potential for reliable phospholipid quantification using chemical standards or relying on a serial dilution of SRM-1950 for estimation of relative response



factors was also demonstrated, whereas lipid identification was supported by their characteristic apparent electrophoretic mobility in conjunction with MS/MS. Complementary analysis of other anionic or polar lipid classes not suitable for methylation and hexane back extraction (*e.g.*, free fatty acids, phosphatidylinositols, phosphatidylethanolamines) can be achieved by their direct analysis using MSI-NACE-MS under negative ion mode conditions using a separate underivatized aliquot. Overall, this work introduces a practical derivatization strategy and standardized protocol that allows for the rapid determination of zwitter-ionic phospholipids using MSI-NACE-MS as required for large-scale lipidomic studies.

### **3.2. Introduction**

The human lipidome comprises a bewildering number of lipid molecular species present in tissues, cells or biofluids, which are defined by their specific polar head group, chemical linkage, fatty acid carbon chain length, number of double bond equivalents, oxygenated fatty acyls, and regio-/stereochemistry.<sup>1,2</sup> As lipid homeostasis plays an important role in energy metabolism, membrane structure, and cell signalling, dysregulation in lipid metabolism (*i.e.*, dyslipidemia) has long been associated with inflammation and the etiology of various cardiometabolic disorders, ranging from obesity, type 2 diabetes, cardiovascular and neurodegenerative diseases.<sup>3,4</sup> Lipidomic studies have also gained traction in nutritional epidemiology as objective indicators of food exposures given the key role of essential dietary fats and fat-soluble vitamins in human health<sup>5</sup> that are not accurately assessed from self-reports.<sup>6</sup> For these reasons, there has been expanding interests in developing mass spectrometry (MS) based methods for untargeted lipid

profiling<sup>7</sup> as a hypothesis-generating approach for gaining new insights into disease mechanisms.<sup>8</sup> However, many technical hurdles impede progress in lipidomics given the lack of chemical standards and reference MS/MS spectra that impact comparative quantitative reporting while also hindering identification of unknown lipids of clinical significance.<sup>9</sup> Recent efforts have focused on developing consensus guidelines in lipid classification and annotation,<sup>10,11</sup> the use of internal standards for data normalization,<sup>12</sup> automated data processing with open-access software tools,<sup>13,14</sup> as well as standardized lipidomic protocols assessed by inter-laboratory ring trials using reference and quality control samples.<sup>15–17</sup> Nevertheless, all aspects of a lipidomics data workflow require careful optimization to avoid bias depending on the specific biospecimen type and analytical platform, including sample pretreatment.<sup>18</sup>

Classical methods for lipid profiling of biological samples have relied on the analysis of esterified fatty acids from lipid hydrolysates using gas chromatography (GC)-MS.<sup>19</sup> However, comprehensive analysis of intact phospholipids was first achieved by MS when using soft ionization methods based on matrix-assisted laser desorption/ionization and electrospray ionization (ESI).<sup>20</sup> Although shotgun lipidomics enables the direct analysis of lipid extracts by direct infusion (DI)-ESI-MS,<sup>21</sup> high efficiency separations are needed to improve method selectivity while reducing isobaric interferences, ion suppression effects and/or generation of artifact signals.<sup>22</sup> To date, liquid chromatography (LC)-MS is the instrumental platform of choice in contemporary lipidomics research.<sup>23</sup> However, LC-MS protocols vary substantially in terms of operation conditions (e.g., column types, elution conditions etc.) used to resolve different lipid species primarily by

reversed-phase, normal-phase and/or hydrophilic interaction chromatography (HILIC).<sup>24,25</sup> For instance, greater sample throughput, separation resolution and/or reproducibility can be achieved in reversed-phase LC-MS lipidomic analyses using core shell particles,<sup>26</sup> vacuum jacked columns,<sup>27</sup> capillaries operated under ultra-high pressure conditions,<sup>28</sup> and via multidimensional separations.<sup>29</sup> Alternatively, supercritical fluid chromatography-MS offers faster separations and broader selectivity for resolving lipids that vary in their polarity with slightly higher robustness than HILIC-MS.<sup>30</sup> Also, ion mobility-MS offers ultra-fast separation times with adequate selectivity to generate a lipidome atlas for confirmatory annotation of phospholipids.<sup>31</sup> On the other hand, nonaqueous capillary electrophoresis-mass spectrometry (NACE-MS) is not an recognized separation technique used in the lipidomics community likely due to a paucity of published studies reported for certain ionic lipids, such as saturated fatty acids<sup>32</sup> lipid A isomers<sup>33</sup> and glycerophospholipids.<sup>34,35</sup> Indeed, a lack of robust NACE-MS protocols, limited vendor support, and sparse method validation in comparison to existing chromatographic methods have deterred its use as a viable separation platform for untargeted lipid profiling.

Recently, we have introduced multisegment injection-nonaqueous capillary electrophoresis mass spectrometry (MSI-NACE-MS) as a multiplexed separation platform for quantitative determination of fatty acids from blood specimens<sup>6,36,37</sup> which can also resolve a broader range of anionic lipids under negative ion mode conditions.<sup>38</sup> Serial injection of seven or more samples within a single capillary allows for higher sample throughput<sup>39</sup> together with temporal signal pattern recognition in ESI-MS<sup>40</sup> for rigorous molecular feature selection and lipid authentication when using untargeted profiling.<sup>38</sup>

However, separation resolution and selectivity was limited for phosphatidylcholines (PC) and other classes of zwitterionic lipids that migrate close to the electroosmotic flow (EOF). Pre-column chemical derivatization strategies have previously been applied to introduce or switch charge states on specific lipid classes as a way to modify their chromatographic retention, reduce isobaric interferences, and improve ionization efficiency with lower detection limits in ESI-MS.<sup>41</sup> For instance, Smith *et al.*<sup>42–44</sup> have used diazomethane for charge inversion on modified cationic phospholipids via methylation to improve sensitivity, selectivity, as well as structural information via collision-induced dissociation in MS/MS. However, given the explosive nature and toxicity hazards of diazomethane,<sup>45</sup> safer methylating agents are required for routine MS-based lipidomic analyses without blast shields and other personal protective equipment. Herein, we introduce a novel two-step chemical derivatization strategy for the quantitative methylation of phospholipids based on 9-fluorenylmethoxycarbonyl chloride (Fmoc) followed by 3-methyl-1-*p*-tolyltriazene (MTT) labeling as a practical way to expand coverage of zwitterionic phospholipids in MSI-NACE-MS. For the first time, we demonstrate that this procedure enables rapid determination (~ 3 min/sample) of methylated phosphatidylcholines and sphingomyelins from SRM-1950 reference plasma sample extracts with acceptable precision and accuracy comparable to existing LC-MS methodologies.<sup>15</sup>

### **3.3. Experimental**

#### **3.3.1 Chemicals and Materials.**

Ultra LC-MS grade methanol, acetonitrile, water and 2-propanol were used to prepare the sheath liquid and the background electrolyte (BGE). Ammonium formate,

formic acid, 1,2-distearoyl-d70-sn-glycero-3-phosphocholine (18:0 PC-d<sub>70</sub>), 1,2-dipalmitoyl-d62-sn-glycero-3-phosphocholine (16:0 PC-d<sub>62</sub>), methyl-*tert*-butyl ether (MTBE), MTT, Fmoc and all other chemical standards were purchased from Sigma-Aldrich Inc. (St. Louis, MO, USA) unless otherwise stated. All lipid standards purchased were either as a powder or dissolved in solution (1:1) of chloroform and methanol. Stock solutions for lipids were then diluted in chloroform and methanol and stored at -80 °C prior to further use. Reference material from the National Institute of Standards and Technology (NIST) SRM-1950 pooled human plasma was purchased from the NIST (Gaithersburg, MD, USA). While certified reference values for SRM-1950 have been reported for several metabolites by NIST, plasma lipids measured in this study were compared to consensus values for SRM-1950 reported in an international study across 31 laboratories that adopted various LC-MS/MS lipidomic workflows,<sup>15</sup> as well as a targeted harmonization study using standardized p400-HR commercial kits for shotgun lipidomics by DI-MS/MS in 14 laboratories worldwide.<sup>17</sup>

### **3.3.2 Plasma Lipid Extraction Using MTBE.**

Plasma samples and lipid calibrant solutions were extracted using a slightly modified MTBE-based liquid extraction procedure previously described for fatty acids and anionic lipids using MSI-NACE-MS in negative ion mode conditions.<sup>36,38</sup> Briefly, 50 µL of a plasma aliquot was mixed with 100 µL of methanol containing PC 16:0-d<sub>62</sub> as a recovery standard and shaken for 10 min. Then, 250 µL of MTBE was added and the mixture was subject to vigorous shaking for 10 min. To induce phase separation, 100 µL of deionized water was then added prior to centrifugation at 10 min at 4000 g. Next, 200

$\mu\text{L}$  of the lipid-rich MTBE layer was transferred into another vial and dried down at room temperature using an Organomation MULTIVAP<sup>®</sup> nitrogen evaporator (Berlin, MA, USA). For underivatized lipids, the dried plasma extracts were then reconstituted to a volume of 50  $\mu\text{L}$  containing acetonitrile/isopropanol/water (70:20:10) with 10 mM ammonium formate containing internal standards PC 18:0-d<sub>70</sub> (5  $\mu\text{M}$ ), benzyltriethylammoniumchloride (BTA) (1  $\mu\text{M}$ ), and of PC 16:0-d<sub>62</sub> (5  $\mu\text{M}$ ) prior to analysis by MSI-NACE-MS.

### **3.3.3 Chemical Derivatization of Zwitterionic Phospholipids Using FMOC and MTT.**

All plasma ether extracts and lipid calibrants were subject to a two-step chemical labeling procedure involving FMOC and MTT. In 2 mL glass vials, ether extracts are subject to 100  $\mu\text{L}$  of 0.85 mM FMOC in chloroform and shaken vigorously for 5 min. Afterwards, samples are blown down to dryness using nitrogen at room temperature prior to reconstitution in 50  $\mu\text{L}$  of MTBE containing 450 mM of MTT. Vials are sealed with Teflon tape and vortexed for 30 s prior to derivatization at 60 °C for 60 min. While reactions were ideally carried out in amber vials to prevent oxidation, solutions noticeably had a darker yellow colour than the original MTT derivatization solution. Afterwards, 100  $\mu\text{L}$  of MeOH, 250  $\mu\text{L}$  of hexane and 200  $\mu\text{L}$  of deionized water was added to back extract polar by-products of the reaction (*e.g.*, p-toluidine). After centrifuging for 10 min at 4000 g, 200  $\mu\text{L}$  of hexane as the supernatant was transferred out to a separate glass vial and then evaporated to dryness under nitrogen. Once completely dried, samples were subsequently reconstituted in 50  $\mu\text{L}$  containing acetonitrile/isopropanol/water (70:20:10) with 10 mM ammonium formate containing internal standards PC 18:0-d<sub>70</sub> (5  $\mu\text{M}$ ) and

benzyltriethylammoniumchloride (BTA) (1  $\mu$ M, and of PC 16:0-d<sub>62</sub> (5  $\mu$ M) prior to analysis by MSI-NACE-MS. Derivatization yields for chemically modified methylated cationic lipids from plasma extracts were calculated using the following formula based on the integrated relative peak area (RPA) for each phospholipid (PL) species relative to PC 18:0-d<sub>70</sub> as an internal standard using equation (1):

$$\% \text{ Derivatization Yield} = 100 * \left( 1 - \frac{\text{FMOc \& MTT treated PL RPA}}{\text{Untreated PL RPA}} \right) \quad (1)$$

### 3.3.4 CE-MS Instrumentation and Serial Injection Configuration.

An Agilent 6230 time-of-flight (TOF) mass spectrometer with a coaxial sheath liquid electrospray (ESI) ionization source equipped with an Agilent G7100A CE unit was used for all experiments (Agilent Technologies Inc., Mississauga, ON, Canada). An Agilent 1260 Infinity isocratic pump and a 1260 Infinity degasser were utilized to deliver an 80:20 MeOH-water with 0.1% vol formic acid at a flow rate of 10  $\mu$ L/min using a CE-MS coaxial sheath liquid interface kit. For mass correction in real-time, the reference ions purine and hexakis(2,2,3,3-tetrafluoropropoxy)phosphazine (HP-921) were spiked into the sheath liquid at 0.02% vol to provide constant mass signals at  $m/z$  121.0509 and 922.0098, which were utilized for monitoring ion suppression and/or enhancement effects. During sample introduction into the capillary, the nebulizer gas was turned off to prevent siphoning effects that may contribute to air bubbles and current errors upon voltage application.<sup>36</sup> This was subsequently turned on at a low pressure of 4 psi (27.6 kPa) following voltage application with the ion source operating at 300 °C with a drying gas of nitrogen that was delivered at 4 L/min. The TOF-MS was operated in 2 GHz extended dynamic range under positive

mode detection. A  $V_{\text{cap}}$  was set at 3500 V while the fragmentor was 120 V, the skimmer was 685 V and the octopole rf was 750 V. All separations were performed using bare fused-silica capillaries with 50  $\mu\text{m}$  internal diameter, a 360  $\mu\text{m}$  outer diameter, and 100 cm total length (Polymicro Technologies Inc., AZ). A capillary window maker (MicroSolv, Leland, NC) was used to remove 7 mm of the polyimide coating on both ends of the capillary to prevent polyimide swelling with organic solvents in the background electrolyte (BGE) or aminolysis under alkaline nonaqueous buffer conditions.<sup>46</sup> An applied voltage of 30 kV was used for CE separations at 25 °C together while using a forward pressure of 5 mbar (0.5 kPa). The BGE was 35 mM ammonium formate in 70% vol acetonitrile, 15% vol methanol, 10% vol water and 5% vol isopropanol with an apparent pH of 2.3 adjusted with the addition of formic acid. Derivatized plasma extracts and lipid standards were introduced in-capillary hydrodynamically at 50 mbar (5 kPa) alternating between 5 s for each sample plug and 40 s for the BGE spacer plug for a total of seven discrete samples analyzed within a single run.<sup>38</sup> Prior to first use, capillaries were subject to a conditioning protocol by flushing at 950 mbar (95 kPa) with MeOH, 0.1 M sodium hydroxide, deionized water, then BGE sequentially for 15 min each. BGE and sheath liquid were degassed prior to use. For analysis of NIST SRM-1950 by MSI-NACE-MS in negative ion mode to verify acidic lipids not amenable by the FMOC/MTT procedure, an alkaline BGE with the same organic solvent composition was used, but with ammonium acetate and ammonium hydroxide as the background electrolyte and pH modifier respectively.<sup>36</sup> In this context, the same MTBE extraction protocol was applied, but concentrated two-fold without the use of FMOC/MTT chemical derivatization.



### 3.4. Results and Discussion

#### 3.4.1 Separation Performance Enhancement After Phospholipid Methylation.

A two-step charge-switch chemical derivatization strategy using FMOc/MTT was developed to generate a permanent positive charge on methylated phospholipids (mPLs) to increase their positive electrophoretic mobility on formerly zwitterionic species, such as phosphatidylcholines (PCs) as depicted in **Figure 3.1(a)**. FMOc was first added as a protecting agent to rapidly react (< 5 min) with phosphatidylethanolamines (PEs) from plasma ether extracts since they can generate isobaric interferences with analogous PCs following their permethylation<sup>44</sup> In this case, MSI-NACE-MS under negative ion mode detection can directly analyze native PEs and other acidic lipids without derivatization.<sup>38</sup> FMOc not only reacts with PE species from plasma extract, but also with excess MTT by-product (*i.e.*, p-toluidine) to form a neutral adduct as shown in the reaction mechanism in **Figure S3.1**. We have provided evidence of p-toluidine reactivity with excess FMOc (**Figure S3.2**) together with its impact on reducing ion suppression effects when using excess MTT following back extraction of mPLs in hexane that was superior to MTBE (**Figure S3.1**) prior to analysis by MSI-CE-MS. Importantly, methylation of phosphoric acid residues on PLs expands the separation window by improving the resolution within lipid class species as demonstrated or mPCs in **Figure 3.1(b)**. Furthermore, mPL species avoid ion suppression effects that occur within the EOF due to co-migration of abundant and electrically neutral plasma lipids (*e.g.*, cholesterol esters, diacylglycerides) while reducing migration times and improving sensitivity with sharper peak shapes. In all cases, a serial injection of seven plasma extracts were analyzed rapidly within a single run by

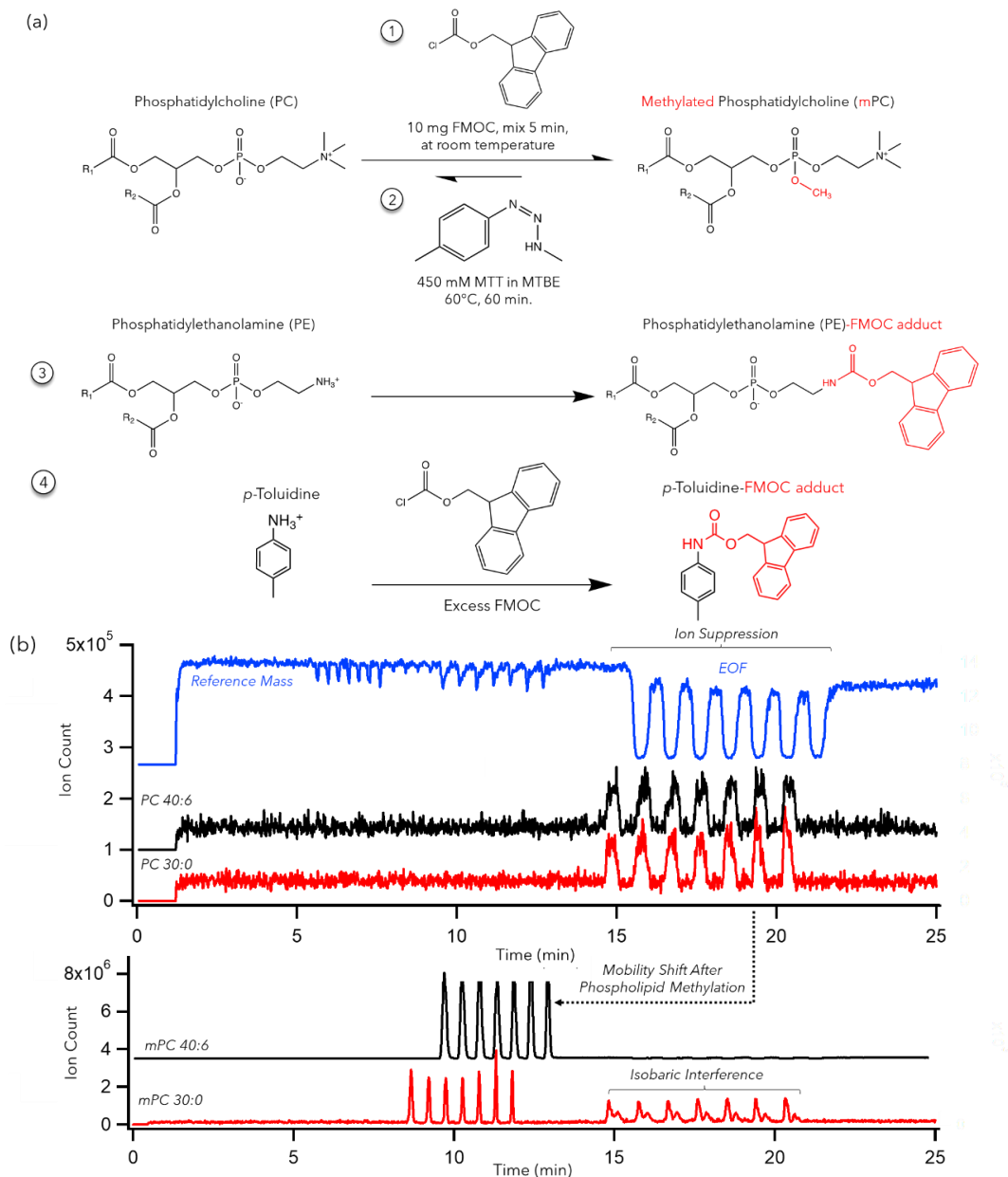


**Figure 3.1.** (a) Overview of FMOC/MTT derivatization scheme that is used as a safer alternative to diazomethane for methylation of phosphate esters to render zwitter-ionic PLs with a net cationic charge as their mPLs. The initial addition of excess FMOC is used react with interfering PEs that may become isobaric with PCs following methylation while also reacting with p-toluidine as major by-product in reaction to reduce ion suppression effects prior to hexane back extraction. (b) Series of extracted ion electropherograms in MSI-NACE-MS under positive ion mode that highlight the large mobility shift that occurs following PL methylation, where cationic mPCs migrate faster prior to the EOF that is prone to ion suppression due to co-migrating neutral plasma lipids. Also, mPCs migrate as sharper peaks resulting in greater concentration sensitivity and better separation resolution as compared to native PCs without chemical derivatization.

MSI-CE-MS (~ 3.5 min/sample) under positive ion mode detection when using full-scan data acquisition. This method is also able to measure methylated sphingomyelin species (mSMs), which also undergo a distinct mobility and mass shift (+14 Da) as shown in their MS/MS spectra acquired under positive and negative ion modes (**Figure S3.4**). Indeed, it has been reported that SM can be methylated a second equivalent on their hydroxyl moiety when using diazomethane, which results in signal splitting and lower sensitivity gain.<sup>42</sup> In our work, dimethylated mSM species were not detected likely due to the lower reactivity of MTT as compared to diazomethane, which does not share the same acute toxicity concerns and explosive workplace hazards.<sup>42-44</sup>

### **3.4.2 Optimization of FMOC/MTT Phospholipid Derivatization.**

MTT was originally reported as a methylation agent for esterification of carboxylic acids<sup>47</sup> that allowed for the analysis of acidic metabolites in urine by GC-MS.<sup>48</sup> Recently, Furukawa *et al.*<sup>49</sup> reported using MTT to methylate oligosaccharides containing sialic acid residues in glycoblotting experiments prior to MALDI-MS analyses. However, this reagent remains unexplored with little information on its reaction mechanism and suitability for comprehensive lipidomic analyses. Importantly, MTT represents a safer liquid reagent to handle as compared to diazomethane that is also commercially available and relatively inexpensive. Initial studies to explore yield optimization of mPLs involved the variation of three key experimental factors, including reaction time (0 to 180 min), MTT concentration (50 to 900 mM) and reaction temperature (20 to 100 °C). This preliminary study demonstrated that maximum yield for mPLs was achieved at 450 mM of MTT, with

a reaction time of 60 min at 60 °C that consistently peaked on average at ~ 70% yield (and as low as 40%) without the use of FMOc given its role on minimizing ionization suppression when using high concentrations of MTT. A kinetic study was next performed to determine that the optimal reaction time when using a two-step chemical derivatization strategy with FMOc/MTT, where progress of the chemical derivatization was evident by a more intense golden/amber hue with longer reaction times as shown in **Figure 3.2(a)**. Optimization of product yield was demonstrated when analyzing the average yield for 16 representative plasma mPC species at 20 min time intervals, where the reaction yield plateaus at 60 min as highlighted in **Figure 3.2(b)**. The incorporation of FMOc not only alleviated the issue of isobaric lipid interference and ion suppression effects after hexane back extraction but resulted in higher and more consistent quantitative yields ( $90.1 \pm 6.4\%$ ) as demonstrated in **Figure 3.2(c)**. In some instances, this nearly doubled the conversion efficiency for certain mPC (*e.g.*, PC 36:5, PC 36:4, PC 40:6) where they only reached a maximum of ~ 45% conversion prior to the introduction of FMOc. In all cases, the derivatization yield was assessed by taking the ratio of the normalized signals of underivatized PC in both a FMOc/MTT treated and untreated sample (refer to equation 1) when using a single sample injection of plasma extract in NACE-MS. In evaluating this, we ensured that PC resolution from the EOF was attained as to not influence signal attenuation that may result in the appearance of higher yields due to suppression of signal as highlighted in **Figure 3.2(d)**. One limitation of use of the hexane washing step on plasma extracts following FMOc/MTT derivatization was that more polar lipid classes were not adequately extracted, including shorter-chain PCs (< C30:0) and lysophosphatidylcholines

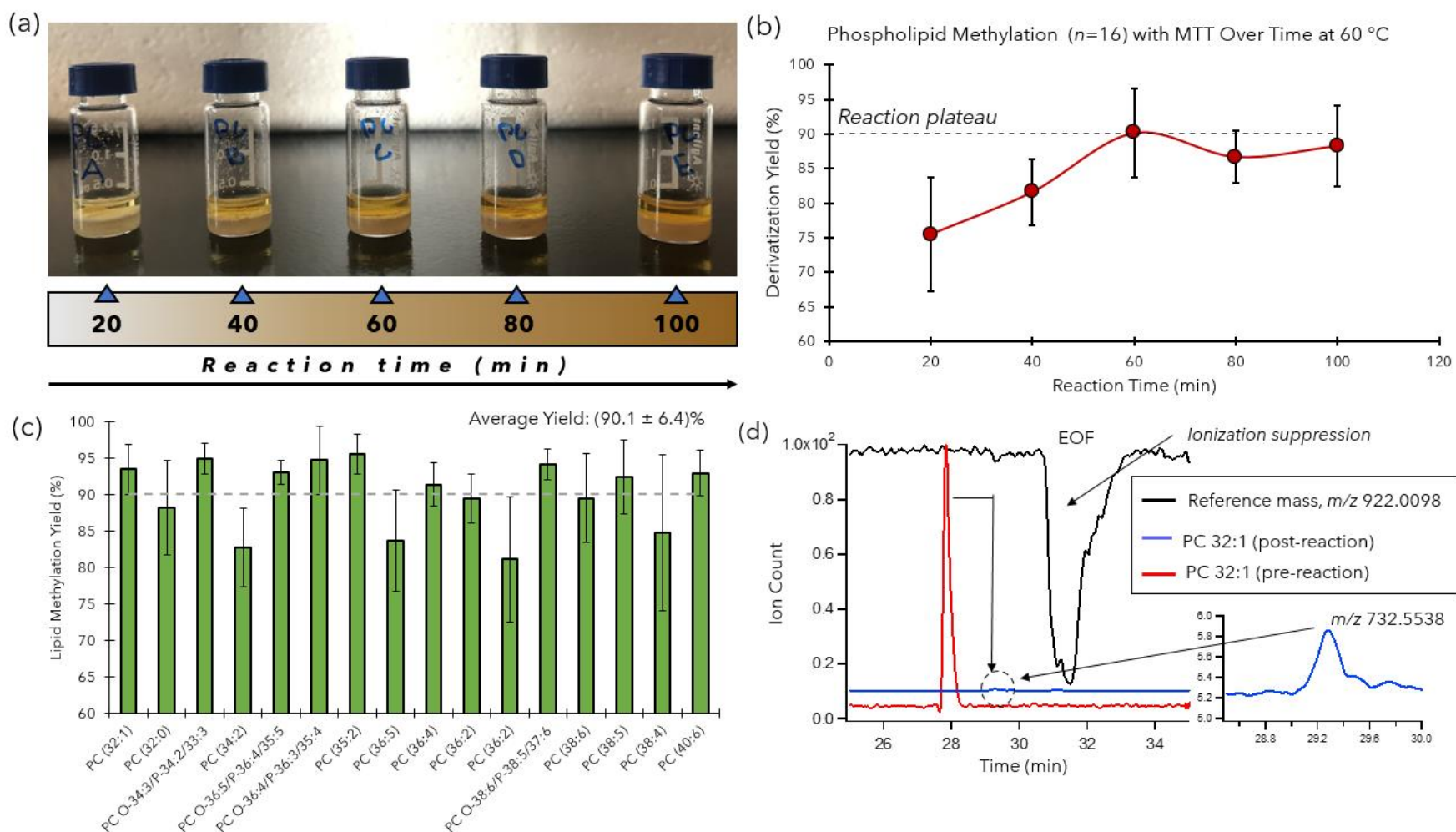


**Figure 3.2.** (a) Optimization of FMOc/MTT derivatization conditions as a function of reaction time that highlights a visible change in yellow color intensity with longer reaction times. (b) A minimum reaction time of 60 min at 60 °C was determined to generate a quantitative and stable yield of mPCs from reference plasma extracts based on analysis of 16 representative PCs in NIST SRM-1950. (c) Bar graphs that compare the average yield of mPCs (~ 90%) in reference plasma extracts, where errors bars represent standard deviation ( $\pm 1s$ ,  $n=5$ ). (d) Representative extracted ion electropherograms highlighting the quantitative yield of mPCs without ion suppression, where reaction yields were assessed on native PCs from plasma reference samples analyzed prior and after FMOc/MTT labeling using NACE-MS with a single sample injection to avoid co-migration with the EOF.

(lysoPCs) which were not detected as their mPCs or had poor precision due to their low abundance. However, most of these polar PC species can be directly analyzed when using MSI-NACE-MS under negative ion mode detection as their acetate adducts without the use of derivatization.<sup>38</sup>

### 3.4.3. Expanded Lipidome Coverage and Classification Via Mobility Maps.

Similar to the use of collisional cross-section areas for classifying lipid structures as gas-phase ions in IMS,<sup>31</sup> the apparent electrophoretic mobility represents an intrinsic physicochemical parameter for classifying ionic lipids in solution by MSI-NACE-MS.<sup>38</sup> Zwitter-ionic PC species that migrated before the EOF under alkaline BGE conditions substantially overlapped with each other resulting in a more narrow separation window as compared to acidic lipids, such as PEs, phosphatidylinositols (PIs), lysophosphatidic acids (PAs), free fatty acids (FFAs). While largely detectable, this scenario was suboptimal due to the greater potential for ion suppression and isobaric interferences that can contribute to false discoveries when performing untargeted lipidomics. In this context, we applied the same modelling principles using the characteristic electromigration behaviour of derivatized mPLs to support their between and within class annotation. **Figure 3.3(a)** highlights that large mobility shift and improved separation resolution that occurs following FMOC/MTT chemical derivatization for two major classes of reactive PLs, namely mPCs ( $n=50$ ) and mSMs ( $n=27$ ). These NIST SRM-1950 plasma mPLs were largely annotated based on their sum composition with low mass error ( $< 5$  ppm) and characteristic relative migration times (RMTs) or electrophoretic mobilities (**Table S3.1, S3.2**) with select mPLs further characterized by MS/MS. Moreover, these mPLs also satisfied our selection criteria when using temporal signal pattern recognition in MSI-NACE-MS to reject spurious signals and background ions,<sup>38</sup> while also being previously reported as consensus lipids consistently measured in an inter-

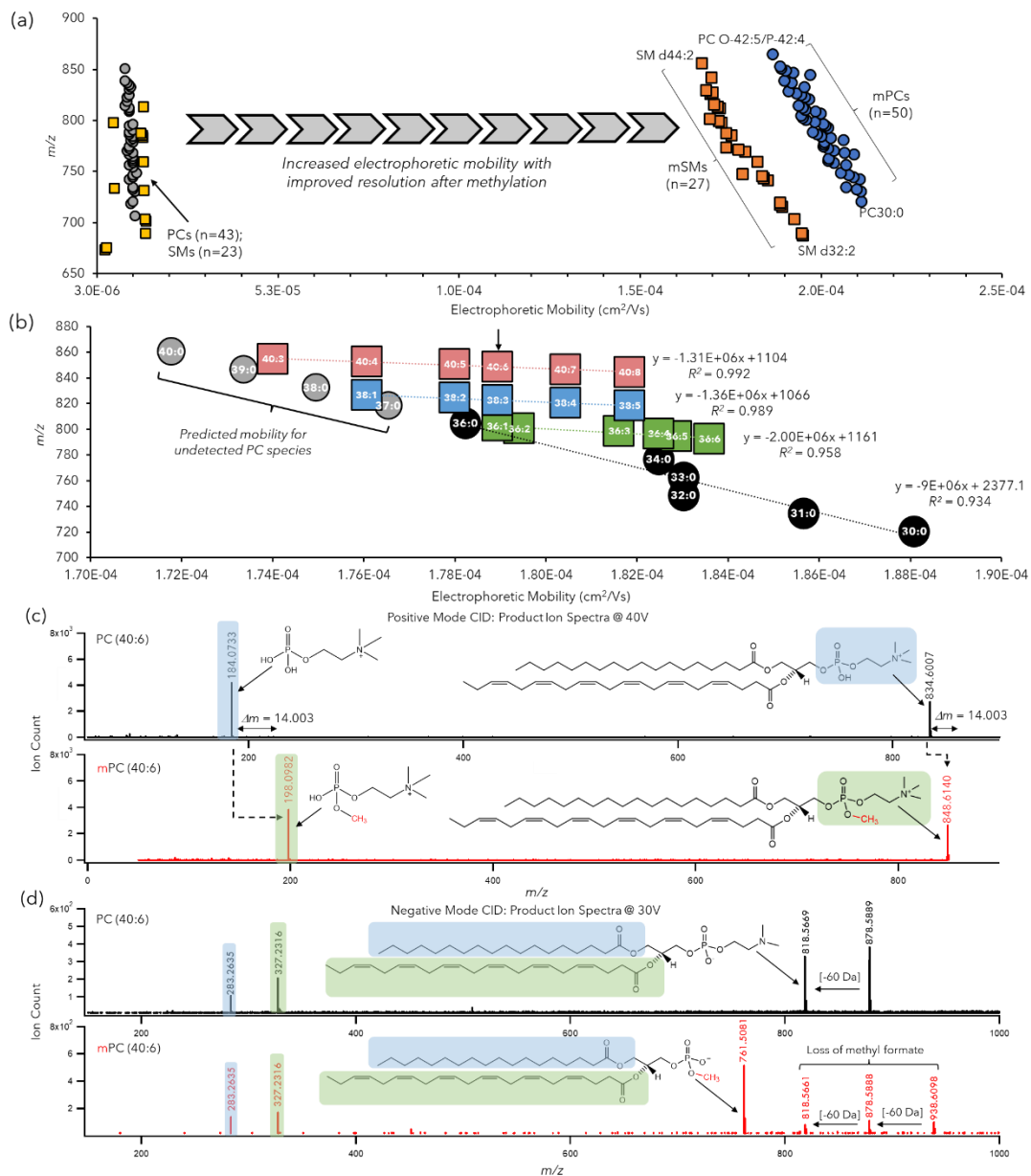


**Figure 3.3** (a) Electrophoretic mobility plot as a function of the accurate mass for 76 PLs measured in reference plasma extracts, including native and methylated PCs and SMs when using MSI-NACE-MS in positive ion mode. As expected, a large mobility shift occurs following quantitative methylation, resulting in better separation resolution of both mSMs and mPCs that are dependent on their chemical linkage, total fatty acyl chain carbon numbers, and degrees of unsaturation. (b) Linear least-squares regression models can be used to predict changes in the apparent electrophoretic mobility for plasma mPLs, as reflected by a homologous series of saturated mPCs (PC 30:0 to PC 36:0), as well as unsaturated mPCs with the same total carbon chain length, such as mPC 36, PC 38 and PC 40 species varying from one to eight degrees of unsaturation. This approach can be used to support lipid identification when using high-resolution MS especially when standards are lacking. A comparison of MS/MS spectra acquired after collision-induced dissociation experiments under (c) positive and (d) negative ion modes on derivatized and underivatized PC 40:6 from reference plasma. This confirmed the methylation of the phosphatidylcholine head group as reflected by a characteristic methyl shift (+14 Da) when comparing the molecular ion and base peak/product ion under positive ion mode, whereas the fatty acyl chain backbone and their relative positioning under negative ion mode was consistent as mPC 18:0\_22:6.

laboratory harmonization study.<sup>15</sup> Overall, mSMs migrate with a lower positive mobility than mPCs due to differences in their chemical linkage bonding that impacts their conformational size in solution for singly charged lipid cations. For instance, similar mass mPC and mSM species (*i.e.*, mPC 32:1  $\approx$  mSM 36:2), the latter mPL sub-class migrates later due to its longer acyl chains that contribute to a slower positive electrophoretic mobility. Additionally, there are characteristic mobility shift patterns evident within both lipid sub-classes,<sup>38</sup> where increasing chain length of the fatty acyl backbone (C30-C44) and greater degrees of unsaturation (n=0-8) predictably reduces or increases the apparent mobility for both mPCs and mSMs, respectively as previously demonstrated for acidic lipids and FFAs.<sup>36,38</sup> In contrast, the separation resolution of zwitter-ionic PLs without methylation was not achieved in MSI-NACE-MS as they migrated with a small positive mobility close to the EOF. The steepness of the slope for underivatized PLs directly reflected their substantial overlap and poor within class separation, which were more readily prone to ion suppression and isobaric interferences with other neutral lipid species. The benefit of methylation of PLs is more clearly depicted in **Figure 3.3(b)**, which compares mobility changes among saturated mPCs (including predicted mobility for non-detected mPCs from extrapolation of linear equation of line), as well as a homologous series of PC 36, PC 38 and PC 40 that demonstrate a linear increase in mobility as a function of increasing degrees of unsaturation when using a least-squares linear regression model ( $R^2 > 0.930$ ). **Figure 3.3(c)** confirms that the large mobility shift for mPLs was a result of formation of a methylated phosphate ester head group as shown in MS/MS spectra acquired for PC 40:6 at optimal collision energies under positive and negative ion mode. Annotation of MS/MS spectra under positive ion mode (at 40 V) for mPC 40:6 as compared to PC 40:6 confirmed a diagnostic product ion for its methylated phosphate headgroup ( $m/z$  190.0982) corresponding to a mass shift of  $m/z$  14 as compared to control ( $m/z$



184.0773). Additionally, annotation of MS/MS spectra acquired under negative ion mode (at 30 V) confirmed that both PC 40:6 and mPC: 40:6 contained a stearic acid (C18:0) and docosahexaenoic acid (C22:6, DHA) with the latter likely in sn-2 position being the more abundant species, as reflected by the signal fragment ratio of the fatty acyl chains. Interestingly, a double formate adduct anion  $[M + 2\text{Formate}]^-$  was detected to be the molecular ion for mPC 40:6 when acquiring MS/MS spectra in negative ion mode when using formic acid in the BGE and sheath liquid as reflected by characteristic neutral loss of  $m/z$  60 (methylformate) that occurred twice as compared to only once for PC 40:6. Moreover, mPC 40:6 generated a unique base peak product ion at  $m/z$  761.5081 under negative ion mode after a neutral loss of methylformate unlike PC 40:6 under the same collision energy conditions. Distinctive MS/MS spectra were acquired for mSM d34:1 under positive and negative ion mode conditions (**Figure S3.4**) that confirmed the same methylated phosphorylcholine head group, but lacked the detection of diagnostic fatty acyl chains at 40 V, which may be better achieved as their lithiated adducts to lower the fragmentation energy barrier in collision-induced dissociation.<sup>50</sup> Also, other approaches are needed to confirm the exact stereochemistry of mPL isomers from plasma extracts, such as the location of unsaturation and/or geometric configuration using techniques such as ozone-induced dissociation experiments with MS/MS.<sup>51,52</sup> Nevertheless, mobility plots generated separately for mPCs and mSMs provide complementary information to characterize the structure of plasma PLs than accurate mass alone when using high resolution MS (**Figure S3.5**), which combines the selectivity of HILIC (*i.e.*, polar head group/chemical linkage) and reversed-phase (*i.e.*, total carbon chain length) chromatography.<sup>38</sup>

#### 3.4.4. Characterization of Consensus mPLs from Reference Plasma Sample.

Previously, Bowden *et al.*<sup>15</sup> used NIST SRM-1950 as a commercially available reference material in an interlaboratory comparison across 31 international laboratories, each using their own analysis data workflows and instrumental methods when performing untargeted lipidomics. Although 1527 unique lipid features were measured quantitatively across all laboratories, only 339 of these lipids were reported consistently by at least 5 or more participating laboratories with adequate precision as determined by a coefficient of dispersion threshold (COD < 40%). As a result, we aimed to validate our two-stage chemical derivatization protocol using MSI-NACE-MS for representative mPCs and mSMs consistently measured from NIST-SRM-1950 plasma extracts using standardized LC-MS protocols. Overall, 83 authenticated plasma mPLs from the harmonization study were screened based on their anticipated methylated ion  $[M+H^+ + 14 \text{ Da}]$  under positive ion mode, including 53 PCs and 30 SMs. Previously, we outlined an iterative workflow to screen for nontargeted lipid features using MSI-NACE-MS under negative ion mode<sup>38</sup> which was performed for mPLs under positive ion mode and then compared independently to validated plasma lipids reported in Bowden *et al.*<sup>15</sup> Overall, MSI-NACE-MS following FMO/MTT chemical derivatization and hexane back extraction was able to measure 94% (50 out of 53) and 90% (27 out of 30) of the consensus PCs and SMs from NIST SRM-1950 plasma.<sup>15</sup> We also performed an untargeted analysis of acidic lipids from NIST SRM-1950 plasma ether extracts when using MSI-NACE-MS under negative ion mode without chemical derivatization in order to expand lipidome coverage for more polar classes of lipids while comparing the benefit of methylation for PCs and SMs. In this case, MSI-NACE-MS was able to quantify 11/14 (79%) bile acids (BAs), 19/25 (76%) of LPCs, but only 24/35 (69%) PE and 7/13 (54%) PI species likely due to their lower responsiveness under negative ion mode detection while introducing small sample

volumes in-capillary (~ 10 nL) in MSI-NACE-MS as compared to LC-MS methods. Although only 8 FFAs acyl species satisfied validation criteria in the lipidomics harmonization study, we noted that MSI-NACE-MS can accurately quantify more than 20 FFAs species from blood extracts as highlighted in our previous studies.<sup>6,53</sup> **Figure S3.6** depicts a Venn diagram of consensus lipids from NIST SRM-1950 that were measured by MSI-NACE-MS under positive and negative ion mode. As expected, a larger fraction (~ 50%) of PCs and SMs were measured consistently by MSI-NACE-MS in positive ion mode as compared to negative ion mode without chemical derivatization. This is likely due to the improved separation resolution and greater ionization response achieved for cationic mPCs and mSMs following FMOC/MTT derivatization. However, electrically neutral plasma lipids were not measured in our study since they remain unresolved and co-migrate with the EOF, including cholesterol esters, diacylglycerols and triacylglycerols. Overall, our work demonstrated that > 150 ionic lipids can be consistently measured in reference plasma extracts when using MSI-NACE-MS under both positive and negative ion mode configurations, including phosphatidylserines (PSs) that were not reported as consensus lipids in the harmonization study.<sup>15</sup>

### **3.4.5. Quantification of Plasma mPLs Using Harmonized Reference Lipid Concentrations.**

A major challenge in contemporary lipidomic research remains the accurate quantification of blood lipids given the lack and/or high costs of lipid standards and stable-isotope internal standards. A key advantage of MSI-NACE-MS is that ionic lipids migrate with a steady-state mobility under isocratic BGE conditions while using a continuous sheath liquid during ionization unlike LC-MS methods relying on gradient elution. Furthermore, multiplexed separations in MSI-NACE-MS not only improve sample throughput, but also allow for versatile serial sample injection configuration to encode mass spectral information temporally in a separation.<sup>38</sup> For instance,

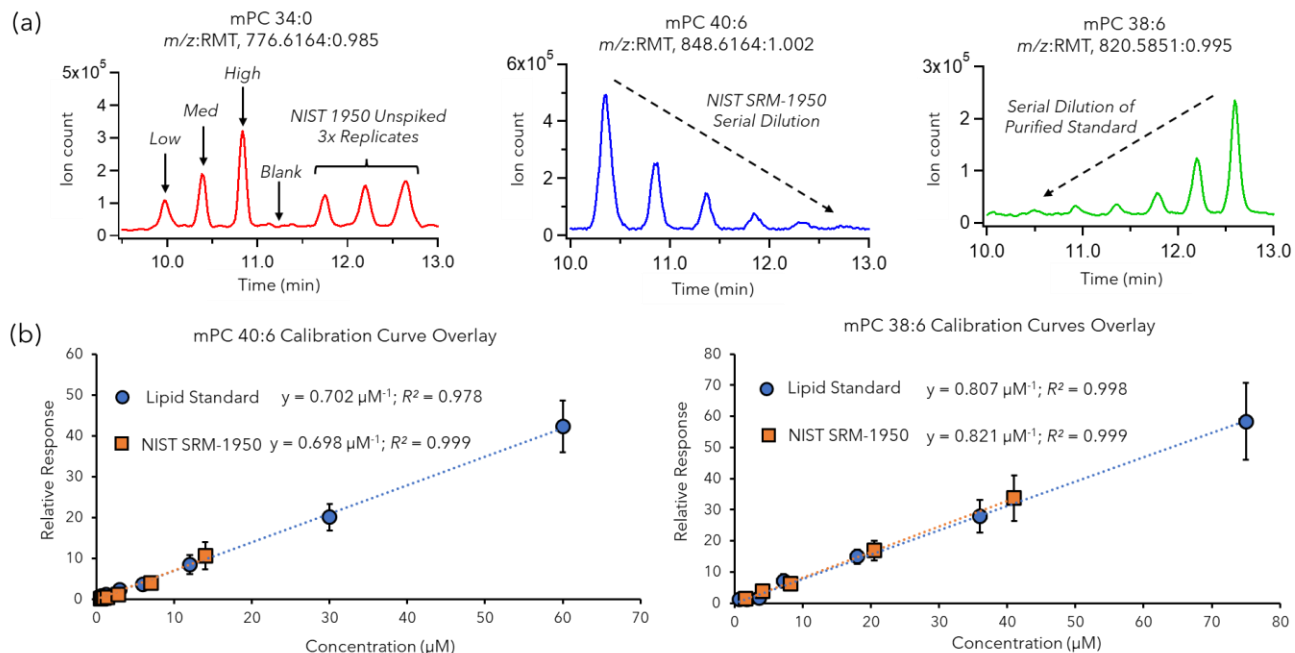


**Figure 3.4.** (a) Representative extracted ion electropherograms for different mPC species when using customized serial injection configuration in MSI-NACE-MS, including spike and recovery studies, serial dilution of NIST SRM-1950, and a serial dilution of a lipid standard. (b) The lack of ion suppression effects for mPC 40:6 and mPC 38:6 was evident based on the good mutual agreement of their relative response factors (*i.e.*, slope of calibration curve,  $\mu\text{M}^{-1}$ ) acquired from 5-point calibration curves from serial dilution of lipid standards or NIST SRM-1950 plasma. This approach allows for the potential of reliable quantitative analysis of plasma lipids even when standards are lacking when using MSI-NACE-MS.

**Figure 3.4(a)** highlights that different serial injection configurations can be designed in MSI-NACE-MS within a single run, such as a spike recovery study in NIST SRM-1950 for mPC 34:0, a serial dilution of NIST SRM-1950 to estimate the relative response ratio of mPC 40:6, and a serial dilution of a lipid standard for mPC 38:6 for generation of a calibration curve. Spike and recovery experiments using four PC lipid standards were performed at three different concentration levels (low, medium, high) ranging from 1.0 to 20  $\mu\text{M}$  ( $n = 5$ ). In all cases, mPCs (and mSMs) were normalized to a single deuterated internal standard (in matching samples) given the lack of ion suppression effects and gradient elution used in MSI-NACE-MS. Quantification of mPCs were then performed using relative response factors (*i.e.*, sensitivity) generated from the

slopes of calibration curves generated for each lipid standard or from serial dilution of NIST SRM-1950 plasma. **Figure 3.4(b)** depicts two representative calibration curve overlays for mPC 38:6 and mPC 40:6, which demonstrates good mutual agreement in measured sensitivity (*i.e.*, slope of calibration curve) based on a least-squares linear regression model with good linearity ( $R^2 > 0.980$ ). This comparison also confirmed the lack of matrix-induced ion suppression effects in MSI-NACE-MS from other plasma lipids given minimal differences (bias < 2%) in the apparent sensitivity derived from serial dilution of calibrant standards as compared to reference plasma. However, the use of serial dilution of NIST SRM-1950 for estimation of the relative response factor ( $\mu\text{M}^{-1}$ ) of mPCs and mSMs was better suited to abundant plasma PLs unlike lipid chemical standards that permitted analysis over a wider linear dynamic range. This strategy was limited to plasma mPLs measured in at least 5 concentration levels with adequate average precision (CV < 20%) upon serial dilution of NIST SRM-1950 using the median of mean consensus lipid concentrations reported by Bowden *et al.*<sup>15</sup> **Table 3.1** summarizes the performance of MSI-NACE-MS for reliable lipid quantification in reference plasma when using external calibration curves as compared to serial dilution of NIST SRM-1950 plasma for four different representative mPCs. As expected, good accuracy was achieved when quantifying mPC 34:0, mPC 38:6, and mPC 40:6 in both spike-recovery studies, as well as unspiked reference plasma (mean bias < 10%) when using external calibration curves by MSI-NACE-MS as compared to untargeted LC-MS methods.<sup>15</sup> Slightly higher bias (< 25%) was found for mPC 38:6 and mPC 40:6 concentrations in reference plasma when compared to a targeted shotgun (separation-free) lipidomic inter-laboratory comparison study by DI-MS/MS using a commercial lipid kit under standardized operating conditions.<sup>17</sup> However, lower precision and poor accuracy (mean bias ~ -50%) was noted for PC 30:0, which was attributed to hexane back extraction favouring the recovery of more lipophilic

**Table 3.1.** Summary of MSI-NACE-MS validation experiments compared to reported concentrations in Bowden *et al.* and Thompson *et al.*

Lipid	Derivatized <i>m/z</i>	Spike & Recovery	%Bias ( <i>n</i> = 5) to plasma PL conc. from Bowden <i>et al.</i>		MSI-NACE-MS		Bowden <i>et al.</i> (2017)			Thompson <i>et al.</i> (2019)			Relative Response Factor	
			External Calibration	Serial Dilution of SRM-1950	External Calibration (μM)	Serial Dilution of SRM-1950 (μM)	Harmonization Study Reported Concentration (μM)	#Labs Detected	COD (%)	p400 - Reported Concentration (μM)	p400 Bias (%)	LOD (μM)	External Calibration, Linearity (slope; <i>R</i> <sup>2</sup> )	Serial dilution of NIST 1950, Linearity (slope; <i>R</i> <sup>2</sup> )
PC 30:0	720.5538	NIST	49.9%	-82.8%										
		High Spike	7.2%	30.7%	2.6 ± 0.7	3.1 ± 0.8	1.6 ± 0.6	11	20	1.8 ± 0.6	39.3%	0.70	0.754 μM <sup>-1</sup> , 0.999	0.618 μM <sup>-1</sup> , 0.990
		Mid Spike	10.2%	34.4%										
		Low Spike	18.3%	44.2%										
		<b>Average</b>	11.9%	49.3%										
PC 34:0	776.6164	NIST	2.1%	-38.4%										
		High Spike	-5.0%	-42.7%	2.2 ± 0.6	1.3 ± 0.4	2.1 ± 0.8	12	18	NA	NA	0.08	0.867 μM <sup>-1</sup> , 0.998	1.438 μM <sup>-1</sup> , 0.979
		Mid Spike	-1.6%	-40.7%										
		Low Spike	-0.6%	-40.1%										
		<b>Average</b>	-1.3%	40.6%										
PC 38:6	820.5851	NIST	0.5%	2.3%										
		High Spike	8.3%	-6.7%	41.2 ± 3.9	41.9 ± 3.3	41.0 ± 8.6	18	11	33.5 ± 8.6	23.1%	0.08	0.821 μM <sup>-1</sup> , 0.999	0.807 μM <sup>-1</sup> , 0.997
		Mid Spike	4.7%	6.5%										
		Low Spike	24.1%	26.3%										
		<b>Average</b>	9.4%	7.1%										
PC 40:6	848.6164	NIST	-5.6%	-6.1%										
		High Spike	-13.2%	-13.7%	13.2 ± 2.1	13.2 ± 2.1	14.0 ± 5.1	17	19	14.9 ± 5.1	-11.2%	0.07	0.698 μM <sup>-1</sup> , 0.999	0.702 μM <sup>-1</sup> , 0.978
		Mid Spike	-5.3%	-5.9%										
		Low Spike	4.9%	4.3%										
		<b>Average</b>	-8.0%	0.6%										

lipid species (> C30) with lower concentration levels below the quantification limit when using MSI-NACE-MS. This discrepancy in accuracy outcomes was not observed in spike-recovery experiments for mPC 30:0 (mean bias < 18%) which demonstrated better accuracy at increasingly higher lipid concentration levels. We also aimed to explore an additional strategy for semi-quantitative estimation of plasma mPL using serial dilutions of NIST SRM-1950 in comparison to external calibration approaches with standards. This may serve as an attractive alternative to measure lipid species when standards are not available provided that ion suppression or enhancement effects are minimal when analyzing plasma ether extracts. Overall, this strategy performs well for abundant mPC 38:6 and mPC 40:6 that have higher reported baseline concentrations in reference plasma (> 10  $\mu\text{M}$ ) as compared to lower abundance mPC 34:0 and mPC 30:0 (< 2  $\mu\text{M}$ ) that also suffer from lower recovery following hexane back extraction. This scenario also corresponded to fewer detectable data points (< 4) upon serial dilution of NIST SRM-1950 needed to generate accurate response factors, which was noted for other lower abundance mPL species.

In summary, expanded lipidome coverage was achieved in MSI-NACE-MS when using a two-step pre-column chemical derivatization strategy to charge switch zwitter-ionic PL species into cationic mPLs using a safer and more convenient methylation reagent than diazomethane. Overall, 77 mPCs and mSMs were measured from reference plasma extracts with adequate precision when using MSI-NACE-MS following FMOC/MTT derivatization that were consistent with consensus lipids reported in an inter-laboratory harmonization study using LC-MS/MS methods. Additionally, 69 other acidic and polar PLs from NIST SRM-1950 plasma extracts can also be measured by MSI-NACE-MS under negative ion mode without chemical derivatization. This approach greatly expands conventional CE-MS metabolomic protocols that rely on aqueous

based BGE systems and are thus limited to the untargeted analysis of hydrophilic/polar metabolites. Lipid annotation and structural classification is also supported based on predictable changes in the apparent electrophoretic mobility for mPCs and mSMs that are dependent on polar head group/chemical linkage, total carbon length and degrees of unsaturation. Advantages of this MSI-NACE-MS protocol include greater throughput (~ 3.5 min/sample) and minimal ion suppression effects that allows for unique data workflows for data acquisition and lipid authentication in comparison to other separation platforms that utilize single sample injections. Also, MSI-NACE-MS offers as a platform more amenable to standardization since it operates using only a bare-fused silica capillary under an isocratic nonaqueous buffer system unlike other competing LC-MS platforms that use different column types and gradient elution programs, including reversed-phase and HILIC-MS. However, MSI-NACE-MS with a coaxial sheath liquid interface suffers from higher detection limits and lower concentration sensitivity for ionic lipids as compared to LC-MS methods due to the smaller sample volume introduced on-capillary (~ 10 nL). Furthermore, certain neutral lipid classes are not resolved or reliably measured by this method as they co-migrate with the EOF. Nevertheless, we anticipate that this two-stage methylation strategy and sample workup protocol may be more widely used than diazomethane and its derivatives when performing lipidomic studies by DI-MS/MS and LC-MS/MS as a way to enhance ionization efficiency and optimize chromatographic performance. For example, labelling using trimethylsilylated diazomethane improved reversed-phase LC analysis of fatty acyl-coenzymes in biological samples due to the high affinity of phosphate groups that absorb onto glass/metallic surfaces.<sup>54</sup> Also, methylation using TMS diazomethane was also applied to increase hydrophobicity and reduce the chelating effect of phytic acid, a common branched-chain fatty acid antioxidant added in foods that can reduce the bioavailability of minerals.<sup>55</sup> Future studies are



underway to better characterize other mPC lipid sub-classes, including isobaric plasmalogens when using MSI-NACE-MS, while applying this approach in larger-scale untargeted lipidomic studies for biomarker discovery. Also, the potential for reliable semi-quantitative determination of PLs by MSI-NACE-MS based on serial dilution of reference serum will be further validated.

### 3.6. Conclusion

In this work, we describe a two-step charge-switch chemical derivatization strategy using FMOCC/MTT for methylation of zwitter-ionic plasma PL species to expand lipid profiling coverage by MSI-NACE-MS under positive ion mode conditions. FMOCC was used as a compatible protecting agent to prevent generation of PE isobaric species that also reduced ion suppression effects from excess MTT by-products prior to hexane back extraction. We optimized the efficacy of this reaction to generate quantitative and reproducible yields of 77 cationic mPCs and mSMs authenticated in reference plasma ether extracts when using MSI-NACE-MS under positive ion mode, which comprised 93% of consensus lipids reported in an inter-laboratory lipidomics harmonization study. Overall, methylation of PLs resulted in improved separation resolution, faster analysis times, reduced ion suppression, and allowed for better lipid structural classification based on changes in their positive electrophoretic mobility using a linear regression model. This method is optimal for large-scale lipidomic studies requiring higher sample throughput with stringent quality control, as well as lower sample volume requirements ( $\sim 2 \mu\text{L}$ ). We also demonstrated good precision and accuracy when quantifying lipophilic mPCs ( $> 30$ ) from reference plasma samples above their quantification limit, including the potential for use of serial dilution of NIST SRM-1950 human plasma to estimate relative response factors for lipids lacking standards. Overall, this work represents the first introduction of a hitherto unrecognized lipidomics platform based on MSI-NACE-MS that takes advantage of a methylation strategy as a cost-

effective and practical alternative to diazomethane without unwarranted hazards and safety precautions.

## ACKNOWLEDGEMENTS

This work was supported by funding from the Natural Sciences and Engineering Research Council of Canada, Genome Canada, and the Canada Foundation for Innovation. R.L. gratefully acknowledges the support of Ontario Graduate Scholarships and McMaster University for several internal scholarships.

## 3.7. References

- (1) Quehenberger, O.; Dennis, E. A. *New Engl J Medicine* 2011, 365 (19), 1812–1823.
- (2) Shevchenko, A.; Simons, K. *Nat Rev Mol Cell Bio* 2010, 11 (8), 593–598.
- (3) Meikle, T. G.; Huynh, K.; Giles, C.; Meikle, P. J. *J Lipid Res* 2021, 62, 100127.
- (4) Han, X. *Nat Rev Endocrinol* 2016, 12 (11), 668–679.
- (5) Hyötyläinen, T.; Bondia-Pons, I.; Orešič, M. *Mol Nutr Food Res* 2013, 57 (8), 1306–1318.
- (6) Azab, S. M.; Souza, R. J. de; Teo, K. K.; investigators), (for the FAMILY; Anand, S. S.; Williams, N. C.; Holzschuher, J.; McGlory, C.; Philips, S. M.; Britz-McKibbin, P. *J Lipid Res* 2020, 61 (6), 933–944.
- (7) Han, X.; Gross, R. W. *J Lipid Res* 2003, 44 (6), 1071–1079.
- (8) Kohno, S.; Keenan, A. L.; Ntambi, J. M.; Miyazaki, M. *Biochem Bioph Res Co* 2018, 504 (3), 590–595.
- (9) Rustam, Y. H.; Reid, G. E. *Anal Chem* 2017, 90 (1), 374–397.
- (10) McDonald, J. G.; Ejsing, C. S.; Kopczyński, D.; Holčapek, M.; Aoki, J.; Arita, M.; Arita, M.; Baker, E. S.; Bertrand-Michel, J.; Bowden, J. A.; et al. *Nat Metabolism* 2022, 1–3.
- (11) O'Donnell, V. B.; FitzGerald, G. A.; Murphy, R. C.; Liebisch, G.; Dennis, E. A.; Quehenberger, O.; Subramaniam, S.; Wakelam, M. J. O. *Circulation Genom Precis Medicine* 2020, 13 (6), e003019–e003019.

- (12) Drotleff, B.; Lämmerhofer, M. *Anal Chem* 2019, *91* (15), 9836–9843.
- (13) Tsugawa, H.; Ikeda, K.; Takahashi, M.; Satoh, A.; Mori, Y.; Uchino, H.; Okahashi, N.; Yamada, Y.; Tada, I.; Bonini, P.; et al. *Nat Biotechnol* 2020, *38* (10), 1159–1163.
- (14) Delabriere, A.; Warmer, P.; Brennsteiner, V.; Zamboni, N. *Anal Chem* 2021, *93* (45), 15024–15032.
- (15) Bowden, J. A.; Heckert, A.; Ulmer, C. Z.; Jones, C. M.; Koelmel, J. P.; Abdullah, L.; Ahonen, L.; Alnouti, Y.; Armando, A. M.; Asara, J. M.; et al. *J Lipid Res* 2017, *58* (12), 2275–2288.
- (16) Initiative, A. D. N.; Consortium, A. D. M.; Barupal, D. K.; Fan, S.; Wancewicz, B.; Cajka, T.; Sa, M.; Showalter, M. R.; Baillie, R.; Tenenbaum, J. D.; et al. *Sci Data* 2018, *5* (1), 180263.
- (17) Thompson, J. W.; Adams, K. J.; Adamski, J.; Asad, Y.; Borts, D.; Bowden, J. A.; Byram, G.; Dang, V.; Dunn, W. B.; Fernandez, F.; et al. *Anal Chem* 2019, *91* (22), 14407–14416.
- (18) Züllig, T.; Trötz Müller, M.; Köfeler, H. C. *Anal Bioanal Chem* 2020, *412* (10), 2191–2209.
- (19) Abel, K.; deSchmertzing, H.; Peterson, J. I. *J Bacteriol* 1963, *85* (5), 1039–1044.
- (20) Han, X.; Gross, R. W. *J Lipid Res* 2021, *63* (2), 100164.
- (21) Han, X.; Gross, R. W. *Mass Spectrom Rev* 2005, *24* (3), 367–412.
- (22) Xu, T.; Hu, C.; Xuan, Q.; Xu, G. *Anal Chim Acta* 2020, *1137*, 156–169.
- (23) Cajka, T.; Fiehn, O. *Methods Mol Biology* 2017, *1609*, 149–170.
- (24) Lange, M.; Ni, Z.; Criscuolo, A.; Fedorova, M. *Chromatographia* 2019, *82* (1), 77–100.
- (25) Harrieder, E.-M.; Kretschmer, F.; Böcker, S.; Witting, M. *J Chromatogr B* 2021, *1188*, 123069.
- (26) Narváez-Rivas, M.; Zhang, Q. *J Chromatogr A* 2016, *1440*, 123–134.
- (27) Plumb, R. S.; Isaac, G.; Rainville, P. D.; Hill, J.; Gethings, L. A.; Johnson, K. A.; Lauterbach, J.; Wilson, I. D. *J Proteome Res* 2022, *21* (3), 691–701.
- (28) Sorensen, M. J.; Miller, K. E.; Jorgenson, J. W.; Kennedy, R. T. *J Chromatogr A* 2020, *1611*, 460575.
- (29) Baglai, A.; Gargano, A. F. G.; Jordens, J.; Mengerink, Y.; Honing, M.; Wal, S. van der; Schoenmakers, P. J. *J Chromatogr A* 2017, *1530*, 90–103.

- (30) Wolrab, D.; Chocholoušková, M.; Jirásko, R.; Peterka, O.; Holčapek, M. *Anal Bioanal Chem* 2020, 412 (10), 2375–2388.
- (31) Leaptrot, K. L.; May, J. C.; Dodds, J. N.; McLean, J. A. *Nat Commun* 2019, 10 (1), 985.
- (32) Lee, J.-H.; Kim, S.-J.; Lee, S.; Rhee, J.-K.; Lee, S. Y.; Na, Y.-C. *Anal Chim Acta* 2017, 984, 223–231.
- (33) Sándor, V.; Berkics, B. V.; Kilár, A.; Kocsis, B.; Kilár, F.; Dörnyei, Á. *Electrophoresis* 2020, 41 (13–14), 1178–1188.
- (34) Gao, F.; Zhang, Z.; Fu, X.; Li, W.; Wang, T.; Liu, H. *Electrophoresis* 2007, 28 (9), 1418–1425.
- (35) Montealegre, C.; Sánchez-Hernández, L.; Crego, A. L.; Marina, M. L. *J Agr Food Chem* 2013, 61 (8), 1823–1832.
- (36) Azab, S.; Ly, R.; Britz-McKibbin, P. *Anal Chem* 2019, 91 (3), 2329–2336.
- (37) Azab, S. M.; Souza, R. J. de; Ly, R.; Teo, K. K.; Atkinson, S. A.; Morrison, K. M.; Anand, S. S.; Britz-McKibbin, P. *Prostaglandins Leukot Essent Fat Acids* 2022, 176, 102378.
- (38) Ly, R.; Ly, N.; Sasaki, K.; Suzuki, M.; Kami, K.; Ohashi, Y.; Britz-McKibbin, P. *J Proteome Res* 2022, 21 (3), 768–777.
- (39) Shanmuganathan, M.; Kroezen, Z.; Gill, B.; Azab, S.; Souza, R. J. de; Teo, K. K.; Atkinson, S.; Subbarao, P.; Desai, D.; Anand, S. S.; et al. *Nat Protoc* 2021, 16 (4), 1966–1994.
- (40) DiBattista, A.; McIntosh, N.; Lamoureux, M.; Al-Dirbashi, O. Y.; Chakraborty, P.; Britz-McKibbin, P. *Anal Chem* 2017, 89 (15), 8112–8121.
- (41) Xia, F.; Wan, J. *Mass Spectrom Rev* 2021, e21729.
- (42) Wasslen, K. V.; Canez, C. R.; Lee, H.; Manthorpe, J. M.; Smith, J. C. *Anal Chem* 2014, 86 (19), 9523–9532.
- (43) Wasslen, K. V.; Tan, L. H.; Manthorpe, J. M.; Smith, J. C. *Anal Chem* 2014, 86 (7), 3291–3299.
- (44) Betancourt, S. K.; Canez, C. R.; Shields, S. W. J.; Manthorpe, J. M.; Smith, J. C.; McLuckey, S. A. *Anal Chem* 2017, 89 (17), 9452–9458.
- (45) Dallinger, D.; Kappe, C. O. *Nat Protoc* 2017, 12 (10), 2138–2147.
- (46) Yamamoto, M.; Ly, R.; Gill, B.; Zhu, Y.; Moran-Mirabal, J.; Britz-McKibbin, P. *Anal Chem* 2016, 88 (21), 10710–10719.

- (47) White, E. H.; Baum, A. A.; Eitel, D. E. *Organic Syntheses* 2003, 48, 102–105.
- (48) Caperos, J. R.; Fernández, J. G. *Brit J Ind Med* 1977, 34 (3), 229.
- (49) Furukawa, T.; Hinou, H.; Takeda, S.; Chiba, H.; Nishimura, S.; Hui, S. *Chembiochem* 2017, 18 (19), 1903–1909.
- (50) Hsu, F.-F.; Turk, J. *J Am Soc Mass Spectr* 2000, 11 (5), 437–449.
- (51) Poad, B. L. J.; Zheng, X.; Mitchell, T. W.; Smith, R. D.; Baker, E. S.; Blanksby, S. J. *Anal Chem* 2018, 90 (2), 1292–1300.
- (52) Claes, B. S. R.; Bowman, A. P.; Poad, B. L. J.; Young, R. S. E.; Heeren, R. M. A.; Blanksby, S. J.; Ellis, S. R. *Anal Chem* 2021, 93 (28), 9826–9834.
- (53) Saoi, M.; Kennedy, K. M.; Gohir, W.; Sloboda, D. M.; Britz-McKibbin, P. *Sci Rep-uk* 2020, 10 (1), 9399.
- (54) Li, P.; Gawaz, M.; Chatterjee, M.; Lämmerhofer, M. *Anal Chem* 2021, 93 (9), 4342–4350.
- (55) Yu, S.; Cai, C.; Wang, Y.; Sheng, C.; Jiang, K. *Rapid Commun Mass Sp* 2021, 35 (22), e9194.

## **3.8. Supporting Information**

### **Chapter III**

#### **Expanding Lipidomic Coverage in Multisegment Injection-Nonaqueous Capillary Electrophoresis-Mass Spectrometry via a Convenient and Quantitative Methylation Strategy**

*Ritchie Ly, Lucas Christian Torres, Nicholas Ly, Philip Britz-McKibbin\**

Department of Chemistry and Chemical Biology, McMaster University, Hamilton, Canada L8S 4M1

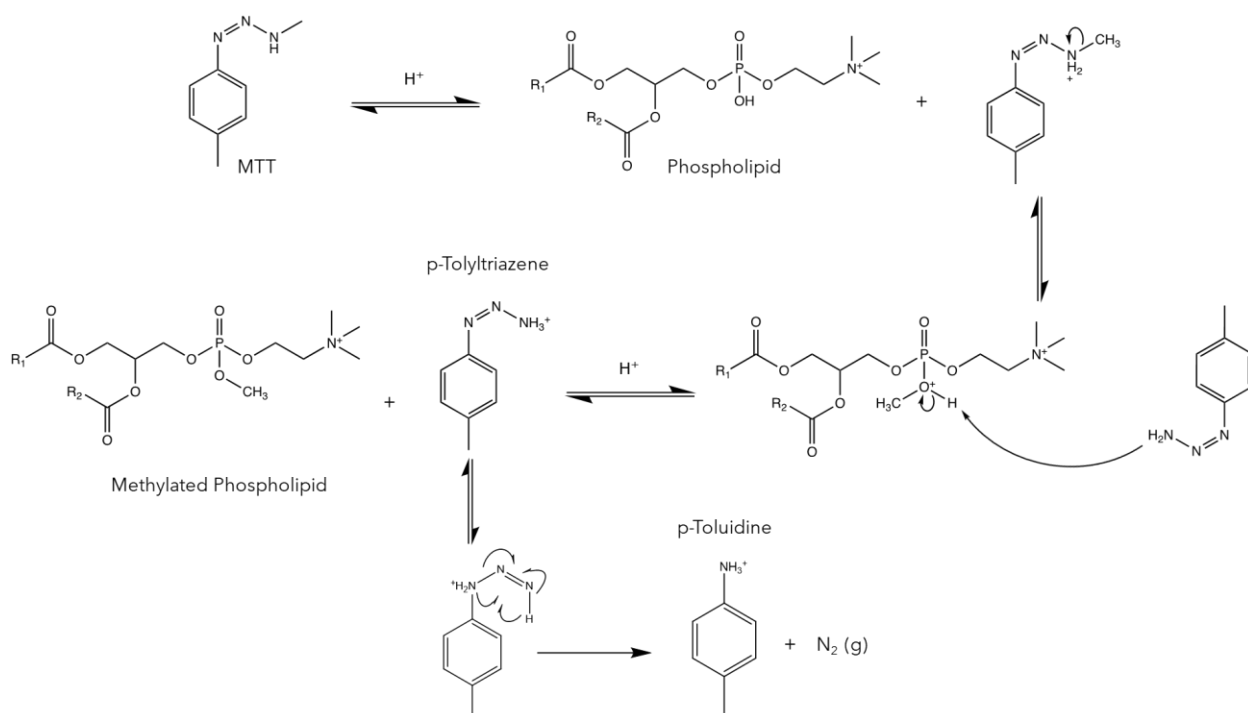


**Figure S3.1.** Proposed mechanism for methylation of phospholipids using MTT. Briefly, this reaction involves a proton transfer to amino group of MTT for activation to increase its electrophilic character resulting in formation of *p*-tolyltriazenium and a methylated phosphate ester head group with a net cationic charge on the phospholipid. This reaction subsequently liberates  $N_2$  gas with concomitant generation of *p*-toluidine as a major by-product.

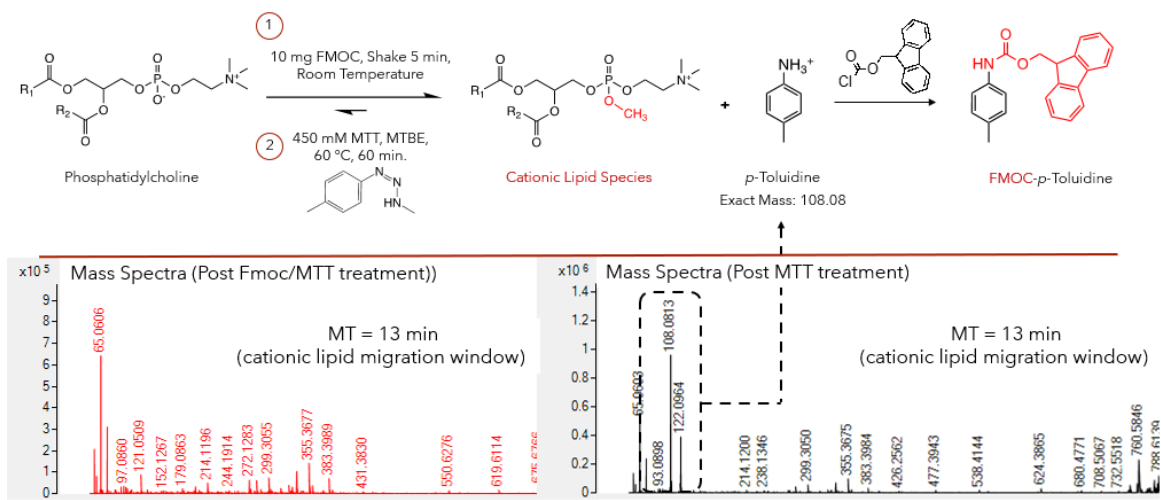


**Figure S3.2.** Reaction scheme depicting *p*-toluidine by-product generation after methylation of phospholipids from MTT. Prior to the introduction of FMOC, a single charged molecular ion  $[M+H]^+$  associated with formation of *p*-toluidine ( $m/z$  108) was observed in the separation window of derivatized PC species. FMOC not only was required to react with PEs to prevent interference with isobaric PC species, but also to react with *p*-toluidine (to form a neutral adduct) and thus prevent ion suppression effects as it otherwise migrated close to methylated phospholipids when using MSI-NACE-MS.



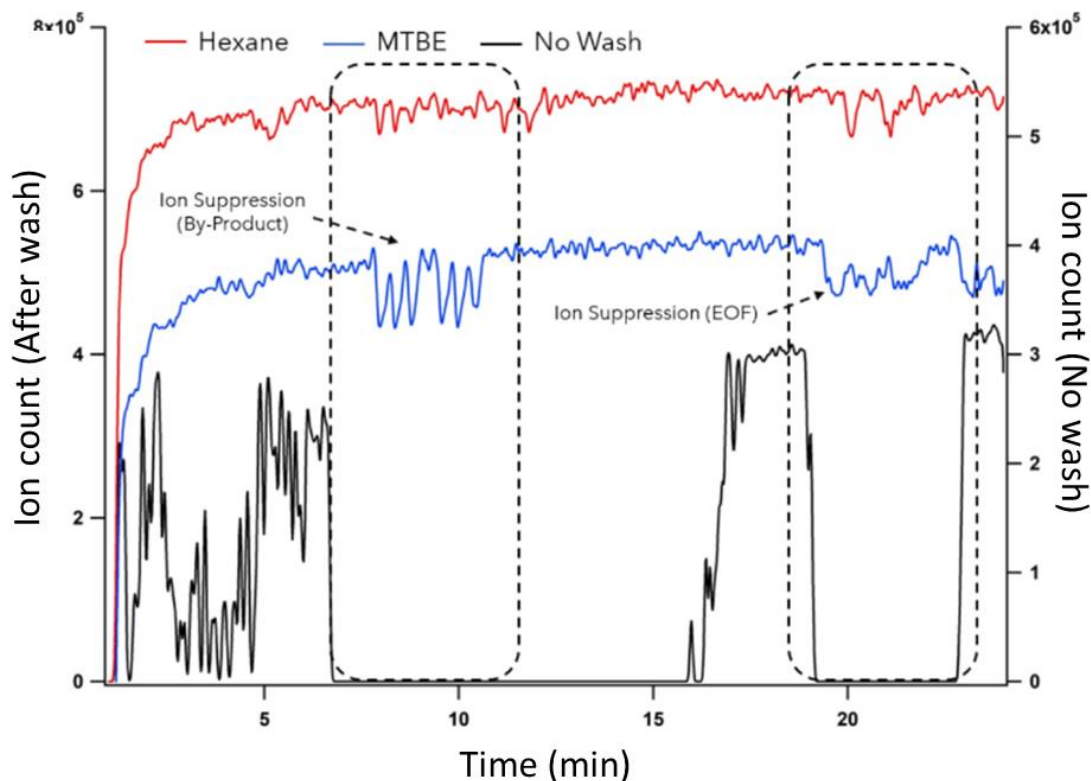


**Figure S3.3.** An extracted ion electropherogram overlay of purine ( $m/z$  121.0509) used as reference mass calibrant in the sheath liquid solution under different sample workup conditions following FMOc/MTT derivatization of NIST SRM-1950 plasma extracts by MSI-NACE-MS under positive ion mode detection. Two major regions of ion suppression correspond to excess MTT by-product (e.g., p-toluidine) and the EOF, where abundant neutral lipid classes co-migrate (e.g., cholesterol esters, diacylglycerides). Two different organic solvents (i.e., MTBE vs. hexane) were used for back extraction of methylated phospholipids following chemical derivatization in order to reduce ion suppression effects as compared to a standard run without washing (black trace). Notably, the use of hexane (red trace) outperformed MTBE (blue trace) resulting in a superior sample cleanup that greatly reduced ion suppression effects from excess reagents in a region where cationic methylated phospholipids migrate in MSI-NACE-MS.

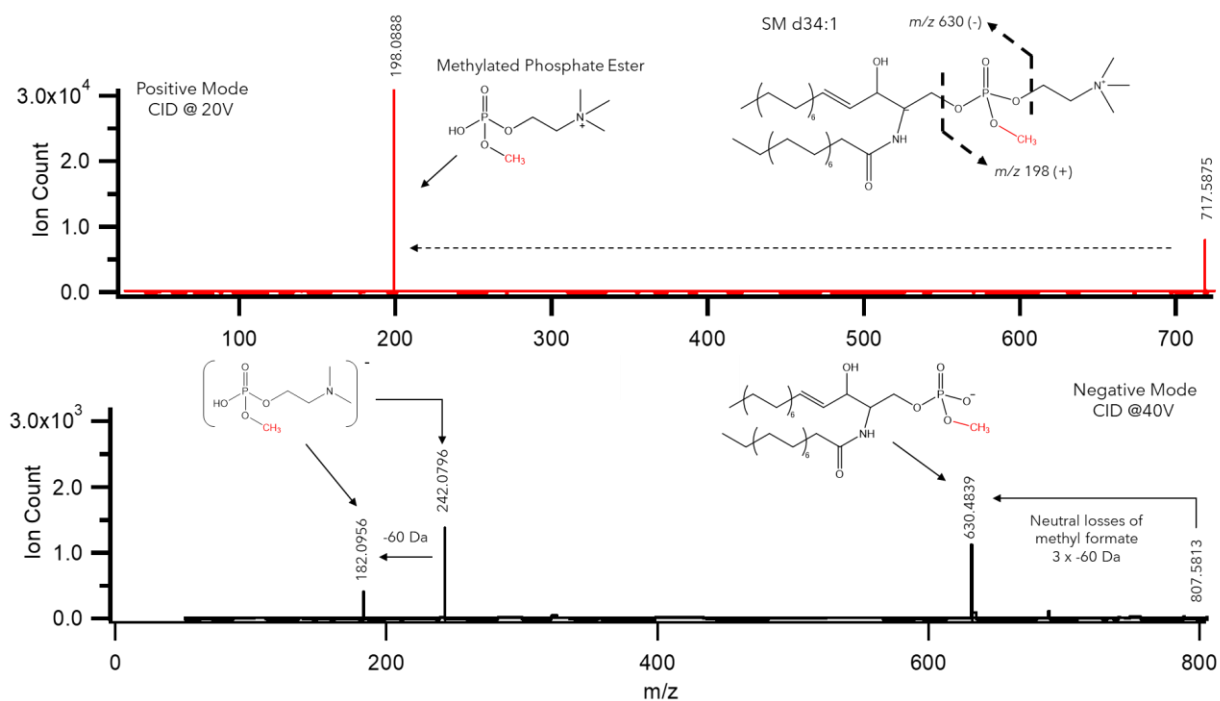


**Figure S3.4.** MS/MS spectra acquired after CID experiments on derivatized mSM d34:1 in positive and negative ion mode. For positive ion mode, a methyl shift [+14 Da] as shown in the base peak product ion ( $m/z$  198.0888). Formate adducts for mSM d34:1 were selected in negative ion mode, however acyl fatty acid product anions were not detected at this collision energy unlike mPCs.

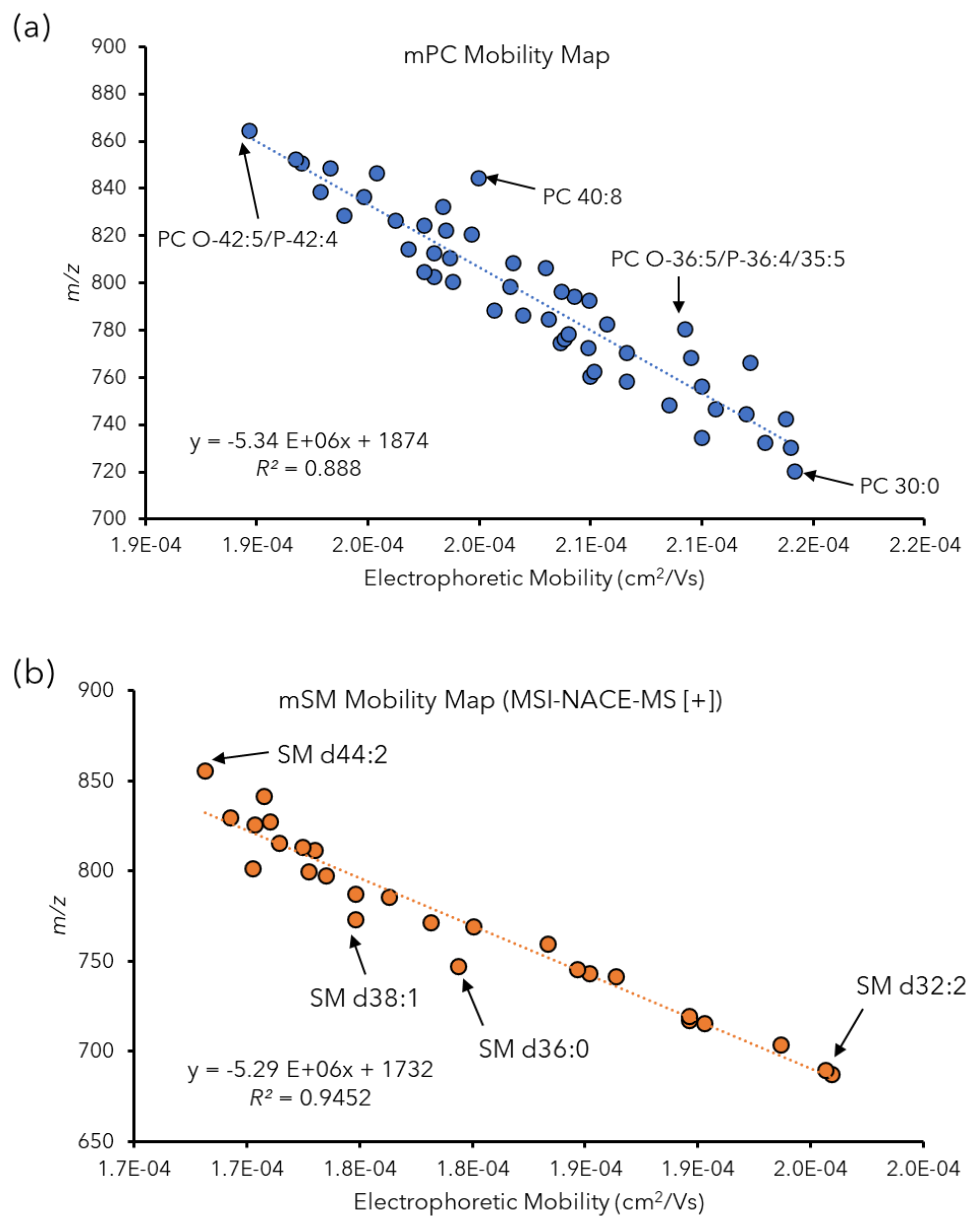


**Figure S3.5.** (a) Mobility map depicting all mPC species ( $n=50$ ) and (b) mSM species ( $n=27$ ) detected from NIST SRM-1950 human plasma extracts after FMOC/MTT derivatization using MSI-NACE-MS in positive ion mode with full-scan data acquisition.

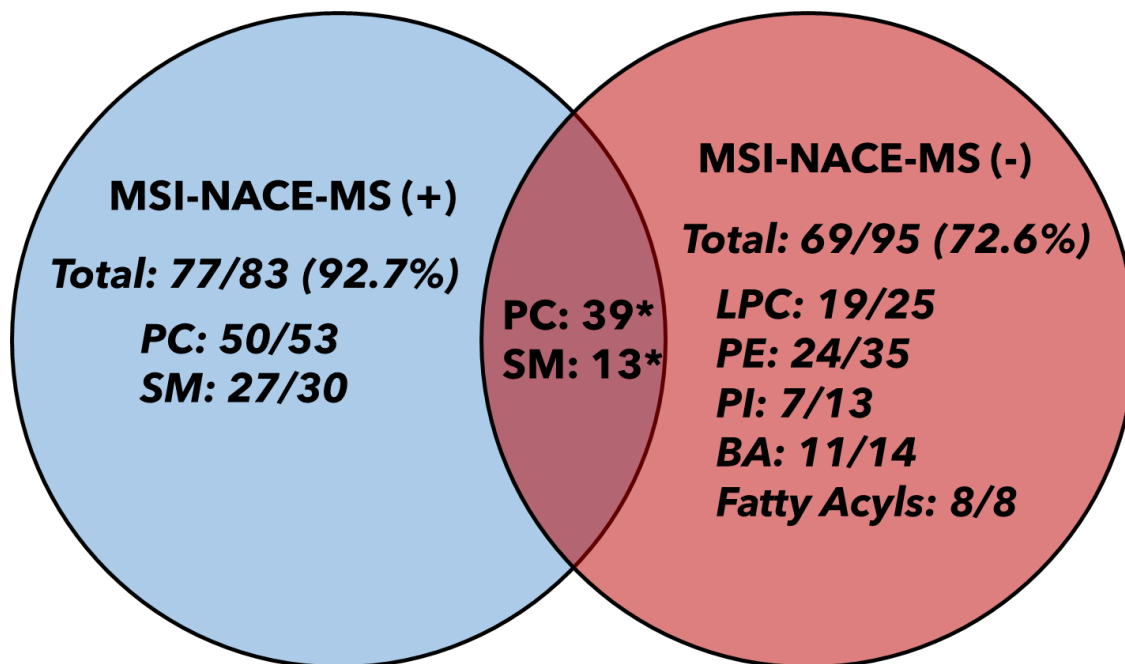


**Figure S3.6.** Venn diagram summarizing the coverage of consensus lipids reported by Bowden *et al.*<sup>15</sup> from NIST SRM-1950 plasma ether extracts when using MSI-NACE-MS under positive (with FMOc/MTT derivatization) and negative ion mode (no derivatization). Due to the hexane back extraction clean up used to reduce ion suppression from excess MTT by-products, hydrophilic/polar PLs (PCs < C30, LPCs, PIs, PAs, FFAs) were better suited for their direct analysis by MSI-NACE-MS under negative ion mode without methylation. Importantly, a larger fraction (~ 50%) of methylated PCs and SMs were measured in MSI-NACE-MS under positive as compared to negative ion mode due to the improved separation resolution and ionization response. Other ionic lipids from plasma extracts that were not reported (e.g., phosphatidylserines) or did not satisfy criteria in the harmonization study have not been included. Also, neutral lipid classes (e.g., cholesterol esters, diacylglycerols) are not reliably quantified by MSI-NACE-MS under these conditions as they co-migrate with the EOF.

**Table S3.1.** Plasma phospholipids measured from NIST-SRM 1950 serum by MSI-NACE-MS in positive ion mode detection that met acceptance criteria in the lipidomics harmonization study.<sup>15</sup>

Lipid Species	Derivatized <i>m/z</i>	Actual Mass	Mass Error (ppm)	Electrophoretic Mobility ( $\text{cm}^2/\text{Vs}$ ) $\times 10^{-4}$	Molecular Formula [Methylated]
PC 30:0	720.5538	720.5518	-2.71	2.142	C39H79NO8P
PC O-32:2/P-32:1/31:2	730.5382	730.5376	-0.75	2.140	C40H77NO8P
PC O-32:1/P-32:0/31:1	732.5538	732.5512	-3.48	2.128	C40H79NO8P
PC O-32:0/31:0	734.5695	734.5624	-9.60	2.100	C40H81NO8P
PC 32:3	742.5382	742.5394	1.68	2.137	C41H77NO8P
PC P-33:1/32:2	744.5538	744.5478	-7.99	2.120	C41H79NO8P
PC 32:1	746.5695	746.5653	-5.56	2.106	C41H81NO8P
PC 32:0	748.5851	748.5798	-7.01	2.085	C41H83NO8P
PC O-34:3/P-34:2/33:3	756.5538	756.5608	9.32	2.100	C42H79NO8P
PC O-34:2/P-34:1/33:2	758.5695	758.5742	6.26	2.066	C42H81NO8P
PC O-34:1/P-34:0/33:1	760.5851	760.5859	1.12	2.050	C42H83NO8P
PC O-34:0/33:0	762.6008	762.5958	-6.49	2.051	C42H85NO8P
PC 34:5	766.5382	766.5341	-5.28	2.121	C43H77NO8P
PC O-35:4/34:4	768.5538	768.55	-4.88	2.095	C43H79NO8P
PC P-35:2/34:3	770.5695	770.5668	-3.44	2.066	C43H81NO8P
PC P-35:1/34:2	772.5851	772.5835	-2.01	2.049	C43H83NO8P
PC 34:1	774.6008	774.6041	4.32	2.036	C43H85NO8P
PC 34:0	776.6164	776.6084	-10.24	2.038	C43H87NO8P
PC P-36:5/35:6	778.5382	778.5457	9.70	2.040	C44H77NO8P
PC O-36:5/P-36:4/35:5	780.5902	780.6045	18.38	2.092	C44H79NO8P
PC O-36:4/P-36:3/35:4	782.6059	782.5923	-7.31	2.057	C44H81NO8P

PC O-36:3/P-36:2/35:3	784.6215	784.6029	-3.64	2.031	C44H83NO8P
PC O-36:2/P-36:1/35:2	786.6372	786.6213	-8.15	2.019	C44H85NO8P
PC O-36:1/P-36:0/35:1	788.6528	788.6235	-7.09	2.006	C44H87NO8P
PC 36:6	792.5538	792.5529	-1.07	2.049	C45H79NO8P
PC 36:5	794.5695	794.5594	-12.65	2.042	C45H81NO8P
PC 36:4	796.5851	796.5834	-2.07	2.037	C45H83NO8P
PC 36:3	798.6008	798.6018	1.31	2.014	C45H85NO8P
PC 36:2	800.6164	800.6123	-5.06	1.988	C45H87NO8P
PC 36:1	802.6321	802.6372	6.42	1.979	C45H89NO8P
PC P-38:6/36:0	804.6477	804.6363	-4.11	1.975	C45H91NO8P
PC O-38:6/P-38:5/37:6	806.5695	806.5703	1.05	2.030	C46H81NO8P
PC O-38:5/P-38:4/37:5	808.5851	808.5925	9.21	2.015	C46H83NO8P
PC O-38:4/P-38:3/37:4	810.6008	810.6009	0.19	1.986	C46H85NO8P
PC O-38:3/P-38:2/37:3	812.6164	812.6074	-11.01	1.979	C46H87NO8P
PC O-38:2/37:2	814.6321	814.6281	-4.85	1.968	C46H89NO8P
PC 38:6	820.5851	820.5828	-2.74	1.996	C47H83NO8P
PC 38:5	822.6008	822.596	-5.77	1.985	C47H85NO8P
PC 38:4	824.6164	824.6153	-1.27	1.975	C47H87NO8P
PC 38:3	826.6321	826.6256	-7.80	1.962	C47H89NO8P
PC 38:2	828.6477	828.6443	-4.04	1.939	C47H91NO8P
PC O-40:7/P-40:6/39:7	832.5851	832.5971	4.47	1.984	C48H83NO8P
PC O-40:5/P-40:4/39:5	836.6164	836.6099	-7.71	1.948	C48H87NO8P
PC O-40:4/P-40:3/39:4	838.6321	838.6276	-5.31	1.928	C48H89NO8P

PC 40:8	844.5851	844.5857	0.77	1.999	C49H83NO8P
PC 40:7	846.6008	846.5933	-8.80	1.954	C49H85NO8P
PC 40:6	848.6164	848.6146	-2.06	1.933	C49H87NO8P
PC 40:5	850.6321	850.633	1.12	1.920	C49H89NO8P
PC 40:4	852.6477	852.6474	-0.29	1.917	C49H91NO8P
PC O-42:5/P-42:4	864.6841	864.6421	-8.51	1.896	C51H95NO7P
SM d32:2	687.5436	687.5316	-7.38	1.979	C38H76N2O6P
SM d32:1	689.5592	689.5532	-8.63	1.976	C38H78N2O6P
SM d33:1	703.5749	703.5685	-9.03	1.956	C39H80N2O6P
SM d34:2	715.5749	715.5746	-0.35	1.923	C40H80N2O6P
SM d34:1	717.5905	717.5886	-2.58	1.916	C40H82N2O6P
SM d34:0	719.6062	719.5999	-8.69	1.916	C40H84N2O6P
SM d36:3	741.5905	741.5911	0.88	1.884	C42H82N2O6P
SM d36:2	743.6062	743.6078	2.22	1.872	C42H84N2O6P
SM d36:1	745.6218	745.6162	-7.44	1.866	C42H86N2O6P
SM d36:0	747.6375	747.6334	-5.42	1.813	C42H88N2O6P
SM d37:1	759.6375	759.6326	-6.38	1.854	C43H88N2O6P
SM d38:3	769.6218	769.6324	3.84	1.820	C44H86N2O6P
SM d38:2	771.6375	771.6292	-10.69	1.801	C44H88N2O6P
SM d38:1	773.6531	773.6426	-13.51	1.768	C44H90N2O6P
SM d39:2	785.6531	785.6445	-10.88	1.783	C45H90N2O6P
SM d39:1	787.6688	787.6634	-6.79	1.768	C45H92N2O6P
SM d40:3	797.6531	797.6523	-0.94	1.755	C46H90N2O6P
SM d40:2	799.6688	799.6628	-7.44	1.747	C46H92N2O6P
SM d40:1	801.6844	801.6764	-9.92	1.722	C46H94N2O6P
SM d41:3	811.6688	811.6622	-8.07	1.750	C47H92N2O6P
SM d41:2	813.6844	813.6793	-6.21	1.744	C47H94N2O6P
SM d41:1	815.7001	815.6894	-13.06	1.734	C47H96N2O6P
SM d42:3	825.6844	825.6804	-4.78	1.724	C48H94N2O6P

SM d42:2	827.7001	827.6957	-5.26	1.730	C48H96N2O6P
SM d42:1	829.7157	829.7111	-5.48	1.713	C48H98N2O6P
SM d43:2	841.7157	841.7108	-5.76	1.728	C49H98N2O6P
SM d44:2	855.7314	855.7512	3.20	1.701	C50H100N2O6P

**Table S3.2.** Plasma phospholipids from NIST SRM-1950 measured by MSI-NACE-MS that did not meet acceptance criteria in the lipidomics harmonization study.<sup>15</sup>

Lipid Species	Derivatized <i>m/z</i>	Actual Mass	Mass Error (ppm)	Electrophoretic Mobility (cm <sup>2</sup> /Vs) × 10 <sup>-4</sup>	Molecular Formula [Methylated]
PC 30:1	718.5382	718.5376	-0.77	2.144	C39H77NO8P
PC 38:1	830.6634	830.6596	-4.51	1.930	C47H93NO8P
PC O-40:6/P-40:5/39:6	834.6008	834.6042	4.13	1.925	C48H85NO8P
PC O-44:5/P-44:4	892.7156	892.7051	-11.71	1.872	C53H99NO7P
SM d38:0	775.6688	775.6788	12.96	1.764	C44H92N2O6P
SM d40:0	803.7001	803.7122	15.12	1.717	C46H96N2O6P
SM d42:4	827.7001	827.6912	-10.69	1.730	C48H96N2O6P
SM d44:3	853.7157	853.7038	-13.88	1.709	C50H98N2O6P



## Chapter IV

### **Lipidomics for Identifying Serum Phospholipids as Surrogate Biomarkers of Omega-3 Index using Multisegment Injection-Nonaqueous Capillary Electrophoresis-Mass Spectrometry**

*Ritchie Ly,<sup>1</sup> Brittany MacIntyre,<sup>2</sup> Stuart Philips,<sup>3</sup> Chris McGlory,<sup>3,4</sup> David Mutch,<sup>2</sup> Philip Britz-McKibbin<sup>1</sup>*

<sup>1</sup> *Department of Chemistry and Chemical Biology, McMaster University, Hamilton, Ontario Canada*

<sup>2</sup> *Department of Human Health and Nutritional Sciences, University of Guelph, Guelph, Ontario Canada.*

<sup>3</sup> *Department of Kinesiology, McMaster University, Hamilton, Ontario Canada*

<sup>4</sup> *School of Kinesiology and Health Studies, Queen's University, Kingston, Ontario Canada*

R.L performed all the experiments including sample preparation, data acquisition using MSI-NACE-MS, data processing, interpretation, statistical analysis and wrote the initial draft for publication. B. M. and D. M. provided plasma samples and data for individual DHA/EPA supplementation study. S.P. and C.M. provided serum samples and data for FO study. P.B.M wrote and provided feedback on the manuscript draft.

#### 4.1. Abstract

Decades of contentious public health guidelines to reduce dietary fat intake has spurred the need for objective biomarkers associated with cardiometabolic health for chronic disease prevention, such as the omega-3 index (O3I). Conventional methods for determination of O3I status however rely on the analysis of omega-3 fatty acid content from erythrocyte phospholipid membrane that is not convenient for routine population-based screening. Herein, we applied a high-throughput method for untargeted lipidomic analysis using multisegment injection-nonaqueous capillary electrophoresis-mass spectrometry to identify circulating phospholipid species that may serve as surrogate biomarkers of O3I status in two independent placebo-controlled intervention trials. An accelerated data workflow using a sub-group analysis of serum extracts from placebo and high-dose fish oil (FO) treatment participants confirmed that dietary omega-3 fatty acids were predominately uptaken as their phosphatidylcholines (PCs) in comparison to other serum phospholipid pools. Consistently in both FO (5.0 g/day) and docosahexaenoic acid (DHA) or eicosapentaenoic acid (EPA)-specific (3.0 g/day) intervention studies, serum PC (16:0/20:5) was most responsive ( $> 7$ -fold change from baseline) to supplementation ( $> 28$  days) as compared to various DHA containing PCs, notably PC (16:0/22:6) ( $> 2$ -fold change from baseline), reflective of preferential incorporation of EPA into these circulating lipid pools. We also demonstrated that the sum of serum PC (16:0/20:5) and PC (16:0/22:6) was positively correlated to O3I measurements when using FO ( $r = 0.717$ ,  $p = 1.62 \times 10^{-11}$ ,  $n=69$ ), as well as DHA or EPA ( $r = 0.764$ ,  $p = 3.00 \times 10^{-33}$ ,  $n=167$ ) with most participants improving their O3I status  $> 8.0\%$ . However, DHA was more efficacious in improving O3I

( $\Delta\text{O3I} = 4.90 \pm 1.33$ ) compared to EPA ( $\Delta\text{O3I} = 2.99 \pm 1.19$ ) that was dose dependent with large between-subject variability. We conclude that MSI-NACE-MS offers a promising multiplexed separation platform for more convenient assessment of O3I status using specific PCs derived from widely available serum or plasma specimens. This work can support nutritional epidemiological studies exploring the role of essential dietary fats in human health while optimizing individual responses to dietary or pharmacological interventions based on specific omega-3 fatty acid formulations.

## 4.2. Introduction

Evidence-based nutritional policies are urgently needed given an alarming increase in the prevalence of obesity and chronic disease burden worldwide<sup>1</sup> despite longstanding recommendations to reduce fat intake as a heart healthy diet.<sup>2</sup> Public health guidelines have historically focused at assessing particular types of fat as opposed to overall diet quality and specific essential nutrients<sup>3</sup>, such as omega-3 fatty acids (FAs) that comprise a small fraction of total fats in contemporary Western diets.<sup>4</sup> For instance, the American Heart Association Nutrition Committee recommends consumption of oily fish/seafood as a source of dietary omega-3 FAs up to twice a week to reduce cardiovascular disease (CVD) risk especially if it replaces less healthy processed foods.<sup>5</sup> This is significant because unlike saturated or monounsaturated FAs, humans are unable to synthesize sufficient amounts of omega-3 FAs that are enriched within the cellular membrane of certain tissues/organs (*e.g.*, retina, brain, heart), such as docosahexaenoic acid (DHA) and eicosapentaenoic acid (EPA) – thus, dietary sources primarily of marine origin are essential.<sup>6</sup> In addition to modifying

membrane composition and cellular function, omega-3 FAs also mediate inflammatory processes via various mechanisms of action, such as formation of resolvins and other anti-inflammatory lipid mediators.<sup>7</sup>

The content of DHA and EPA from commonly consumed wild fish species can vary more than a 100-fold, with larger variation in farmed fish depending on local feeding practices.<sup>8</sup> Alternatively, commercial fish oil (FO) dietary supplements offer a way to ensure adequate omega-3 FA nutrition in conjunction with emerging microalgae sources<sup>9</sup> and prescription omega-3 FA products.<sup>10</sup> Nevertheless, most childbearing age and pregnant women do not meet their recommended dietary intake of omega-3 FAs.<sup>11</sup> This is critical to early stages of fetal neurodevelopment with growing evidence that greater intake of omega-3 FAs may reduce premature and low weight births.<sup>12</sup> Yet, there have been conflicting results from clinical trials on omega-3 FAs in cardiovascular disease protection.<sup>13</sup> This likely stems from inadequate dosage regimens using impure formulations that do not target responsive patients with hypertriglyceridemia,<sup>14</sup> which may also effectively reduce CVD events in current and former smokers.<sup>15</sup>

To date, nutritional epidemiological studies have largely relied on food frequency questionnaires to estimate omega-3 FA dietary fat intake for chronic disease risk assessment.<sup>16</sup> Alternatively, biomarkers may offer a more reliable way to assess nutritional status<sup>17</sup> given between-subject differences in omega-3 FA bioavailability and metabolism, while also verifying dietary adherence during intervention studies. In this case, the omega-3 index (O3I), defined as the erythrocyte EPA + DHA content from phospholipid (PL) as a mole percent to total fatty acids, has been proposed as a novel biomarker of coronary

heart disease risk and sudden cardiac death complementary to traditional risk factors.<sup>18</sup> Moreover, O3I status can be stratified based on defined cut-off values, where < 4% is considered high risk, 4-8% being intermediate risk, and low risk > 8%,<sup>19</sup> as confirmed independently in a meta-analysis from 19 cohort studies.<sup>20</sup> For example, the mean O3I index for Canadian adults has been reported as 4.5% with less than 3% of the population classified with high cardioprotection (*i.e.*, O3I > 8%) that was dependent on age, ethnicity, fish consumption, supplement use, smoking status and obesity.<sup>21</sup> Although PL erythrocytes reflect habitual omega-3 FA intake patterns over a medium-term time interval (~ 2 months) as compared to other more dynamic circulating PL class pools,<sup>22,23</sup> previous studies have demonstrated a moderate correlation of O3I with EPA and DHA PL content measured in plasma or whole dried blood.<sup>19</sup> Indeed, disadvantages of existing O3I index and omega-3 FA protocols include the need to access erythrocytes, which are not widely available in biorepositories unlike fasting plasma, serum or whole blood.<sup>24</sup> Also, gas chromatography (GC) is often used for omega-3 FA determination from PL erythrocyte hydrolysates, but requires complicated sample workup and PL fractionation procedures not amenable to large-scale clinical or epidemiological studies.<sup>25</sup>

Herein, we performed an untargeted lipidomic analysis on fasting serum or plasma samples to identify robust PL biomarkers of O3I in young Canadian adults that were replicated independently in two placebo-controlled intervention trials using high-dose omega-3 FAs (~ 3 or 5 g) derived from either FO, DHA or EPA.<sup>26,27</sup> We previously demonstrated that the sum of DHA and EPA measured as their free (non-esterified) FAs in serum ether extracts were associated with daily intake of fish/FO daily servings,<sup>28,29</sup>

however serum EPA was more responsive than DHA to high-dose FO ingestion.<sup>23</sup> In this study, we aimed to validate a panel of specific PL species that may serve as convenient surrogates of O3I when using a multisegment injection-nonaqueous capillary electrophoresis-mass spectrometry (MSI-NACE-MS).<sup>30</sup> This multiplexed separation method allows for higher throughput analyses (~ 3.5/min sample) while using novel data workflows for biomarker discovery, which allows for comprehensive PL screening when combined with a two-step chemical derivatization protocol. Our work offers a convenient way to measure O3I status for risk assessment of cardiovascular health while requiring only small volumes of blood as a way to expand its overall clinical utility.

### **4.3. Experimental**

#### **4.3.1. Study Designs, Participants and Cohorts**

In the first study, fasting serum samples were derived from participants in a randomized, double-blinded, placebo-controlled intervention study that investigated the effects of FO supplementation on attenuating skeletal muscle disuse atrophy following leg immobilization.<sup>26</sup> This clinical trial was registered at the US National Library of Medicine (<https://clinicaltrials.gov/>) as NCT03059836. Briefly, this study involved a cohort of healthy young women with a mean age of 22 years (range: 19-31 years) and BMI of 24 kg/m<sup>2</sup> (range: 18-26 kg/m<sup>2</sup>) that were recruited locally from the Hamilton area. These participants received either an active treatment arm of a high-dose omega-3 FA from FO (3.0 g EPA and 2.0 g DHA daily;  $n = 9$ ) or a placebo control based on an isoenergetic and volume equivalent sunflower oil (SO) daily ( $n = 9$ ). Repeat serum samples were collected from participants at baseline and at 28, 42 and 56 days throughout the intervention. All

fasting serum samples were then stored frozen at  $-80^{\circ}\text{C}$ . Further details on blood collection, participant selection and exclusion criteria, and erythrocyte PL omega-3 FA analysis for O3I determination are described elsewhere.<sup>26</sup> Briefly, lipids were extracted from red blood cells using the Folch method<sup>31</sup> in chloroform-methanol (2:1 v/v) containing butylated hydroxytoluene (0.01%) as an antioxidant and heptadecanoic acid as an internal standard. From here, PL fractions were isolated by thin-layer chromatography silica plates (Silica Gel 60, 0.22 mm; Merck, Kenilworth, NJ, USA) where heptane:isopropylether:acetic acid (60:40:3, v/v/v) was used as the resolving solution. Gel bands were scraped off the plate and transferred into screw cap tubes to be subjected to transmethylation with  $\text{BF}_3$  in methanol. Fatty acid methyl esters (FAMES) were then dissolved in hexane and analyzed using a Hewlett-Packard 5890 Series II GC with flame-ionization detector while using a Varian CP-SIL capillary column (100 m, internal diameter of 0.25 mm) (Palo Alto, CA, USA). These measurements were then used to calculate the O3I by taking the sum of quantified EPA and DHA relative to the total sum of measured lipids.

In the second study, fasting plasma samples were collected from participants in a randomized, double-blinded, multiarm, placebo-controlled parallel group trial comparing the effects of supplementing with either  $\sim 3$  g/day EPA, DHA, or olive oil (OO) over a 12-week period.<sup>27</sup> Anthropometric measurements (age, height, body weight and BMI) were obtained for participants on study day visits and summarized in **Table S1**. Purified EPA (KD-PUR EPA700TG) and DHA (KD-PUR DHA700TG) oils, as well as OO were obtained from KD Pharma (Bexbach, Germany) where EPA and DHA were in their triglyceride forms. The FA content of these supplements was previously reported to be

75.7%  $\pm$  0.01% for oleic acid (C18:1) in the OO supplement, 74.7%  $\pm$  0.09% EPA and 0.55%  $\pm$  0.01% DHA in the EPA supplement, and 72.3%  $\pm$  1.3% DHA and 1.05  $\pm$  0.11% EPA in the DHA supplement.<sup>32</sup> All of the capsules contained 0.2% tocopherol to prevent oxidation of fatty acids. Exclusion criteria included use of FO supplements within the previous 3 months, > 2 servings of fish/seafood or other omega-3 FA-rich products per week, prescribed medication use (except oral contraceptives), current smoking and history of CVD. Participants were assigned via block randomization with stratification by sex to one of three treatment arms, namely 1) OO supplement ( $n = 30$ ), 2) EPA supplement ( $n = 30$ ) and 3) DHA supplement ( $n = 30$ ). In this context, participants were instructed to maintain their regular exercise and dietary habits throughout the entirety of the study. After overnight fasts, participants were subject to blood sampling at the Human Nutraceutical Research Unit at the University of Guelph before (baseline) and after (endpoint) of the 12-week supplementation period. Blood was collected into EDTA-treated vacutainers was used to isolate plasma and erythrocytes. Samples were separated by centrifugation at 700  $\times$  g at 4 °C for 15 min. Frozen erythrocyte samples were shipped to the Medical University of Bialystok, Poland on dry ice for fatty acid composition analysis using a standardized protocol as described above.

#### **4.3.2. Sample Workup, Extraction and Derivatization Procedure for MSI-NACE-MS**

Serum and plasma samples were subject to a two-step derivatization protocol using 9-fluorenylmethoxycarbonyl chloride (FMOC) and 3-methyl-1-p-tolyltriazene (FMOC/MTT) as outlined in *Chapter III*. This was needed to improve separation resolution and ionization efficiency by converting zwitter-ionic PL species that co-migrate with the



electroosmotic flow (EOF) into methylated phosphatidylcholines (mPCs) and methylated sphingomyelins (mSMs) with a permanent positive charge when using MSI-NACE-MS under positive ion mode detection. Briefly, in a glass sample vial, a 50  $\mu\text{L}$  aliquot of sample was first subject to a methyl-*tert*-butyl ether (MTBE) extraction, where 100  $\mu\text{L}$  of methanol with 0.01% of butylated hydroxytoluene as antioxidant, was added to samples containing PC 16:0-d<sub>62</sub> as a recovery standard. Samples were briefly shaken to induce protein precipitation. Next, 250  $\mu\text{L}$  of MTBE is added and shaken prior to adding 100  $\mu\text{L}$  of water to induce phase separation. Samples are then centrifuged at 4000 g at 4 °C where then 200  $\mu\text{L}$  of the organic layer is transferred into a new glass vial and dried down. Next samples are then subject to 100  $\mu\text{L}$  of 0.2 mg/mL FMOc containing PC 18:0-d<sub>70</sub> as a secondary internal standard and shaken for 5 min before drying down again. Next, 50  $\mu\text{L}$  of MTBE containing 450 mM of MTT is added to the glass vial with the lid sealed with Teflon tape. This vessel was then heated to 60 °C for 60 min. Once the reaction is complete, the solution was dried down and then subject to a back extraction, where 100  $\mu\text{L}$  is added, followed by 250  $\mu\text{L}$  of hexane and then 200  $\mu\text{L}$  of water before centrifuging for 10 min at 4000 g at 4 °C. Then, 200  $\mu\text{L}$  of the organic layer was transferred out and dried down. Once completely dried, samples were subsequently reconstituted in 50  $\mu\text{L}$  containing acetonitrile/isopropanol/water (70:20:10) with 10 mM ammonium formate containing internal standards PC 18:0-d<sub>70</sub> (5  $\mu\text{M}$ ) and benzyltriethylammoniumchloride (BTA) (1.0  $\mu\text{M}$ , and of PC 16:0-d<sub>62</sub> (5  $\mu\text{M}$ ) prior to analysis by MSI-NACE-MS with full-scan data acquisition in positive ion mode. Plasma and serum ether extracts were also analyzed directly without methylation, namely acidic/polar PLs (*e.g.*, lysophosphatidylcholines,

phosphatidylethanolamines, phosphatidylinositols) when using MSI-NACE-MS under negative ion mode detection as described elsewhere.<sup>30</sup> Briefly, a 50  $\mu\text{L}$  aliquot were first subject to a methyl-*tert*-butyl ether extraction where 100  $\mu\text{L}$  of MeOH with 0.01% of butylated hydroxytoluene, antioxidant, is added to samples containing deuterated myristic acid C14:0-d<sub>27</sub> as a recovery standard. Following rigorous shaking, phase separation was then induced through the addition of water where samples are then centrifuged to sediment protein at the bottom of the vial at 4000 *g* at 4°C for 30 min. The formation of a biphasic solution enables for the top, lipid rich ether layer to be extracted at a fixed volume (200  $\mu\text{L}$ ) where then it was dried under a gentle stream of nitrogen gas at room temperature. The dried extracts were then concentrated 2-fold by reconstitution in 25  $\mu\text{L}$  acetonitrile-isopropanol-water (70:20:10 v/v/v) with 10 mM ammonium acetate and 50  $\mu\text{M}$  of deuterated stearic acid C18:0-d<sub>35</sub> as an internal standard.

#### **4.3.3. Untargeted and Targeted Lipidomics of Serum/Plasma Ether Extracts by MSI-NACE-MS**

An Agilent 6230 TOF mass spectrometer equipped with a coaxial sheath liquid ESI ionization source was used with an Agilent G7100A capillary electrophoresis (CE) unit for all experiments (Agilent Technologies Inc.). To supply a sheath liquid during separations, an Agilent 1260 Infinity isocratic pump delivered a solution containing 80% vol methanol with 0.1% vol. formic acid at a flow rate of 10  $\mu\text{L}/\text{min}$  into the sprayer. All separations were performed using bare fused-silica capillaries with an internal diameter of 50  $\mu\text{m}$ , outer diameter of 360  $\mu\text{m}$  and total length of 110 cm (Polymicro Technologies Inc.). During electrophoresis, the applied voltage was set to 30 kV with the CE operating at 25 °C and

providing an isocratic pressure of 10 mbar (1 kPa). The background electrolyte was 35 mM ammonium formate in 70% vol acetonitrile, 15% vol methanol, and 5% vol isopropanol with an apparent pH of 2.3 that was adjusted by the addition of formic acid. Derivatized ether extracts were injected hydrodynamically at 50 mbar (5 kPa) alternating between 5 s for each sample plug and 40 s for the background electrolyte spacer plug to total seven discrete samples that were analyzed within 30 min for a single experimental run. Repeat QC samples were created by pooling samples from different study cohorts and introduced in a randomized position for each MSI-NACE-MS run to assess and monitor the technical precision of the method in both FO ( $n = 13$ ) and EPA or DHA ( $n = 29$ ) supplementation trials. All extracts were analyzed in positive ion mode acquisition with a  $V_{\text{cap}}$  at 3500V with full-scan data acquisition over the range of ( $m/z$  50-1700). For negative mode analysis of sub-group samples, the sheath liquid consisted of 80% vol methanol with 0.5% vol ammonium hydroxide delivered at a flow rate of 10  $\mu\text{L}/\text{min}$  using a CE-MS coaxial sheath liquid interface kit. The separations were performed on the same bare fused-silica capillaries with internal diameter of 50  $\mu\text{m}$ , outer diameter of 360  $\mu\text{m}$  and total length of 95 cm. The applied voltage was set to 30 kV at 25  $^{\circ}\text{C}$  for CE separations using an isocratic pressure of 20 mbar (2 kPa). The background electrolyte consisted of 35 mM ammonium acetate in 70% vol acetonitrile, 15% vol methanol and 5% vol isopropanol with an apparent pH of 9.5 that was adjusted using the addition of 12% vol ammonium hydroxide. These underivatized serum and plasma ether extracts were injected hydrodynamically at 50 mbar (5 kPa) alternating between 5 s for each sample plug and 40 s for the background electrolyte spacer for a total of seven discrete samples that were analyzed within a 30 min run.<sup>30,33,34</sup>

The TOF was operated in negative ion mode acquisition with  $V_{\text{cap}}$  at 3500 V for full-scan data acquisition over the range of ( $m/z$  50-1700).

#### 4.3.4. Data Processing and Statistical Analysis

All MSI-NACE-MS data was analyzed using Agilent MassHunter Workstation Software (Qualitative Analysis Version 10.0, Agilent Technologies, 2012). All molecular features were extracted in profile mode within a 10 ppm mass window where derivatized lipids were annotated on the basis of the characteristic  $m/z$  corresponding to their derivatized molecular ion (mPC) and relative migration time (RMT), reflecting the electrophoretic mobility for cationic lipids. The manually integrated peak areas obtained from the extracted ion electropherograms were normalized to PC-16<sub>d62</sub> to determine relative peak areas and RMT. Extracted ion electropherograms were integrated after smoothing using a quadratic/cubic Savitzky-Golay filter (7 points). Regression analysis and correlation plots were performed using Excel (Microsoft Office). Visualization of data, heat maps, comparing technical variance of QC samples with overall biological variance between subjects was conducted using MetaboAnalyst version 5.0 ([www.metaboanalyst.ca](http://www.metaboanalyst.ca)). Normality tests and nonparametric statistical analysis was performed using IBM SPSS version 23 (IBM), whereas MedCalc version 12.5.0 (MedCalc Software) was used to generate boxplots and control charts. A two-way between and within-mixed-model ANOVA (treatment; time) was used for assessing the impact of high-dose FO supplementation at three time points as compared to baseline. For the study involving separated DHA or EPA supplementation, a Wilcoxon-Signed Ranked test was performed to evaluate treatment effects after confirming non-normally distributed data. A

Pearson correlation coefficient was used to test association between lead candidate omega-3 PLs and FAs analyzed from the hydrolyzed erythrocyte PL fraction.

## 4.4 Results and Discussion

### 4.4.1. Rapid Screening for Serum Phospholipids Responsive to High-Dose FO Supplementation

In this work, we initially performed an untargeted screen for serum PLs associated with omega-3 FA intake based on an analysis of pooled serum extracts from all participants in the placebo/baseline as compared to the FO treatment arm (EPA, 3 g/day + DHA, 2 g/day). These two sub-groups of participants were analyzed in triplicate together with a blank extract to rapidly identify differentiating PL species that respond to high-dose FO ingestion when using MSI-NACE-MS under two complementary configurations as shown in **Figure 4.1(a)**. This strategy takes advantage of a serial injection of 7 serum extracts within a single run while using temporal signal pattern recognition,<sup>30</sup> which allows for rigorous credentialing of PL features responsive to high-dose DHA and EPA intake while rejecting spurious signals, background ions and importantly, a majority of non-responsive PLs. **Figure 4.1(b)** illustrates four representative PL classes annotated by their accurate mass, relative migration time, ionization mode ( $m/z$ :RMT:mode) together with their likely sum compositions, such as mSM d32:1, mPC 36:5, lysoPC 20:5, and PE 38:6. As expected, non-omega-3 containing PLs with low degrees of unsaturation, such as mSM d32:1 did not exhibit a significant change in response following FO supplementation as compared to baseline/placebo. Surprisingly, two other acidic PL classes measured

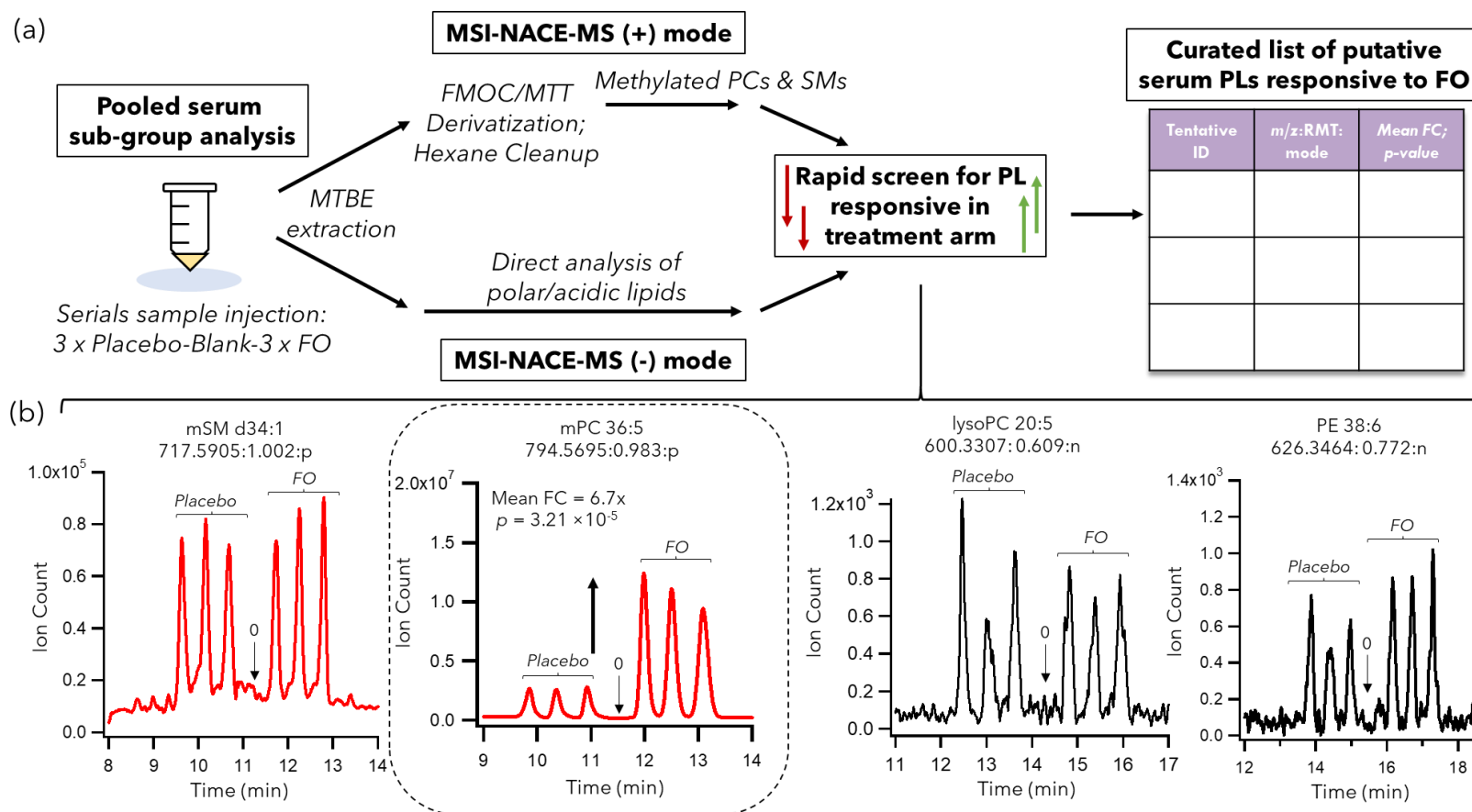


**Figure 4.1** (a) Overview of an accelerated data workflow for rapid identification of putative serum biomarkers of omega-3 fatty acid intake following high-dose FO supplementation as compared to placebo/baseline when using MSI-NACE-MS with temporal pattern signal pattern recognition under two complementary configurations. (b) Representative extracted ion electropherograms highlighting various PL classes/species that do not change following FO supplementation (e.g., SM d34:1, lysoPC 20:5, PE 38:6) in contrast to specific serum PC species that undergo a notable increase after FO ingestion, such as mPC 36:5. In all cases, a sub-group analysis was performed by MSI-NACE-MS under positive and negative ion modes when analyzing a serial injection of pooled serum samples from participants in the placebo/baseline and FO treatment arms in triplicate together with a blank extract as control.

directly from serum extracts by MSI-NACE-MS under negative ion mode, including a putative EPA-containing lysoPC (lysoPC 20:5), and a DHA-containing PE (PE 38:6), did not show a significant change in their ion response between the two sub-groups. In contrast, mPC 36:5 that was subsequently confirmed as mPC (16:0\_20:5) following annotation of its MS/MS spectra, exhibited a striking 6.7-fold average increase in response (from baseline/placebo) after high-dose FO supplementation. **Figure S4.1** highlights that other DHA-containing PCs, such as mPC 40:6, identified as mPC (16:0\_22:6), exhibited a notable increase after high-dose FO intake relative to baseline/placebo sub-group, together with free fatty acids of EPA and DHA as we previously reported.<sup>28,29</sup> Furthermore, underivatized PC 36:5 (detected as its acetate adduct in negative ion mode) was independently shown to also undergo a similar response increase with FO supplementation. However, as zwitter-ionic PCs migrate close to the EOF, resolution is poor and they are more prone to on suppression effects that attenuate overall responsivity. For these reasons, we applied a quantitative PC and SM methylation reaction as a charge-switching derivatization strategy in lipidomics to greatly improve their separation resolution and detectability when using MSI-NACE-MS under positive ion mode. Overall, select PC species containing DHA and EPA were determined to be the primary PL class that were most responsive to FO ingestion as compared to free FAs, whereas no significant response changes were noted with omega-3 FA containing lysoPCs, PIs, and PEs. The latter observation contradicts Dawczynski *et al.*<sup>35</sup> who reported that PE and plasmalogen together with PC species were increased following microalgae supplementation as compared to SO placebo. As microalgae supplements primarily contain DHA in PL form, this discrepancy

may be attributed to differences in dosage, purity and lipid form of ingested omega-3 FA that not only impact bioavailability, but also its metabolic fate.<sup>36</sup> As a result, we subsequently focused on data integration predominately on serum mPCs, including lead candidate biomarkers of omega-3 nutritional status identified in this untargeted lipidomic screening strategy.

#### **4.4.2. Discovery of Serum PC Species and Panels Associated with High-dose FO Supplementation**

Overall, 47 PC species and several mSM were quantified in all serum ether extracts from a cohort of young women ( $n = 8$ ) at baseline and then at three time points following high-dose FO or SO placebo intervention over an 8-week (or 56 day) period as shown in **Figure 4.2(a)**. In this case, all mPCs measured were analyzed after normalization of their ion responses to a single deuterated internal standard where they were annotated by characteristic their  $m/z$ :RMT and their sum composition annotation. We previously reported a participant who was likely nonadherent in the FO intervention trial based on a lack of concentration changes measured in their serum EPA and DHA trajectories,<sup>29</sup> which we confirmed independently in this work based on a lack of response change measured in their serum mPC 36:5 and mPC 40:6 profiles unlike other participants in the FO treatment arm. The overall data structure is shown in **Figure 4.2(b)**, which depicts a 2D PCA scores plot and hierarchical cluster analysis (HCA) heat map for 47 mPC and mSM species following *glog*-transformation and autoscaling. Good technical precision was achieved using repeat analysis of a pooled QC sample (median CV = 13%,  $n = 13$ ) as compared to



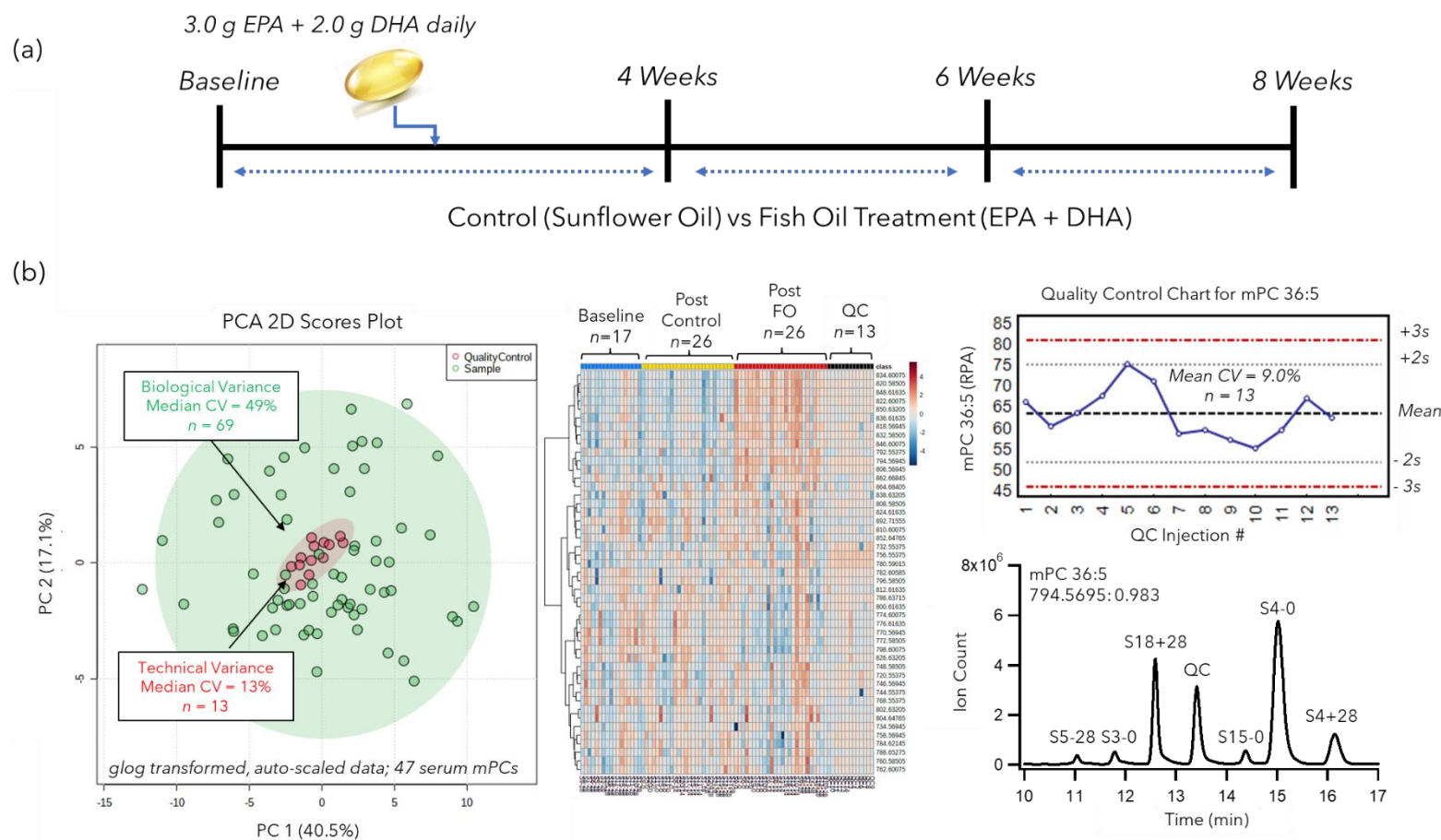


**Figure 4.2 (a)** Study design overview of serum samples from a cohort of young women ingesting either sunflower oil (SO) or high-dose FO supplement over an 8-week interval. **(b)** Summary of lipidomic data structure and data quality when using a 2D PCA scores plot and 2D hierarchical cluster analysis heatmap based on analysis of 47 mPCs and mSMs, including putative omega-3 index serum biomarkers identified after the subgroup analysis. For instance, the technical precision based on the repeat analysis of pooled QC serum samples was acceptable (median CV = 13%,  $n = 13$ ) when compared to the biological (between-subject) variability for the serum lipidome (median CV = 49%,  $n = 69$ ) as also demonstrated in the control chart for serum mPC 36:5. Extracted ion electropherogram depicts changes in the ion response for a randomized series of serum extracts analyzed by MSI-NACE-MS under positive ion mode conditions. Samples representing FO supplementation are noted by their large ion responses as compared to baseline or placebo samples, whereas the QC represents a pooled average response for the entire cohort.

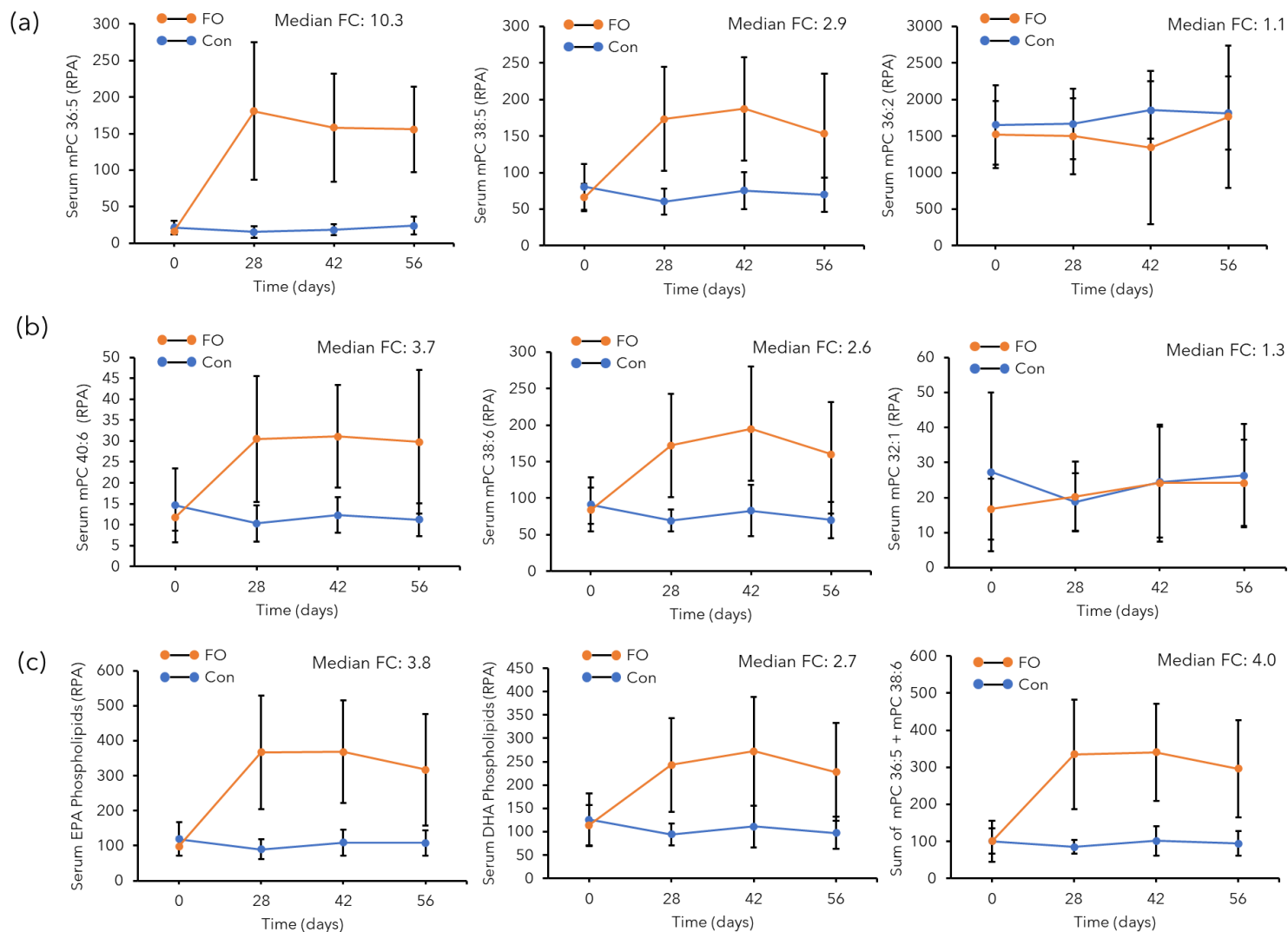


**Figure 4.3.** Serum lipid trajectory plots measured in young women ( $n = 9$ ) from baseline after ingesting high-dose FO supplement (3 g/day EPA+2 g/day DHA) as compared to a SO placebo over a 56-day period. **(a)** Highlights two top-ranked serum EPA containing PCs (mPC 36:5; mPC 38:5) that were most responsive to FO intake unlike a linoleic acid containing PC as control (mPC 36:2). **(b)** Highlights two top-ranked serum DHA containing PCs (mPC 40:6; mPC 38:6) that were most responsive to FO intake unlike an oleic acid containing PC as control (mPC 32:1). **(c)** Compares treatment response trajectories to FO intake based on the sum of three EPA- or DHA-containing PCs, as compared to the sum of the two best EPA and DHA-specific biomarkers (mPC 36:5+mPC 38:6).

the biological (between-subject) variance in the serum lipidome for all participants (median CV = 49%,  $n = 69$ ). **Figure 4.3** depicts box plots for a series of top-ranked serum biomarkers associated with high-dose FO ingestion as compared to placebo that received SO when using a repeat measure mixed 2-way ANOVA model. Since SO consumed contains linoleic (C18:2) and oleic acid (C18:1) as major FA constituents, serum levels of mPC 32:1 and mPC 36:2 were also included as PL controls for comparison, but they showed no significant response change ( $p > 0.05$ ) in both placebo and FO treatment arm. Overall, changes in serum lipidome profiles demonstrate that PCs containing EPA (as a single species or as sum) responded to FO supplementation to a greater extent than DHA containing mPC species. These results are consistent with serum free fatty acid trajectories measured previously in this cohort, where serum EPA strongly was correlated to EPA concentrations measured from erythrocyte PL hydrolysates while being more responsive to FO ingestion than DHA.<sup>29</sup> This likely reflects the 50% higher dosage of EPA (3 g/day) as compared to DHA (2 g/day) used in the FO supplement. Additionally, differences in the underlying kinetics and lipid distribution patterns for these two distinct yet essential omega-3 FA species may also contribute to these findings. For instance, DHA in erythrocytes take longer to trans-esterify and incorporate within plasma PLs than EPA,<sup>25</sup> whereas DHA preferentially incorporates into the PE of lipid membrane bilayers while EPA incorporates more readily into PCs.<sup>25</sup> Indeed, our sub-group analysis using MSI-NACE-MS under negative ion mode did not reveal any PE species that displayed a significant response changes following high-dose FO supplementation as compared to baseline/placebo (**Figure S4.1**). As expected, our omega-3 mPC lipid panel was able to readily detect a nonadherent

participant (S10) in the FO treatment arm that was also previously reported to not be compliant with leg immobilization protocols (**Figure S4.2**). Overall, [DHA + EPA] concentrations measured in PL hydrolysates demonstrated a median fold-change of 2.6 from baseline that was similar to the sum of serum EPA and DHA as their NEFAs,<sup>29</sup> but less than the sum of mPC 36:5+mPC 38:6 with a median FC of 4.0 as shown in the right panel of **Figure 4.3(c)**. Interestingly, moderate positive correlations were found for all participants ( $n = 69$ ) when associating serum specific omega-3 PCs to their corresponding EPA or DHA erythrocyte PL fractions as highlighted in **Figure S4.2(a,b)**. When exploring serum lipidome changes using a two-way mixed model ANOVA (**Table 4.1**), it was clear that a specific serum lipid profile containing a combination of EPA and DHA containing PCs would perform best to incorporate responses from ingestion to both essential omega-3 FA nutrients. Overall, the sum of PC 36:5 and PC 38:6 together performed exceptionally well as a sensitive yet specific metric of omega-3 FA intake relative to placebo when compared to all other combinatorial profiles or single serum PC biomarkers. In fact, both these PC species contain palmitic acid in their *sn*-1 position (*i.e.*, PC 16:0/20:5 and PC 16:0/22:6), which was found to exhibit a moderate positive correlation ( $r = 0.717$ ,  $p = 4.39 \times 10^{-12}$ ) to O3I measurements from red blood cell PL membranes as highlighted in **Figure S4.2(c)**. This supports the potential that these two specific circulating PCs species may offer a clinically useful surrogate measure for O3I status that is also responsive to lifestyle changes associated with habitual dietary omega-3 intake, such as high-dose FO supplements.

**Table 4.1.** Responsive fasting serum mPCs associated with high-dose FO intake classified by a two-way mixed-model ANOVA with repeated time points for within subject effects when comparing FO and control (sunflower oil) treatment arms.

Serum PCs	Within-Subject Effects				Between-Subject Effects			
	<i>F</i>	<i>p</i> value <sup>a</sup>	Effect Size <sup>b</sup>	Study Power	<i>F</i>	<i>p</i> value	Effect Size <sup>b</sup>	Study Power
mPC 36:5 + mPC 38:6 <sup>c</sup>	6.89	$7.81 \times 10^{-4}$	0.346	0.965	74.1	$9.93 \times 10^{-7}$	0.851	1.000
Total EPA mPCs ( <i>n</i> = 3)	6.76	$8.83 \times 10^{-4}$	0.342	0.962	54.2	$6.00 \times 10^{-6}$	0.806	1.000
mPC 36:5	6.69	$9.42 \times 10^{-4}$	0.340	0.960	33.4	$6.30 \times 10^{-5}$	0.720	1.000
Total ω-3 mPCs ( <i>n</i> = 6)	6.30	$1.37 \times 10^{-3}$	0.326	0.949	14.8	$2.00 \times 10^{-3}$	0.533	0.945
Total DHA mPCs ( <i>n</i> = 3)	5.39	$3.36 \times 10^{-3}$	0.293	0.909	32.8	$7.00 \times 10^{-5}$	0.716	1.000
mPC 38:5	5.12	$4.43 \times 10^{-3}$	0.282	0.893	39.0	$3.00 \times 10^{-5}$	0.750	1.000
mPC 38:6	4.94	$5.27 \times 10^{-3}$	0.276	0.882	20.2	$6.01 \times 10^{-4}$	0.609	1.000
mPC 40:6	4.51	$8.26 \times 10^{-3}$	0.258	0.848	25.6	$2.17 \times 10^{-4}$	0.664	0.997
mPC 36:1	1.37	$2.66 \times 10^{-3}$	0.095	0.336	0.01	$9.35 \times 10^{-1}$	0.001	0.051
mPC 36:2	0.23	$8.72 \times 10^{-1}$	0.018	0.090	0.16	$6.95 \times 10^{-1}$	0.012	0.066

<sup>a</sup> Mixed-model ANOVA applied where data sphericity satisfied using Mauchly's test of sphericity.

<sup>b</sup> Effect size based on Partial Eta Squared.

<sup>c</sup> mPC 36:5 = mPC (16:0/20:5) + mPC 38:6 = mPC (16:0/22:6)

#### 4.4.3. Validation of Serum PC Biomarkers of O3I Status Following DHA or EPA Specific Supplementation

While the previous study identified specific PC species that were responsive to FO supplementation, it relied on an unequal mixture of omega-3 FAs while only including a modest number of women, such that the results may not be generalizable. There is growing interest investigating the specific effects of DHA and EPA for improved understanding of their complementary mechanisms of action while elucidating optimal therapeutic interventions for precision health. However, this can be difficult to elucidate using mixed omega-3 FA supplements given the capacity for *in-vivo* retroconversion of DHA to EPA in humans, whereas EPA does not retroconvert to DHA.<sup>32,37</sup> Additionally, the rapid

incorporation of EPA into erythrocyte membranes can result in the masking of nonadherence to long-term FO intervention whereas circulating PCs may serve as more sensitive biomarkers for dietary surveillance.<sup>38</sup> However, there have been few studies that have compared the specific effects of EPA from DHA supplementation in humans to date. For instance, the Japan EPA Lipid Intervention Study (JELIS)<sup>39</sup> and The Reduction of Cardiovascular Events with Icosapent Ethyl-Intervention Trial (REDUCE-IT)<sup>40</sup> have both reported reduced risks of cardiovascular events after 5 years using EPA ethyl ester supplementation with patients taking statins. Although some smaller trials do indeed directly compare EPA and DHA supplementation in humans, they demonstrate that DHA is more efficacious than EPA in reducing triglycerides<sup>41,42</sup> while previous work demonstrated that EPA lacked triglyceride lowering effects.<sup>27</sup> Thus, we aimed to validate lead candidate serum PC biomarkers of O3I in a second independent clinical trial involving a larger cohort of participants using DHA or EPA specific supplementation at the same dosage level (3 g/day) as highlighted in **Figure 4.4(a)**. In this case, fasting (EDTA) plasma samples were collected as the blood specimen type rather than serum. **Table S4.1** summarizes the characteristics of the participants in this second validation study, which included a cohort of young, normal weight, Canadian adults of both sexes who had an average baseline O3I of  $(3.98 \pm 0.73)$  and  $(3.46 \pm 0.77)$  for women ( $n=14$ ) and men ( $n=13$ ), respectively. After previously authenticating several omega-3 containing PCs responsive to FO supplementation, we performed a targeted lipidomic analyses of these same PCs when using MSI-NACE-MS in positive ion mode. For the participants assigned to ingest the high-dose (3 g/day) EPA dietary supplement, the same plasma PCs as FO showed

significant increases following ingestion over 12 weeks, primarily mPC 36:5 and mPC38:5 as shown in **Figure 4.4(b)**. Notably, the same DHA containing mPC species also demonstrated increases after DHA intake, but it was more attenuated (~ 2 fold) compared to EPA intervention (up to 7-fold) as highlighted in **Figure 4.4(c)** that is consistent with the preferential uptake and enrichment of EPA into circulating blood PCs. These observations also suggest that DHA may be distributed to other lipid pools and/or stored in specific tissues to a greater extent than EPA, further demonstrating their distinct mechanisms of metabolism and distribution. Given that the constituents of olive oil primarily consist of linoleic and oleic acids, we also profiled various mPC species that would likely contain these unsaturated FAs as well. Indeed, there was a modest, yet significant change (~ 1.2-fold) observed in mPC 36:1 and mPC 38:2 from baseline following olive oil ingestion after 12 weeks in this study that was still lower in magnitude as compared to omega-3 FAs that derive primarily from seafood in the diet.

#### **4.4.4. Circulating $\omega$ -3 Phosphatidylcholines as Surrogate Markers to Measure Omega-3 Index**

The omega-3 index (O3I) can serve as a predictive biomarker of sudden cardiac death since the DHA+EPA content of erythrocyte membranes are correlated with human cardiac membrane EPA + DHA levels that can alter myocardium function.<sup>19</sup> A recent surveillance study reported that 43% of Canadian adults had O3I levels that were associated with a high risk for coronary heart disease.<sup>21</sup> However, routine screening for O3I is often difficult as erythrocytes isolated from whole blood are prone to hemolysis during processing and often are not available in biobank repositories in comparison to other biospecimen types, such as

(a) 3.0g/day of either EPA, DHA or Olive Oil

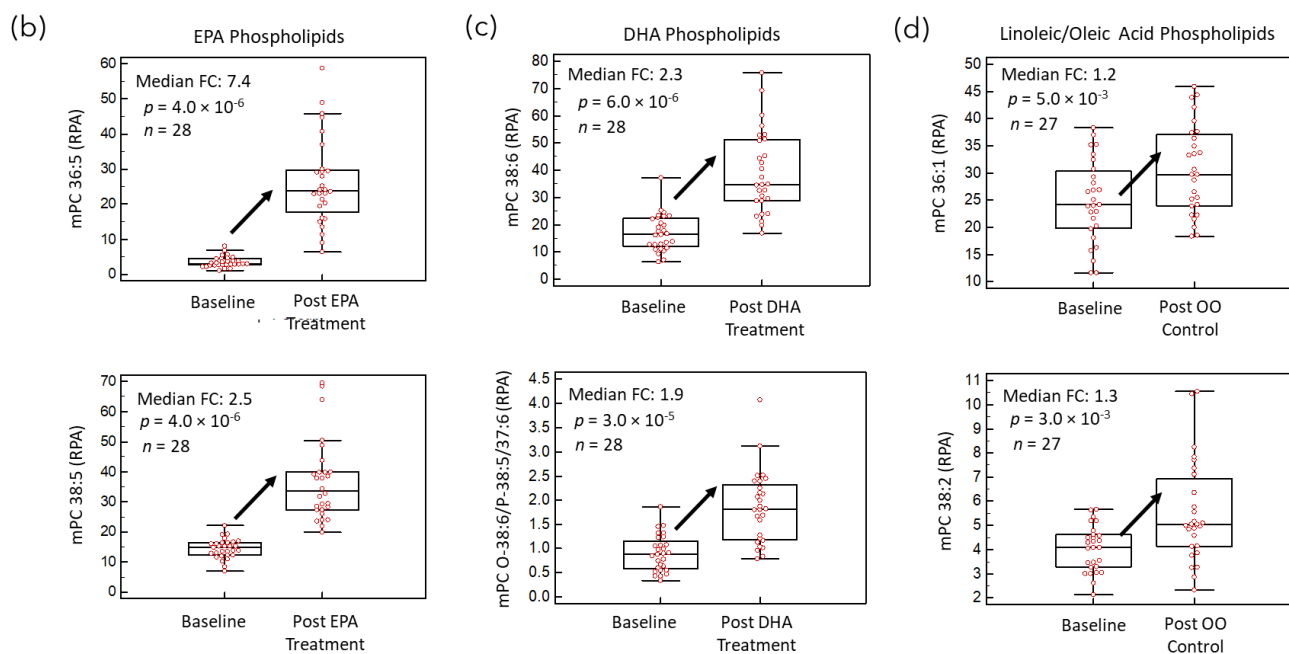
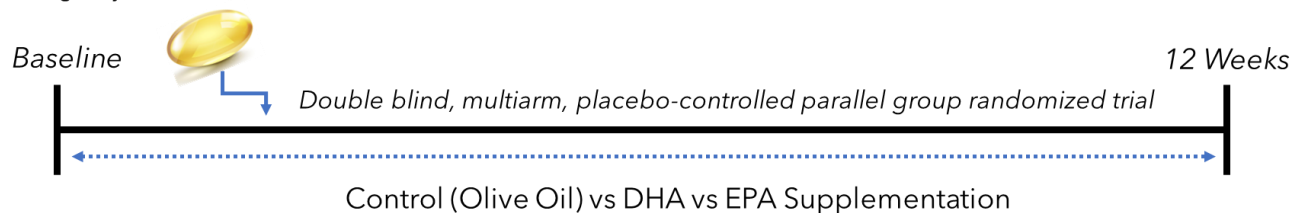


**Figure 4.4** (a) Overview of the validation cohort involving a placebo-controlled clinical trial of participants ingesting either olive oil (OO), DHA or EPA supplementation (3 g/day) over a 12-week period. Representative box-plots shown for (b) two top-ranked EPA and (c) two top-ranked DHA containing PCs that exhibited a significant increase in response after EPA or DHA supplementation, respectively as compared to (c) linoleic/oleic acid containing PCs as olive oil placebo/control. Notably, PC 36:5 is more sensitive to EPA ingestion at the same dosage level than DHA consistent with outcomes from the previous study with a modest treatment response from olive oil ingestion.



**Table 4.2.** Serum  $\omega$ -3 phospholipid models and their associated Pearson correlation to erythrocyte O3I.

Lipid Panel	Number of Lipids (EPA, DHA)	Pearson Correlation ( <i>r</i> )	<i>p</i> -value
mPC 36:5 + mPC 38:6 <sup>a</sup>	2 (EPA: 1, DHA: 1)	0.764	$3.0 \times 10^{-33}$
mPC 36:5 + mPC 38:5 + mPC 38:6 + mPC 40:6	4 (EPA: 2, DHA: 2)	0.711	$5.6 \times 10^{-27}$
mPC 36:5 + mPC 38:5 + mPC 38:6	3 (EPA: 2, DHA: 1)	0.706	$1.7 \times 10^{-26}$
mPC 38:6	1 (EPA: 0, DHA: 1)	0.663	$1.5 \times 10^{-22}$
mPC 36:5 + mPC 38:5 + mPC 40:5 + mPC 36:6 + mPC 38:6 + mPC 40:6	6 (EPA: 3, DHA: 3)	0.636	$2.5 \times 10^{-20}$
mPC 36:5	1 (EPA: 1, DHA: 0)	0.494	$1.2 \times 10^{-11}$
mPC 38:5	1 (EPA: 1, DHA: 0)	0.484	$3.5 \times 10^{-11}$
mPC 40:6	1 (EPA: 0, DHA: 1)	0.387	$2.5 \times 10^{-7}$
mPC 36:6	1 (EPA: 0, DHA: 1)	0.225	$3.5 \times 10^{-3}$
mPC 40:5	1 (EPA: 1, DHA: 0)	0.222	$4.0 \times 10^{-3}$

<sup>a</sup> *mPC 36:5 = mPC (16:0\_20:5) + mPC 38:6 = mPC (16:0\_22:6)*

serum or plasma. We aimed to further validate that specific circulating PCs in fasting serum or plasma samples can serve as useful surrogate measures of O3I that can reflect changes in dietary omega-3 FA intake when using purified supplements of DHA, EPA or olive oil (control) at the same dosage level. While the total sum of all ( $n = 6$ ) pertinent omega-3 lipid species demonstrated moderate correlation ( $r = 0.636$ ) to O3I, the performance further improved when using fewer serum PCs as summarized in **Table 4.2**. Similar to the FO supplementation study, the strongest correlation to O3I was based on the sum of plasma levels of mPC 36:5 and mPC 38:6, which represent two of the most abundant circulating EPA and DHA PL species ( $r = 0.764$ ,  $p = 3.0 \times 10^{-33}$ ). **Figure 4.5(a)** depicts a correlation plot for plasma mPC 36:5 + mPC 38:6 as a function of O3I which highlights the striking yet differential enhancement in omega-3 nutrition status after 12 weeks of intervention,

where 64% and 11% of participants intaking DHA and EPA had their O3I status in the low-risk level for optimal cardiovascular health ( $> 8\%$  O3I). Although EPA had a less efficacious response to changing O3I, all participants improved to a moderate risk level (4-8%). In contrast, the majority of participants at baseline or ingesting placebo (74% or 82/110) had high-risk O3I status ( $< 4\%$ ). Additionally, we explored the differential efficacy of omega-3 FA supplementation by investigating DHA and EPA-specific correlations to plasma mPC 36:5 + mPC 38:6 with changes in O3I from baseline as depicted in **Figure 4.5(b)**. As expected, DHA supplementation alone contributed to a 63% greater relative efficacy overall ( $\Delta$  O3I =  $4.90 \pm 1.33$ ) as compared to participants ingesting a similar dosage regimen for EPA ( $\Delta$  O3I =  $2.99 \pm 1.19$ ). This difference in responsivity is also captured by comparing the slopes determined from the correlation of DHA (slope = 5.36) and EPA (slope = 9.17) only supplement sub-groups based on a least-squares linear regression model. As a result, this model can be used to adjust for the attenuated DHA response relative to EPA in the circulating PC lipid pool to estimate their content more accurately in erythrocyte membrane given their localized functional consequences on cellular/tissue activity. Although sex-dependent supplementation differences are observed (**Table S4.2**), more study power is needed to draw conclusions given that some subjects demonstrated no change in O3I and/or reduced serum lipid responses after treatment, which heavily influenced comparisons. Nevertheless, routine surveillance of O3I status and monitoring of treatment responses to omega-3 supplements may be realized via high throughput screening of serum/plasma mPC 36:5 + mPC 38:6 for chronic disease prevention and promotion of human health based on modifiable lifestyle factors, such as

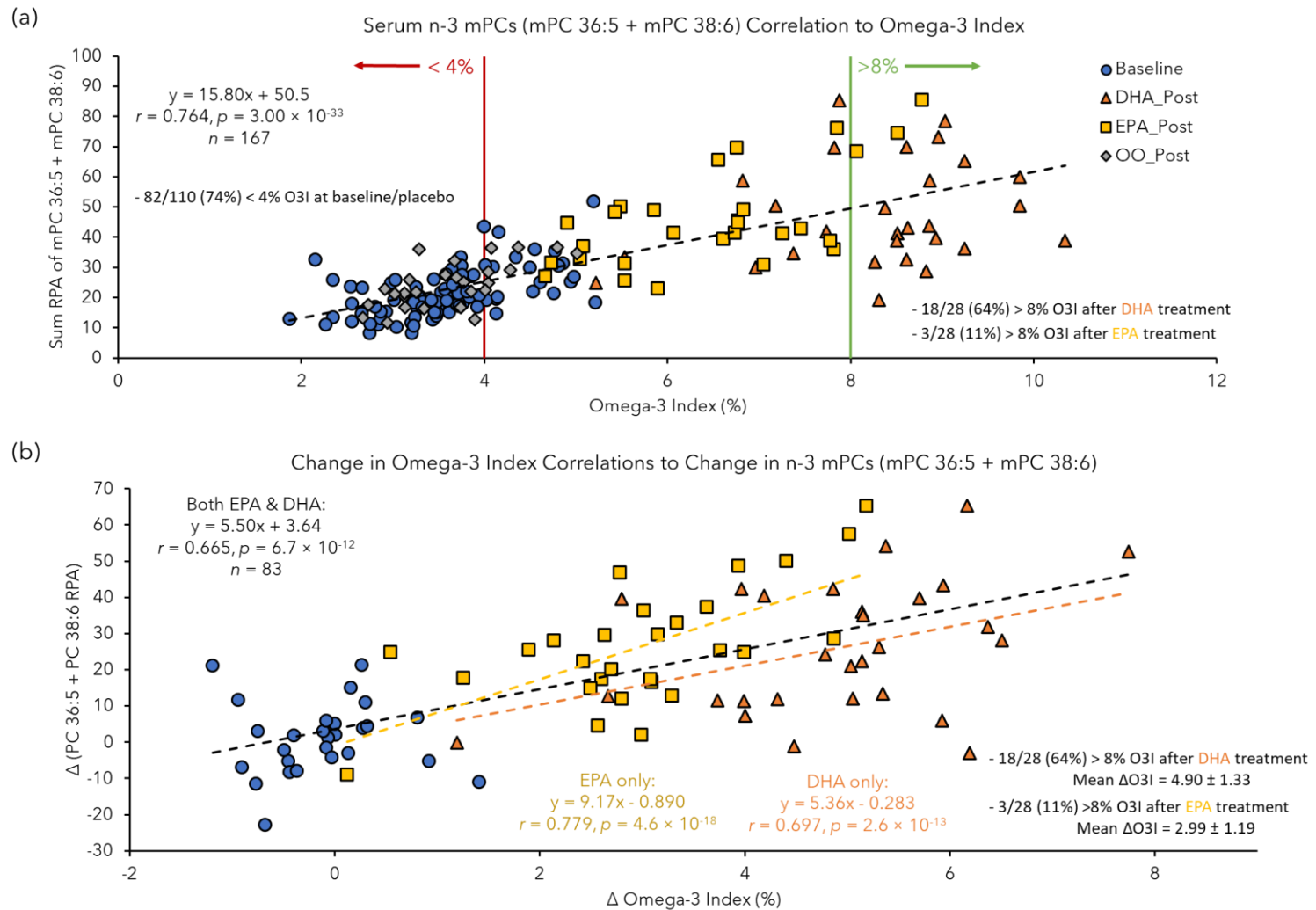


**Figure 4.5 (a)** Scatter plot showing strong correlation ( $r = 0.764, p = 3.0 \times 10^{-33}$ ) of O3I to PC 36:5 and PC 38:6, a single EPA and DHA phospholipid at all time points ( $n = 167$ ) in separate DHA/EPA supplementation study. Defined O3I boundaries set at suggested cut off levels where  $< 4\%$  is considered high risk, 4-8% is intermediate and  $> 8\%$  is low risk for cardiovascular events. Notably, this demonstrates that DHA supplementation contributes more to improved O3I quality scores compared to EPA. This is further evidenced in (b) which correlates the change in these phospholipids to change in O3I.

diet and nutraceutical supplements.

#### **4.5. Conclusion**

In this work, we explored and validated the impact of high-dose omega-3 supplementation using FO, as well as DHA and EPA specific formulations, on changes in the phospholipid profiles of healthy participants in two independent intervention studies. We first introduced an accelerated data workflow when using MSI-NACE-MS based on a sub-group analysis to identify putative circulating biomarkers associated with dietary intake of omega-3 FAs relative to placebo. In both studies, we determined that EPA containing PCs were more sensitive to supplementation than DHA containing PCs. However, all other phospholipid classes measured in this work did not significantly incorporate DHA or EPA, including PEs, PIs, SMs and lysoPCs with the exception for free fatty acids of EPA and DHA. Overall, the combination of circulating PC 36:5 (or PC 16:0\_20:5) and PC 38:6 (PC 16:0\_22:6) provided the strongest correlation to O3I that reflects local changes in erythrocyte PC membrane composition and cellular function. Shorter sampling time points are needed to better assess the minimum time frames required for equilibration of omega-3 specific PCs in circulation that may likely be impacted by other factors given large between-subject variability, such as age, BMI, dosage, specific lipid formulation, and specific comorbidities impacting fat absorption (e.g., cystic fibrosis, inflammatory bowel disease). Limitations to this study include use of a lipidomics platform that cannot resolve neutral lipids classes, such as cholesterol esters, triglycerides and diglycerides. However, these abundant lipid classes have much shorter lifetimes than PCs and other phospholipid pools and thus may be too sensitive to recent food intake patterns. Future work will further validate these findings in a larger cohort as required for better calibration and adjustment for differential uptake patterns of EPA as compared to DHA within circulating phospholipid pools for accurate O3I determination. We anticipate that the

development of assays based on direct infusion-MS/MS may allow for rapid screening of PC 36:5 and PC 38:6 as surrogate biomarkers of O3I, which can be applied in smaller volumes of blood, including dried blood spots. This work is critical to provide better risk assessment tools for cardiovascular health and sudden cardiac death in the population while also guiding evidence-based nutritional guidelines.

#### 4.6. References

- (1) Mente, A.; Dehghan, M.; Rangarajan, S.; McQueen, M.; Dagenais, G.; Wielgosz, A.; Lear, S.; Li, W.; Chen, H.; Yi, S.; et al. *Lancet Diabetes Endocrinol* 2017, 5 (10), 774–787.
- (2) Temple, N. J. *Nutrients* 2018, 10 (1), 39.
- (3) Siri-Tarino, P. W.; Chiu, S.; Bergeron, N.; Krauss, R. M. *Annu Rev Nutr* 2015, 35 (1), 517–543.
- (4) Surette, M. E. *Can Med Assoc J* 2008, 178 (2), 177–180.
- (5) Rimm, E. B.; Appel, L. J.; Chiuve, S. E.; Djoussé, L.; Engler, M. B.; Kris-Etherton, P. M.; Mozaffarian, D.; Siscovick, D. S.; Lichtenstein, A. H.; Cardiology, O. behalf of the A. H. A. N. C. of the C. on L. and C. H. C. on E. and P. C. on C. D. in the Y. C. on C. and S. N. and C. on C. *Circulation* 2018, 138 (1), e35–e47.
- (6) Field, C. J.; Robinson, L. *Adv Nutr* 2019, 10 (4), 722–724.
- (7) Calder, P. C. *Nutrients* 2010, 2 (3), 355–374.
- (8) Cladis, D. P.; Kleiner, A. C.; Freiser, H. H.; Santerre, C. R. *Lipids* 2014, 49 (10), 1005–1018.
- (9) Ryckebosch, E.; Bruneel, C.; Termote-Verhalle, R.; Goiris, K.; Muylaert, K.; Foubert, I. *Food Chem* 2014, 160, 393–400.
- (10) Siscovick, D. S.; Barringer, T. A.; Fretts, A. M.; Wu, J. H. Y.; Lichtenstein, A. H.; Costello, R. B.; Kris-Etherton, P. M.; Jacobson, T. A.; Engler, M. B.; Alger, H. M.; et al. *Circulation* 2017, 135 (15), e867–e884.
- (11) Zhang, Z.; Fulgoni, V. L.; Kris-Etherton, P. M.; Mitmesser, S. H. *Nutrients* 2018, 10 (4), 416.
- (12) Middleton, P.; Gomersall, J. C.; Gould, J. F.; Shepherd, E.; Olsen, S. F.; Makrides, M. *Cochrane Db Syst Rev* 2018, 2018 (11), CD003402.

- (13) Abdelhamid, A. S.; Brown, T. J.; Brainard, J. S.; Biswas, P.; Thorpe, G. C.; Moore, H. J.; Deane, K. H.; Summerbell, C. D.; Worthington, H. V.; Song, F.; et al. *Cochrane Db Syst Rev* 2020, 2020 (3), CD003177.
- (14) Watanabe, Y.; Tatsuno, I. *J Atheroscler Thromb* 2020, 27 (3), 183–198.
- (15) Miller, M.; Bhatt, D. L.; Steg, P. G.; Brinton, E. A.; Jacobson, T. A.; Jiao, L.; Tardif, J.-C.; Ballantyne, C. M.; Budoff, M.; Mason, R. P.; et al. *European Hear J - Cardiovasc Pharmacother* 2022.
- (16) Garneau, V.; Rudkowska, I.; Paradis, A.-M.; Godin, G.; Julien, P.; Pérusse, L.; Vohl, M.-C. *Nutr J* 2012, 11 (1), 46.
- (17) Rafiq, T.; Azab, S. M.; Teo, K. K.; Thabane, L.; Anand, S. S.; Morrison, K. M.; de Souza, R. J.; Britz-McKibbin, P. *Adv Nutr* 2021, 12 (6), 2333–2357.
- (18) Harris, W. S.; Schacky, C. von. *Prev Med* 2004, 39 (1), 212–220.
- (19) Harris, W. S. *Am J Clin Nutrition* 2008, 87 (6), 1997S-2002S.
- (20) Harris, W. S.; Gobbo, L. D.; Tintle, N. L. *Atherosclerosis* 2017, 262, 51–54.
- (21) Langlois, K.; Ratnayake, W. M. N. *Health Rep* 2015, 26 (11), 3–11.
- (22) Baylin, A.; Campos, H. *Curr Opin Lipidol* 2006, 17 (1), 22–27.
- (23) Andersen, L. F.; Solvoll, K.; Johansson, L. R. K.; Salminen, I.; Aro, A.; Drevon, C. A. *Am J Epidemiol* 1999, 150 (1), 75–87.
- (24) Albert, C. M.; Campos, H.; Stampfer, M. J.; Ridker, P. M.; Manson, J. E.; Willett, W. C.; Ma, J. *New Engl J Medicine* 2002, 346 (15), 1113–1118.
- (25) Stark, K. *Lipid Technology* 2008, 20 (8), 177–179.
- (26) Mcglory, C.; Gorissen, S. H. M.; Kamal, M.; Bahniwal, R.; Hector, A. J.; Baker, S. K.; Chabowski, A.; Phillips, S. M. *Faseb J* 2019, 33 (3), 4586–4597.
- (27) Klingel, S. L.; Metherel, A. H.; Irfan, M.; Rajna, A.; Chabowski, A.; Bazinet, R. P.; Mutch, D. M. *Am J Clin Nutrition* 2019, 110 (6), 1502–1509.
- (28) Azab, S. M.; Souza, R. J. de; Ly, R.; Teo, K. K.; Atkinson, S. A.; Morrison, K. M.; Anand, S. S.; Britz-McKibbin, P. *Prostaglandins Leukot Essent Fat Acids* 2022, 176, 102378.
- (29) Azab, S. M.; Souza, R. J. de; Teo, K. K.; Anand, S. S.; Williams, N. C.; Holzschuher, J.; McGlory, C.; Phillips, S. M.; Britz-McKibbin, P. *J Lipid Res* 2020, 61 (6), 933–944.

- (30) Ly, R.; Ly, N.; Sasaki, K.; Suzuki, M.; Kami, K.; Ohashi, Y.; Britz-McKibbin, P. *J Proteome Res* 2022, 21 (3), 768–777.
- (31) FOLCH, J.; LEES, M.; STANLEY, G. H. S. *J Biological Chem* 1957, 226 (1), 497–509.
- (32) Metherel, A. H.; Irfan, M.; Klingel, S. L.; Mutch, D. M.; Bazinet, R. P. *Am J Clin Nutrition* 2019, 110 (4), 823–831.
- (33) Azab, S.; Ly, R.; Britz-McKibbin, P. *Anal Chem* 2019, 91 (3), 2329–2336.
- (34) Kuehnbaum, N. L.; Kormendi, A.; Britz-McKibbin, P. *Anal Chem* 2013, 85 (22), 10664–10669.
- (35) Dawczynski, C.; Plagge, J.; Jahreis, G.; Liebisch, G.; Höring, M.; Seeliger, C.; Ecker, J. *Nutrients* 2022, 14 (15), 3055.
- (36) Lemaitre-Delaunay, D.; Pachiaudi, C.; Laville, M.; Pousin, J.; Armstrong, M.; Lagarde, M. *J Lipid Res* 1999, 40 (10), 1867–1874.
- (37) Brenna, J. T. *Am J Clin Nutrition* 2019, 110 (4), 789–790.
- (38) Brenna, J. T.; Plourde, M.; Stark, K. D.; Jones, P. J.; Lin, Y.-H. *Am J Clin Nutrition* 2018, 108 (2), 211–227.
- (39) Yokoyama, M.; Origasa, H.; Matsuzaki, M.; Matsuzawa, Y.; Saito, Y.; Ishikawa, Y.; Oikawa, S.; Sasaki, J.; Hishida, H.; Itakura, H.; et al. *Lancet* 2007, 369 (9567), 1090–1098.
- (40) Bhatt, D. L.; Steg, P. G.; Miller, M.; Brinton, E. A.; Jacobson, T. A.; Ketchum, S. B.; Doyle, R. T.; Juliano, R. A.; Jiao, L.; Granowitz, C.; et al. *New Engl J Med* 2019, 380 (1), 11–22.
- (41) Allaire, J.; Vors, C.; Harris, W. S.; Jackson, K. H.; Tchernof, A.; Couture, P.; Lamarche, B. *Brit J Nutr* 2019, 121 (11), 1223–1234.
- (42) Grimsgaard, S.; Bonna, K. H.; Hansen, J. B.; Nordøy, A. *Am J Clin Nutrition* 1997, 66 (3), 649–659.

## 4.7. Supplemental Information

### Chapter IV

#### **Lipidomics for Identifying Serum Phospholipids as Surrogate Biomarkers of Omega-3 Index using Multisegment Injection-Nonaqueous Capillary Electrophoresis-Mass Spectrometry**

*Ritchie Ly,<sup>1</sup> Brittany MacIntyre,<sup>2</sup> Stuart Philips,<sup>3</sup> Chris McGlory,<sup>3,4</sup> David Mutch,<sup>2</sup>  
Philip Britz-McKibbin<sup>1</sup>*

<sup>1</sup> *Department of Chemistry and Chemical Biology, McMaster University, Hamilton, Ontario Canada*

<sup>2</sup> *Department of Human Health and Nutritional Sciences, University of Guelph, Guelph, Ontario Canada.*

<sup>3</sup> *Department of Kinesiology, McMaster University, Hamilton, Ontario Canada*

<sup>4</sup> *School of Kinesiology and Health Studies, Queen's University, Kingston, Ontario Canada*



**Table S4.1.** Clinical characteristics of participants in a placebo-controlled DHA or EPA (3.0 g/day) treatment intervention over 84 days.

Grouping	Sex	Clinical Characteristic			
		Age	BMI	O3I (Baseline)	O3I (Post)
Placebo (OO)	Female, $n = 14$	$21 \pm 1$	$24.6 \pm 3.3$	$3.98 \pm 0.73$	$3.76 \pm 0.60$
	Male, $n = 13$	$21 \pm 2$	$24.0 \pm 4.0$	$3.46 \pm 0.77$	$3.45 \pm 0.59$
DHA	Female, $n = 15$	$22 \pm 2$	$22.7 \pm 2.7$	$3.73 \pm 0.51$	$8.04 \pm 1.34$
	Male, $n = 13$	$23 \pm 3$	$24.3 \pm 3.3$	$3.15 \pm 0.64$	$8.73 \pm 0.97$
EPA	Female, $n = 14$	$21 \pm 2$	$22.5 \pm 2.8$	$3.61 \pm 0.64$	$6.75 \pm 1.20$
	Male, $n = 14$	$21 \pm 2$	$23.4 \pm 2.7$	$3.40 \pm 0.87$	$6.23 \pm 1.10$

**Table S4.2.** Sex-dependence of DHA or EPA treatment intervention on lipid panel measured by MSI-NACE-MS and O3I.

Treatment	Sex	Age <sup>a</sup>	$\Delta$ (mPC 36:5 + mPC 38:6) RPA <sup>a</sup>	$\Delta$ O3I <sup>a</sup>	p-value	
					$\Delta$ mPC Panel <sup>b</sup>	$\Delta$ O3I <sup>c</sup>
Placebo (OO)	F = 14	$21.0 \pm 1.4$	$0.43 \pm 11.38$	$-0.22 \pm 0.54$	$7.38 \times 10^{-1}$	$6.16 \times 10^{-1}$
	M = 13	$20.9 \pm 2.2$	$1.74 \pm 8.51$	$-0.01 \pm 0.65$		
EPA	F = 14	$21.0 \pm 2.1$	$33.71 \pm 16.15$	$3.14 \pm 1.25$	$1.89 \times 10^{-2}$	$5.71 \times 10^{-1}$
	M = 14	$21.6 \pm 2.0$	$19.30 \pm 14.26$	$2.83 \pm 1.14$		
DHA	F = 15	$21.5 \pm 1.8$	$26.11 \pm 16.15$	$4.31 \pm 1.26$	$9.66 \times 10^{-1}$	$1.90 \times 10^{-2}$
	M = 13	$22.6 \pm 2.8$	$25.80 \pm 20.88$	$5.57 \pm 1.10$		

<sup>a</sup> Reported values are mean  $\pm$  standard deviation<sup>b</sup> p-values calculated with Student's t-test after confirming normality using Shapiro-Wilk ( $p > 0.05$ )<sup>c</sup> p-values calculated with Mann-Whitney U test after confirming normality using Shapiro-Wilk ( $p < 0.05$ )

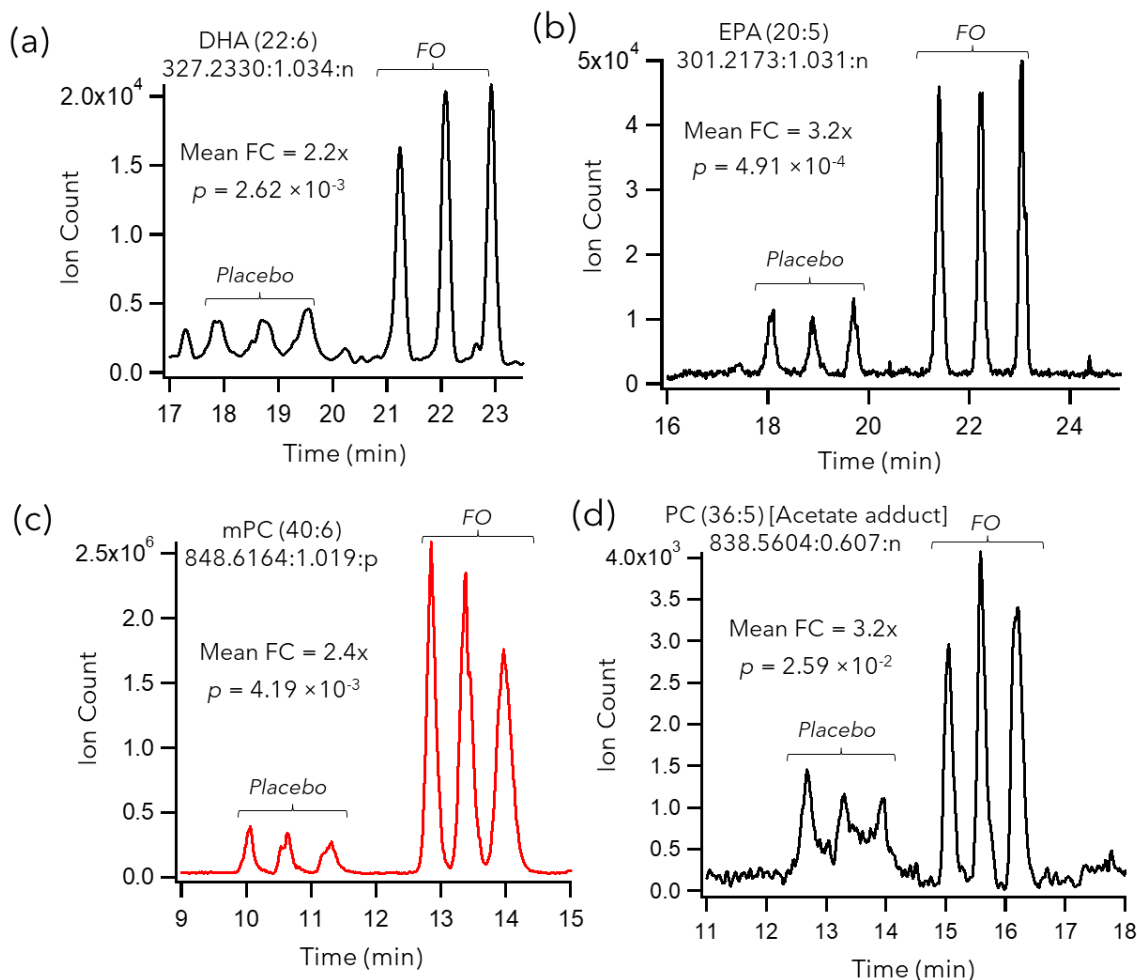


**Figure S4.1.** Sub-group analysis of high-dose FO supplementation as compared to placebo/baseline showing response changes for (a) DHA and (b) EPA as their free FAs that were measured by MSI-NACE-MS under negative ion mode. (c) Furthermore, a DHA-containing PC species (mPC 40:6) was confirmed to have a major increase in response following FO ingestion albeit a lesser extent than mPC 36:5 when using MSI-NACE-MS under positive ion mode (with FMOC/MTT labeling). (d) Independent replication of increase to PC 36:5 (detected as acetate adduct) by MSI-NACE-MS with FO ingestion under negative ion mode conditions, which is sub-optimal for quantitative analysis given impact of matrix induced ion suppression effects under these operating conditions

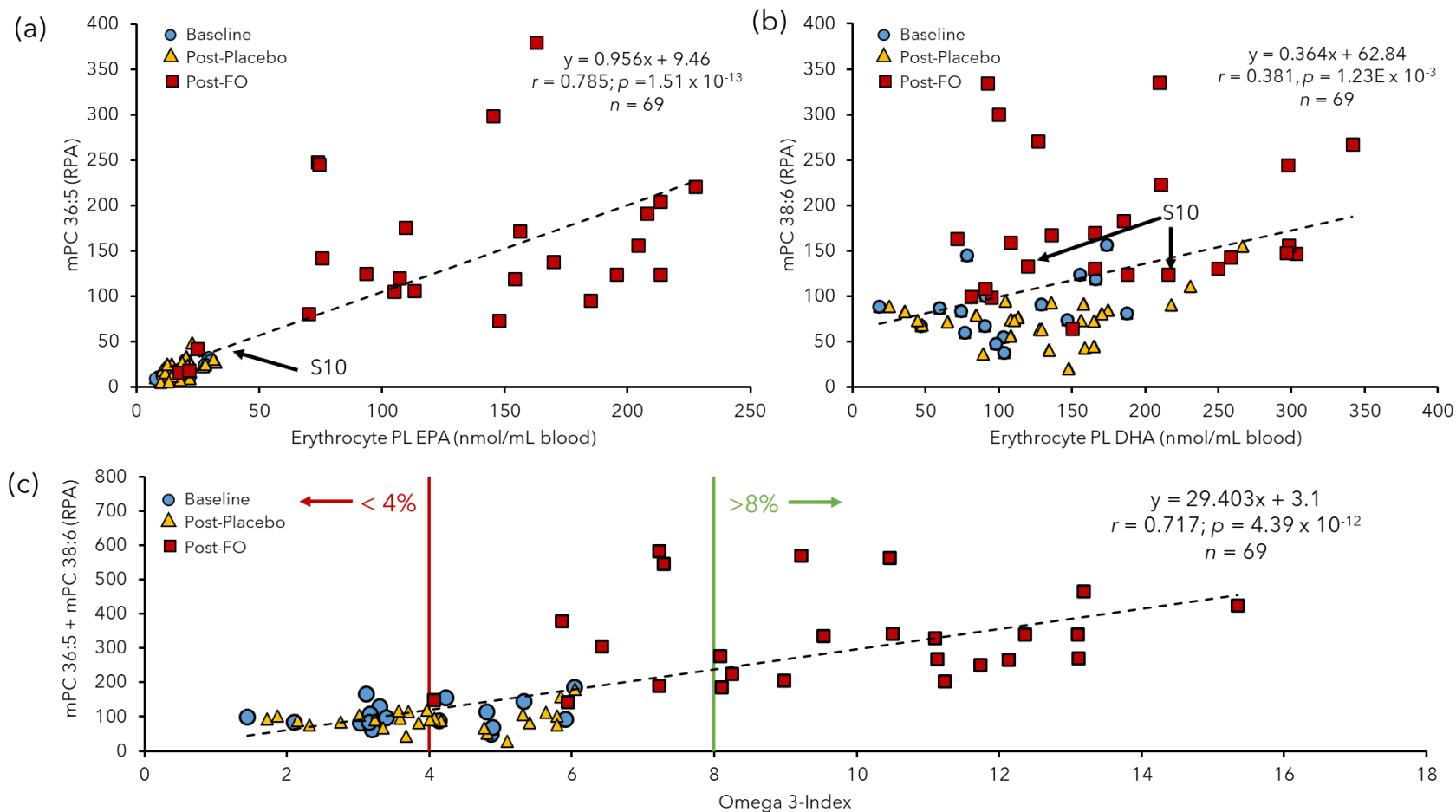


**Figure S4.2.** Scatter plots showing moderate linear correlation ( $r = 0.738$ ) between measured PCs containing (a) EPA ( $n = 3$ ) with erythrocyte PL EPA measurements that is more sensitive to detecting dietary nonadherence to FO supplementation (S10) in comparison to PCs containing (b) DHA and previously reported EPA as its NEFA at all time points ( $n = 69$ ). PCs containing DHA show weaker correlation ( $r = 0.428$ ). (c) Scatter plot demonstrating strong correlation ( $r = 0.717$ ) between proposed lipid profile (mPC 36:5 + mPC 38:6) to O3I measured traditionally using fatty acid content in red blood cell membranes from FO study

**Chapter V:**

**Future Directions in Lipidomics Using NACE for Biomarker Discovery**

## Chapter V: Conclusions and Future Directions

### 5.1 Overview of Major Thesis Contributions

As the field of lipidomics continues to flourish, several movements by the community have been made to harmonize approaches given the complexity and disarray in reporting and publication. This has spawned several actions by the community such as several ring trials using standard reference materials<sup>1,2</sup> and even the introduction of reporting a dynamic checklist to standardize language across the community.<sup>3</sup> Whilst this aims to increase the quality of work and tackle issues of reproducibility within the field, this can act as a deterrent for new and innovative approaches to progress the field forward. For example, the sheer cost of the necessary deuterated and purified lipid standards alone requires large investment that when coupled to the general unavailability of many species – drastically inhibits quantitative efforts. These issues can be further exacerbated when extending to larger scale projects to attain the necessary study power for lipid biomarker discovery, which introduces more issues in itself (*i.e.*, batch variation, quality control, etc). Coupled to the continual development and additions to the wide variety of bioinformatics tools available for the field – more efforts should be made to devise approaches to make the lipidomics field more accessible to the broader community. Thus, this thesis presents several major contributions by spearheading the movement for presenting MSI-NACE-MS as a new approach that is a viable, cost-effective, yet robust platform for lipidomics studies. This was demonstrated using several strategies and tools to facilitate accelerating lipidomic biomarker discovery through nontargeted approaches and in larger-scale studies that build on the many advancements already made by the lipidomics community.

In *Chapter II*, we construct an iterative workflow using new software tools to aid in filtering of nontargeted features. Furthermore, studies from our group that involved the use of MSI-NACE-

MS since its successful introduction had primarily been targeted in nature with a focus on nonesterified fatty acids. In this work, we then introduce a formalized, multi-tiered strategy to approach nontargeted studies using MSI-NACE-MS to unveil impressive lipidomic profiling capabilities of several lipid species over a wide polarity range. This was conducted in collaboration with Human Metabolome Technologies in Tsuruoka, Yamagata, Japan where this assay was demonstrated on a unique CE-Orbitrap-MS system that was connected using a custom in-house developed ESI source. In this context, we substantially expanded the number of lipids profiled by MSI-NACE-MS to > 260 lipids with 128 that met the credentialing criteria of our iterative workflow. Briefly, open source-software MZmine was used to visually screen through the dilution trend pattern to quickly eliminate features with the use of implemented tools (*i.e.*, CAMERA) to filter through adducts and isotope peaks. This filtered list was then integrated and subjected to quantitative criteria to address repeatability, linearity and absence of background signals to further refine. This was then subject to a frequency filter as this study was ultimately applied to a cohort of Japanese patients of varying severity of nonalcoholic fatty liver disease. Thus, lipid features were eliminated based on CVs of their QCs in the entire study as well as their frequency within all samples prior to creation of the data matrix. We further validate our features through the use of a mobility map to classify charged lipid species over a wide polarity range that demonstrates selectivity complimentary to chromatographic separations. Using this, the serum lipidome profiles were able to differentiate high- from low-risk NASH patients where elevated circulating NEFAs were then associated to other clinical characteristics such as increased glucose intolerance and more severe liver fibrosis and greater disease burden. While a major limitation of the study was that it did not contain a control group of subjects, this work demonstrates the capabilities of MSI-NACE-MS as a multiplexed lipidomic platform to screen for several lipid species, while still

providing robustness for larger lipidomic studies.

*Chapter III* represents an expansion to the profiling capabilities demonstrated previously using MSI-NACE-MS as another major limitation of the study was that many phosphatidylcholine (PC) species were unable to be reliably measured due to their zwitterionic nature resulting in comigration in regions of major ion suppression. While responses were enhanced when switching to an acidic buffer and operating under positive ion acquisition mode, PC still largely overlapped within species as well as with ion suppression regions resultant from the EOF. Derivatization strategies using diazomethane exist to fix a permanent positive charge on PC species with quantitative yields but require handling of dangerous reagents which can be a deterrent in large scale studies. In this work, we introduce an alternative methylation strategy that involves the use of MTT, an underutilized reagent that is inexpensive and safer relative to diazomethane. To combat the possibility of generating isobaric species via permethylation of phosphatidylethanolamine (PE), we introduce the use of Fmoc as a first-tier step to cap PE head groups and effectively move them away as being isobaric interferences as they can be analyzed using our complimentary negative mode assay. For the first time, we discuss the reaction kinetics of MTT through conducting rigorous validation and optimize derivatization yields to reach 90% over several PC species using a 60 min reaction at 60 °C. A simple hexane wash is introduced to clear residual by-product of the reaction and produce a clean extract of derivatized, diacyl PC species. This derivatization strategy effectively induces a positive mobility shift of PC species away from ion suppressive regions that additionally improves separation resolution of within species by further augmenting their electrophoretic mobility. We demonstrate this by extending our mobility map models that highlight mobility differences between saturated and unsaturated species as well as highlighting the capacity to analyze sphingomyelin (SM) which demonstrates a characteristic later

mobility due to their extended acyl chain lengths. Using a validated standard reference material (SRM NIST 1950), we were able to extend our profiling capabilities to an additional >80 lipid species by implementing this derivatization strategy. Overall, this work further extends and demonstrates the capabilities of MSI-NACE-MS as a robust high-throughput platform for large scale lipidomic studies. Furthermore, this chapter contributes a unique derivatization strategy using an underutilized reagent that can be applicable for methylation in other analytical approaches.

## **5.2. Further Method Development to Expand Lipid Profiling Capabilities by NACE**

While we indeed, successfully demonstrate the capabilities of MSI-NACE-MS to profile several ionic lipid species, we were limited to the solvent combinations available due to compatibility when coupling to MS. A unique quality that has been previously highlighted and demonstrated in the few existing applications of NACE is the ability to extort unique separations by modulating unique solvent combinations based on their physicochemical properties.<sup>4,5</sup> This is the result of various solvent-solvent interactions as well as their influence on  $pK_a$  shifts due to relative permittivity, autoprotolysis constant and hydrogen bonding capability of the solvents in use.<sup>6</sup> For example, it has been previously demonstrated that the use of methanol as a BGE solvent was able to achieve complete separation of  $\beta$ -blockers with improved responses and reduced analysis times using UV detection in comparison to conventional aqueous BGE.<sup>7</sup> In the context of lipidomics, there have been few applications that demonstrate the ability to separate cis- and trans-isomers of fatty acids using Brij 35 as a surfactant additive using UV detection without the need for derivatization.<sup>8</sup> Thus, NACE-UV can present as a cost-effective platform for more focused/targeted lipid profiling that can offer unique separation selectivity or to supplement studies that are interested in resolving isomer species.



### **5.3. Applications of Strategies to Uncover Lipid Based Biomarkers for Cystic Fibrosis Using Neonatal Dried Blood Spots**

Notably, this thesis sets the foundation for more comprehensive, exploratory work to be conducted to uncover biomarkers in volume restricted samples, using MSI-(NA)CE-MS as a robust platform. In this context, these projects will enable for comprehensive screening of biomarkers in cystic fibrosis (CF) neonates using dried blood spots that were provided in a collaborative project with CHEO. Cystic fibrosis remains as a disease implemented in newborn screening that does not use MS based screening and typically relies on a two-tiered design involving detection of elevated immunoreactive trypsinogen with confirmatory sweat chloride testing.<sup>9</sup> While whole genome sequencing has recently been implemented into the screening algorithm, this results in many transient cases of CF that may present variable phenotypes. Notably, pancreatic insufficiency is a common complication associated with CF due to the development of thick mucus that block the entry of pancreatic enzymes from entering the small intestine.<sup>10</sup> Consequently, this results in fat malabsorption which puts patients at risk for steatorrhea (excretion of abnormal quantities of fat with feces), malnutrition as well as fat-soluble vitamin deficiencies. Smaller molecules such as metabolites and particularly lipids may then represent an interesting target in biomarker search. For example, it was revealed that the dysregulation of metabolite profiles involving amino acids, and lactate represented markers of inflammation in broncho-alveolar fluid from CF patients. Interestingly, volatile organic compounds presented as markers of *Pseudomonas aeruginosa* colonization, which is the most common bacteria in CF patients and is a prognostic indicator of progressive lung disease.<sup>11</sup> In the context of lipidomics however, it has been noted that circulating essential fatty acids and other lipids were decreased as well as decrease in PUFAs in lung, intestine and pancreas of mice as well

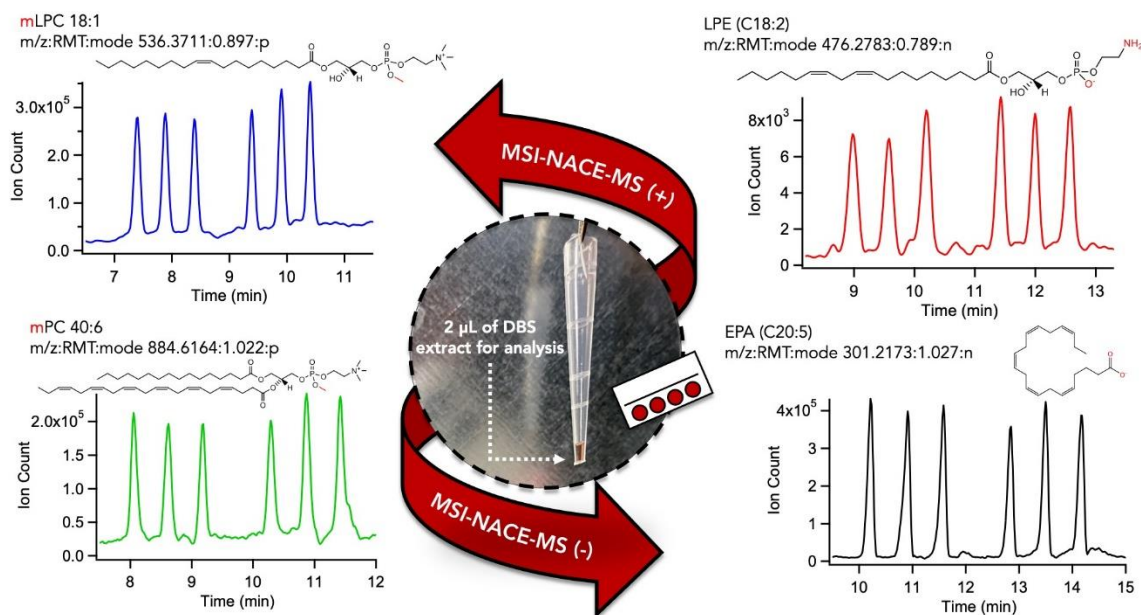


**Figure 5.1.** Analysis of lipid species using MSI-NACE-MS from a single dried blood extract using pipette tip adapters following an MTBE extraction. Extract is split into fractions for analysis in negative mode, whilst other fraction is derivatized for analysis in positive mode. Figure adapted from Ly *et al.*<sup>15</sup>

as the nasal cells of patients, with particular reference to imbalances in omega-3/omega-6 ratios.<sup>12,13</sup> However, the development and expansion of profiling capabilities presented in this thesis using MSI-(NA)CE-MS represent a venue to comprehensively profile and analyze hydrophilic and hydrophobic metabolites using a single dried blood spot punchout as outlined in work that we have recently published (**Figure 5.1**). This study will not only confirm the preliminary discoveries that our group previously unveiled,<sup>14</sup> but will expand to provide more comprehensive insights to the underlying metabolic pathways that may differentially impact affected CF neonates while also providing context to transient cases that may demonstrate ambiguous phenotypes with the recent inclusion of whole genome sequencing in the screening algorithm.

#### **5.4. Uncovering Lipid-Based Biomarkers in Large-scale Epidemiological Studies Using MSI-NACE-MS**

This thesis demonstrates and presents several developments to improve and expand the screening capabilities of MSI-(NA)CE-MS that initially focused on polar/ionic hydrophilic metabolites. While organic solvent-based buffer systems have been demonstrated for small, targeted lipidomic studies previously, the use of NACE-MS for lipidomic studies remained deterred due to several technical issues. We address these issues when we initially introduced MSI-NACE-MS which includes acetonitrile induce swelling of polyimide capillary coating, precise control of nebulising gases during separation and injection sequences to prevent siphoning (which is exacerbated using less viscous organic solvents), capillary breakages due to corona discharge and optimal combinations of compatible solvent systems. While we have overcome these issues, we only demonstrate stability for studies involving < 200 samples. Our group has recently ventured into conducting larger epidemiological studies ( $n = 1000$ ) using our conventional aqueous based methods and successfully demonstrate MSI-CE-MS as a viable platform. With the current direction of lipidomic studies and race to uncover lipid-based biomarkers, application of MSI-NACE-MS in larger scale studies to provide stronger study power would further solidify its place as a platform in the field. Furthermore, this would enable us to provide critical study aspects in the lipidomics field such as more robust quality control and enhanced batch control correction algorithms to further increase data fidelity.

#### **5.5. Development of Targeted DI-MS/MS Assay for High-Throughput Screening of Vitamin D and Omega-3 Status**

In *Chapters IV & V*, I introduced and successfully applied a unique derivatization strategy that enables the analysis of zwitterionic lipid species by fixing a positive charge through

methylation. While we apply this strategy to improve separation of PC species by MSI-NACE-MS, we uncover several phospholipid species that demonstrated a response to treatment involving EPA and DHA. With this, we challenge the measurement and use of O3I with the use of PC species that contain omega-3 lipids as a more reflective indicator of omega-3 status that is more readily measurable in serum, plasma or other readily available bio-banked specimens. More specifically, the combination of PC 36:5 and PC 38:6 strongly correlated to O3I and works well as a surrogate to O3I measurements but in more readily available biospecimens (*i.e.*, serum, plasma). Thus, we opt to implement this strategy for more targeted, high-throughput screening of omega-3 status using DI-MS/MS. Additionally, we recently introduced a protocol to analyze vitamin D using a click-derivatization strategy using 2-nitrosopyridine to affix a positive charge as an alternative that offers improved precision and accuracy than immunoassays.<sup>16</sup> Given the recent spotlight on initiatives to improve public health, both vitamin D and omega-3 lipids remain largely deficient that can provide substantial health benefits, especially if the capability to monitor individual levels is available in a quick, yet efficient manner. Thus, this work offers the ability to assess status in support of large-scale studies in nutritional epidemiology and in clinical settings to rapidly screen individual patients that may benefit from supplementation from vitamin D and/or omega-3 supplementation.

## **5.5. General Conclusions**

In conclusion, this thesis pushes significant boundaries by providing unique strategies to accelerate biomarker discovery and profile polar, ionic lipids in a cost-effective manner using multiplexed separations via MSI-NACE-MS. We incorporate the use of an iterative nontargeted data workflow to screen and validate lipid species using signal pattern recognition strategies. Additionally, we further expand lipid profiling by introducing a unique derivatization strategy to

affix a permanent positive charge that serves as an alternative to more dangerous protocols (*i.e.*, diazomethane), yet applicable universally for other analytical applications. In addition to the robust quality control and enhanced batch correction that MSI-NACE-MS provides, we demonstrate the use of supplemental annotation tools through intrinsic mobility maps that further increase confidence when conducting nontargeted studies for biomarker discovery. Furthermore, we build on foundations developed by the greater lipidomics community with semi quantitative approaches using serial dilution of a standard plasma reference material (NIST SRM-1950) that has been validated through various international ring trials. Lastly, we apply this accelerated workflow to reveal serum and plasma phospholipids that can be used as convenient surrogate markers to rapidly screen for omega-3 nutritional status to reduce risk for cardiovascular events. Overall, this thesis paves the way in demonstrating the capabilities of MSI-NACE-MS as a viable platform for large-scale lipidomic studies to accelerate biomarker discovery and achieving deeper insights to lipid related pathophysiology and functionality.

## 5.7. References

- (1) Thompson, J. W.; Adams, K. J.; Adamski, J.; Asad, Y.; Borts, D.; Bowden, J. A.; Byram, G.; Dang, V.; Dunn, W. B.; Fernandez, F.; et al. *Anal Chem* 2019, *91* (22), 14407–14416.
- (2) Bowden, J. A.; Heckert, A.; Ulmer, C. Z.; Jones, C. M.; Koelmel, J. P.; Abdullah, L.; Ahonen, L.; Alnouti, Y.; Armando, A. M.; Asara, J. M.; et al. *J Lipid Res* 2017, *58* (12), 2275–2288.
- (3) McDonald, J. G.; Ejsing, C. S.; Kopczynski, D.; Holčapek, M.; Aoki, J.; Arita, M.; Arita, M.; Baker, E. S.; Bertrand-Michel, J.; Bowden, J. A.; et al. *Nat Metabolism* 2022, 1–3.
- (4) Kenndler, E. *J Chromatogr A* 2014, *1335*, 16–30.
- (5) Kenndler, E. *J Chromatogr A* 2014, *1335*, 31–41.
- (6) Steiner, F.; Hassel, M. *Electrophoresis* 2000, *21* (18), 3994–4016.

- (7) Geiser, L.; Cherkaoui, S.; Veuthey, J.-L. *J Chromatogr A* 2002, 979 (1–2), 389–398.
- (8) Barra, P. M. de C.; Castro, R. de J. C.; Oliveira, P. L. de; Aued-Pimentel, S.; Silva, S. A. da; Oliveira, M. A. L. de. *Food Res Int* 2013, 52 (1), 33–41.
- (9) Coward, R. M.; Davis, E. L.; Young, S. L. *Fertil Steril* 2020, 114 (3), 495–496.
- (10) Freedman, S. D.; Blanco, P. G.; Zaman, M. M.; Shea, J. C.; Ollero, M.; Hopper, I. K.; Weed, D. A.; Gelrud, A.; Regan, M. M.; Laposata, M.; et al. *New Engl J Medicine* 2004, 350 (6), 560–569.
- (11) Lyczak, J. B.; Cannon, C. L.; Pier, G. B. *Clin Microbiol Rev* 2002, 15 (2), 194–222.
- (12) Worgall, T. S. *Curr Opin Clin Nutr* 2009, 12 (2), 105–109.
- (13) Strandvik, B. *New Engl J Medicine* 2004, 350 (6), 605–607.
- (14) DiBattista, A.; McIntosh, N.; Lamoureux, M.; Al-Dirbashi, O. Y.; Chakraborty, P.; Britz-McKibbin, P. *J Proteome Res* 2018, 18 (3), 841–854.
- (15) Ly, R.; Azab, S.; Shanmuganathan, M.; Britz-McKibbin, P. In *Capillary Electrophoresis-Mass Spectrometry for Proteomics and Metabolomics*; Ramautar, R., Chen, D. D. Y., Eds.; WILEY-VCH, 2022; pp 179–193.
- (16) Helmecci, E.; Fries, E.; Perry, L.; Choong, K.; O’Hearn, K.; McNally, D.; Britz-McKibbin, P. *J Lipid Res* 2022, 63 (5), 100204.